RESTRICTED PHASE-LOCKING DYNAMICS OF PERIODICALLY FORCED NETWORK GAMMA RHYTHMS

JONATHAN CANNON AND NANCY KOPELL

1. Introduction

The observation of gamma (30-100Hz) oscillations in many areas of the brain has inspired numerous modeling efforts and theoretical investigations [**Buzsaki2012a**] into the possible mechanisms and functions of the rhythm. Most of these studies have focused on the effects of network architecture and parameter values on network synchronization at gamma frequencies [**Wang1996**][**Gouwens2010**] [**Christoph2003**][**Borgers2012**] [**Karbowski2000**] [**Chow1998**] [**Buzsaki2012a**]. More recently, some have considered these mechanisms in the broader neural context in which gamma-generating populations may receive temporally patterned inputs, including inputs modulated at gamma frequencies [**Borgers2005**] [**Christoph2008**] [**dorea2008**] [**Gielen2010**] [**Serenevy**]. An increasing number of researchers in this area are focusing on the hypothesis that coherence between gamma-rhythmic neuron populations modulates the effectiveness of information transfer, often called the "Communication Through Coherence" (CTC) hypothesis [**Fries2009**] [**Womelsdorf2007b**]. But only a handful have posed the important question of how such coherence is maintained and manipulated, and these focus mainly on numerical observations and heuristic arguments. None that we know of have taken a systematic, theoretical approach to the problem of establishing coherence between multiple gamma-rhythmic populations.

In this manuscript, we use an assortment of mathematical tools in order to investigate the properties under periodic forcing of gamma-generating circuits. We focus on the simplest model of gamma generation, called Interneuronal Network Gamma (ING), in which a self-inhibiting neuronal population alternatingly fires a volley of spikes and recovers from its self-inhibition on the time scale of a gamma cycle [**Whittington1995**][**Whittington2000**]. We also consider Pyramidal-Interneuronal Network Gamma, in which pyramidal cells fire a spike volley, evoke an inhibitory spike volley, recover slowly from inhibition, and repeat [**Whittington1997**] [**Whittington2000**]. These two processes share the key mechanism of slowly-decreasing inhibition that rapidly resets when it is overcome by excitation.

We do not examine the mechanisms of synchronization and desynchronization: these have already been studied extensively [**Wang1996**] [**Gouwens2010**] [**Christoph2003**] [**Borgers2012**] [**Karbowski2000**] [**Chow1998**] [**Buzsaki2012a**]. Instead, we will consider only systems

that have already reached and are maintaining tight synchrony, and are driven homogeneously by a temporally-patterned signal. By restricting our scope in this way, we are better able to tease out the properties distinctive to the rhythmic mechanism itself, as opposed to those brought about by noise, heterogeneity, etc.

Here we make two major claims about this rhythmic mechanism when it is subjected to periodic forcing, both of which we explain and qualify analytically:

(1) Its dynamics are constrained to periodic and quasiperiodic behavior.

(2) When it is phase-locked to a periodic pulse, it is monostable (only one stable phase-locked trajectory exists).

The distinctive properties of this mechanism are easiest to identify and understand in contrast to the properties of the relaxation oscillator. As a representative example of the relaxation oscillator, we use the well-studied Fitzhugh-Nagumo (FN) model. In the next three sections, we compare the mechanism of relaxation oscillations to the ING/PING mechanism, and we use this comparison to help us contextualize and explain the unique properties listed above.

The first section reviews results from the theory of forced oscillators. We review the properties of flows on a torus, and in particular the limitation of such flows to periodic and quasiperiodic motion. We recall that a limit-cycle oscillator under sufficiently weak forcing is constrained to an attracting invariant torus in phase space; however, the strength of forcing that is sufficiently weak to guarantee the persistence of the invariant torus depends on the properties of the system.

In particular, the Fitzhugh-Nagume (FN) relaxation oscillator close to its singular limit retains an invariant torus only for extremely weak forcing. Once the torus vanishes, the forced relaxation oscillator also acquires a wider range of dynamic behaviors, including stable period doubling and chaos [**Croisier2009**]. We also note that forced relaxation oscillators generally have parameter regimes in which two periodic orbits are simultaneously stable when the forcing period is slightly longer or slightly shorter than the natural period. We argue in the discussion section that these properties make a forced relaxation oscillator a poor candidate for communication through coherence (CTC).

In the second section, we define a simple three-dimensional model of forced ING, in which a synchronous population of inhibitory neurons repeatedly emerges from decaying mutual inhibition, spikes, and instantly restores maximal mutual inhibition, all under the influence of periodically-patterned drive. We find that this system maintains a globally attracting invariant torus when trajectories converge sufficiently between each spike. Such convergence may arise from two different sources: synaptic saturation and sustained inhibition. When this convergence condition is met, the ING system's asymptotic dynamics are strictly constrained to an invariant torus, and therefore consist entirely of periodic and quasiperiodic orbits.

We also show that when the ING oscillator phase-locks to periodic pulsatile input (assumed for purposes of the proof to consist of square pulses), only one stable periodic orbit may exist, so it always phase-locks with the same phase offset from the forcing. We argue that the combination of a persistent attracting invariant torus and monostable phase-locking makes it an ideal candidate for CTC.

In the third section, we define a model of a forced PING oscillator that lives in five dimensions (including forcing) instead of three, but behaves very similarly to the ING oscillator when the E-cell is periodically forced and the membrane time-constant of its inhibitory population is small. We show that for sufficiently low I-cell membrane time-constant, the dynamics of PING with a forced excitatory population are very similar to the dynamics of forced ING; in particular, the asymptotic dynamics of periodically forced PING are also constrained to an invariant torus, on which its dynamics are similarly restricted.

2. Context

2.1. **Flows on Tori.** We shall find it very useful do draw a distinction between systems constrained to an invariant torus and systems free from this constraint. We recall that periodic forcing may be introduced into a model by adding a circular variable Φ representing the phase of the forcing period, with $\dot{\Phi}$ constant. If this variable is introduced into a system with an asymptotically stable limit cycle but remains uncoupled from the rest of the system, the limit cycle in full phase space is an asymptotically attracting invariant torus. By Fenichel's result on the persistence of normally-hyperbolic invariant manifolds [**Fenichel**], this torus must persist and continue to attract when the coupling between Φ and the other variables is sufficiently weak. If the forcing is made stronger, however, this torus may be topologically altered or destroyed. This generally corresponds to a transition to chaotic dynamics. For more information on this transition and the discussion that follows, see e.g. [**Schuster**] and [**Rasband**].

While this torus persists (and forward and backward flows on it are unique), the asymptotic dynamics of the forced oscillator are limited to the dynamics possible on the surface of a two-dimensional torus. Flows on the 2-torus do not allow period-doubling bifurcations: a period-doubled solution would necessarily cross the unstable solution that remains after period-doubling. For the same reason, two phase-locked solutions with different locking ratios (e.g. 1:1 and 2:1 locking) cannot coexist on a torus. The only dynamics possible on the surface of a 2-torus are quasiperiodic (described by a function of two periodic motions with an irrational ratio) and periodic. Generally the phase-locked states on the torus are arranged in order of phase locking ratio along a "devil's staircase," in which phase locking ratios with smaller denominators persist over a larger subset of a parameter space, all phase locking ratios are represented, and phase locked states are separated by short windows of quasiperiodicity.

We note that the existence of an invariant torus is implied by the existence of an invariant circle under a Poincare map. (This is directly analogous to the fact that a fixed point under a Poincare map implies the existence of a limit cycle.) If a Poincare map on a transverse section of a continuous flow takes a topological circle of points back to itself and preserves the circle's orientation, then the forward flow of the circle traces out a torus; since the torus is made up of complete trajectories, it is invariant under the flow. If the circle asymptotically attracts all initial points in the section, then all trajectories passing through the section are asymptotically attracted to the torus. We use this simple result to prove the existence of attracting invariant tori in later sections.

This method of proving the existence of an invariant torus is particularly useful for systems with discontinuous jumps: the induced map on a section may still be a homeomorphism on an invariant circle. In this case, the invariant set in the full space is a broken torus; but if the circle of points is mapped homeomorphically across each jump, then by identifying points before the jumps with points after them we can create a topology in which the invariant flow takes place on an unbroken invariant torus, and dynamics on its surface are constrained to periodic and quasiperiodic orbits (see Figure 1).

Invariant tori are particularly useful in spiking systems. In a neural model with a Poincare section corresponding to a "spike," we can define a Poincare map from the state at one spike to the state at the next. If the full state space is only two-dimensional, this is a one-dimensional map, so the value of a single variable at a spike determines the system state at the next spike. In the following sections and in a number of other publications, this variable is time or the phase of an ongoing forcing oscillation, and the map is called a "spike map" [**Brette2003**] (though other publications refer to it as a "firing map" [**Carrillo2001**], "firing time map" [**Goel2002**] or "spike-time map" [**Tiesinga2002a**]). In higher dimensional systems, no single variable at a spike can determine the state at the next. But if the Poincare map possesses an attracting invariant circle (i.e. the full system possesses an attracting invariant torus), a one-dimensional map may be defined on the invariant circle; after the system becomes close to the torus, this map begins to act as a spike map and can be used to study the asymptotic dynamics of the system.

2.2. **The Relaxation Oscillator and Phase-Locking.** Here we study the phase-locking properties of a periodically-forced relaxation oscillator. As a generic exemplar of such an oscillator, we study the periodically-forced Fitzhugh-Nagumo (FN) oscillator, defined by the equations

$$\begin{cases} \tau \dot{v} = & v - v^3 - w + \epsilon I(\Phi) \\ \dot{w} = & v - c - rw \\ \dot{\Phi} = & 1 \end{cases} \tag{2.1}$$

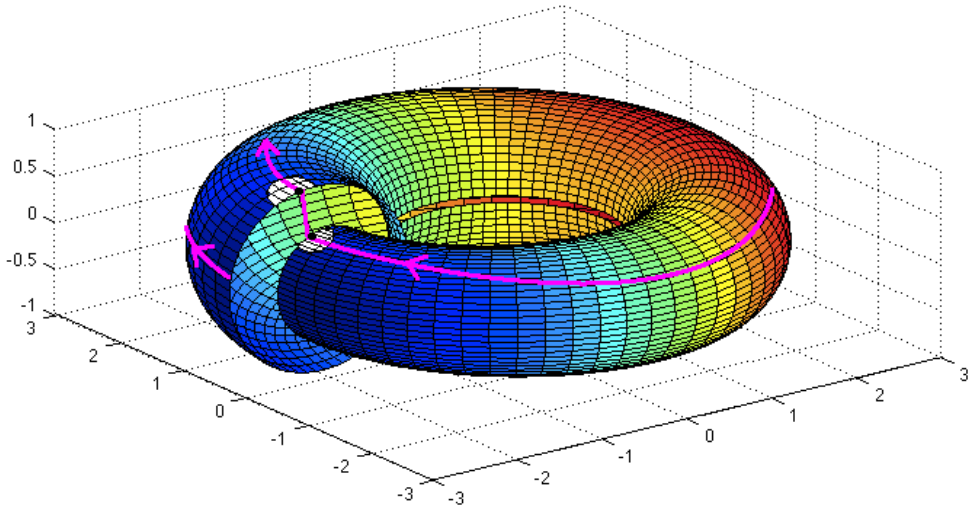

Figure 1: A flow on a torus with a discontinuous jump. Points are identified across the jump (e.g., the black points on the magenta trajectory), and in the induced topology the white set is open. The jump is a homeomorphism on the circle, so this topology glues the two circular faces together one-to-one and continuously to create an unbroken torus on which flows are continuous.

In these equations, $\Phi \in \mathbb{T}^1 = [0, T_I)$, $I(\cdot)$ is a piecewise-continuous function from $\mathbb{T}^1$ to $\mathbb{R}^+$ and hence a periodic current with period T_I, and $0 < \tau \ll 1$. This model has been studied in [**Alexander1990**](in which only the w variable is forced), [**Guckenheimer2006**], [**Croisier2009**], [**Izhikevich2000**], and [**Coombes2000**], to name a few; our analysis is intended only to compare these results to the properties of ING oscillators.

2.2.1. *The Breakup of the Invariant Torus.* Though any system with a globally attracting limit cycle is globally attracted to an invariant torus for sufficiently weak periodic forcing, the strength of forcing required to break up the torus varies by system. One factor that can reduce the requisite forcing strength necessary to break the torus is a separation of time scales. This effect is apparent in the case of the forced relaxation oscillator.

Croiser et. al [**Croisier2009**] conduct a numerical study of the FN oscillator under forcing. They find that interesting dynamics emerge at a forcing strength ϵ that decreases precipitously as $\tau \to 0$. These dynamics include the period-doubling of stable 1:1 phase-locked orbits, and bistability between 1:1 and 2:1 phase-locked solutions, both for forcing periods close to the system's natural period. As discussed above, neither of these behaviors is possible if there exists a globally attracting invariant torus; therefore, their observations prove that when τ is small, the attracting invariant torus breaks up at very small ϵ.

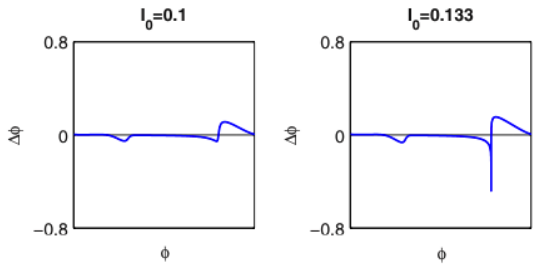

Figure 2: The phase response curve (PRC) of the FN oscillator with small τ in response to two different pulse strengths (both very weak), reproduced from Croisier et al. 2009 [**Croisier2009**].

2.2.2. *Bistable Phase-Locking.* Even when the forced FN oscillator possesses an invariant torus, it still tends to support stable 1:1 phase-locking at two different phases. Croiser et. al [**Croisier2009**] demonstrate by numerical simulation that when a FN oscillator (with small, nonzero ϵ) is given pulsatile periodic forcing, the stable phase-locking tongue has bistable regions for forcing periods immediately to the right and left of the natural period.

Croisier et al. point out that the bistability is directly related to the fact that the phase-response curve (PRC) makes two downward excursions from the zero line (see Figure 2). Here, the phase response curve (PRC) is defined as a function from an oscillator's phase at the arrival of a temporally localized pulse to the resulting advance (or delay) in phase [**Winifree**] [**Ermentrout2002**] [**Canavier2012**]. It can be used to produce a "phase-resetting map" from the oscillator's phase at one stimulus to its phase at the next:

$$\phi_{i+1} = \phi^i + f(\phi^i) + T_I \bmod T_0 \tag{2.2}$$

where $f(\cdot)$ is the PRC, $\phi \in \mathbb{T}^1 = [0, T_0)$ (see [**Croisier2009**]), and T_I and T_0 are the forcing period and natural period as before. When the PRC crosses $T_0 - T_I$, the phase-resetting map crosses the diagonal and phase-locking is possible; when this crossing is from above to below, the phase-resetting map crosses from above the diagonal to below, so phase-locking may be stable (as long as the slope of the phase-resetting map at the crossing is greater than -1). The PRC for the FN oscillator is reproduced from [**Croisier2009**] in Figure 2. Note its two downward excursions. If the forcing period is just above the natural period, then $T_0 - T_I$ is just below zero, and these downward excursions may cause the PRC to cross $T_0 - T_I$ downwards twice with shallow slopes, giving rise to two stably phase-locked trajectories.

3. ING: Robust, Monostable Phase-Locking on an Invariant Torus

Here we investigate the phase-locking properties of the forced ING mechanism.

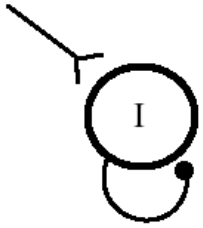

Figure 3: Schema of the ING circuit.

As we discuss above, our treatment of ING assumes a periodically-forced synchronous population of I-cells in a cycle of creating and then slowly recovering from mutual inhibition. The components of this system are:

- A fast voltage variable V (the shared membrane potential of the inhibitory population) goes from excitable to oscillatory as drive passes above a threshold, causing it to blow up (spike) and then reset.
- A slow inhibition variable $s > 0$ (the level of synaptic inhibition) that resets to a higher value when the voltage variable spikes, and otherwise decays with time.
- A forcing phase variable Φ that advances steadily with time and may be either on a circle or lifted to $\mathbb{R}$ (in which case we write $\bar{\Phi}$).

Like the forced relaxation oscillator, this system is characterized by a slow variable, a faster variable, and a periodic forcing variable, and dynamics are characterized by gradual change in the slow variable punctuated by sudden jumps in the fast variable. In its definition, this system differs from the FN oscillator in two key respects:

- The slow variable has fast resets triggered by the faster variable, and the resetting map induces a contraction in the slow direction. In this respect, it is like a relaxation oscillator with a very fast right branch. (See **[Somers1993]** for an explanation of how a difference between the speeds along the two branches of a forced relaxation oscillator creates "compression" in the slow direction.)
- Excitation always pushes the system closer to a spike. This is possible because the fast variable is circular, so it never has to reverse direction like the fast variable in the FN oscillator.

These differences have important consequences for the phase-locking properties of the system that distinguish it from a relaxation oscillator:

- The attracting invariant torus that exists for $\epsilon = 0$ persists for strong forcing for a broad range of parameters, precluding period-doubling and any other behavior that cannot exist on the torus.

- In general, when the forced ING oscillator phase-locks to a periodic pulse, only one phase-locked trajectory is stable. (We prove this claim for forcing by square pulses within a particular parameter regime described below, and we observe it in simulation in a broader range of forcing scenarios.)

We study one instantiation of the forced ING oscillator described above, using the voltage V of a QIF neuron [**Latham2000**] to model the voltage of the synchronous inhibitory population and an exponentially decaying scalar $s^i \in (0,1]$ to model the slowly decaying inhibition. We use the equations

$$\begin{cases} \dot{V} = & \frac{1}{\tau}(V^2 + G) \\ \dot{s} = & -\frac{s}{\tau_s} \\ \dot{\Phi} = & 1 \end{cases} \tag{3.1}$$

where

$$G = b - gs + \epsilon I(\Phi).$$

is the net flux of current; g is the maximal conductance of the I-cell autapse; τ_s is the decay time constant of inhibition; τ is the I-cell membrane time constant; and b is the baseline level of tonic excitation of the I-cell. The forcing phase $\Phi \in [0, T_I)$ is on $\mathbb{T}^1$, and $I(\cdot)$ is a T_I-periodic piecewise-continuous function representing the periodic drive to the I-population. V resets to $-\infty$ when it blows up to ∞, and s resets instantly to

$$\rho(s) = 1 + c(s-1) \tag{3.2}$$

when V blows up. We call this synaptic resetting rule ρ "linearly resetting synapses." We show in Appendix 6.1 that this synapse model approximates more realistic synapses if the spikes that cause synaptic rise are narrow. Models in which synapses increase by a fixed amount at every spike can also be reproduced in this framework by making g large and c close to 1. Similar equations to ours were used to model forced gamma rhythms in [**Borgers2005**].

We also assume that the sum of b and $I(\Phi)$ becomes sufficiently positive for long enough each period that the forward flow from any initial state is eventually followed by another spike, and that the next spike occurs within time C for some $C < \infty$. (The existence of an upper bound C on inter-spike interval can be shown to follow from the first assumption and the compactness of state space.)

We treat the synaptic current s as a directly injected current. We believe that under most circumstances, introducing a synaptic reversal potential would not compromise our qualitative results; however, that is outside the scope of this paper.

Additional Notation:

- When we want to consider a circular variable (e.g., Φ) in its lift to $\mathbb{R}$, we use an overbar (e.g., $\bar{\Phi}$).

- We write V_t to refer to the value of V at time t. Given an ODE and a set of initial conditions V_0, s_0, Φ_0, we write $V_t(V_0, s_0, \Phi_0)$ to refer to the value of V when the system is initialized with these initial conditions and allowed to flow forward by time t. We use s_t and Φ_t similarly.

3.1. **Existence of a Globally Attracting Invariant Torus for Non-Small ϵ.** *Here we discuss the broad conditions under which a periodically-forced ING system as described in (3.1) possesses a globally attracting invariant torus.*

In order to avoid the inconvenience of resetting membrane potentials at a spike, we switch from a QIF neuron with voltage V to the equivalent theta neuron with phase θ, using the change of variables presented in [**Ermentrout1986**]:

$$V = \tan\left(\frac{\theta}{2}\right) \tag{3.3}$$

where $\theta \in \mathbb{T}^1 = [0, 2\pi)$. We can replace the first equation in (3.1) with

$$\dot{\theta} = \frac{1}{\tau}\left[1 - \cos(\theta) + (1 + \cos(\theta))G\right]. \tag{3.4}$$

In θ coordinates, the invariant manifold (when it exists) is a torus with one jump discontinuity at $\theta = \pi$ corresponding to the instantaneous synaptic resetting event at each spike. If each trajectory is connected across the jump by identifying the point (π, s, Φ) at the left-hand limit of a spike time with $(\pi, \rho(s), \Phi)$ at the right-hand limit of the spike, then the invariant set is a topological torus in phase space, as discussed in Section 2.1 and illustrated in Figure 4. Importantly, though the vector field on this torus is not continuous across $\theta = \pi$, it points in the positive direction on either side of it, so trajectories have unique continuations across the boundary and it is accurate to describe the invariant set as a flow constrained to a torus [**Alexander1990**]. As discussed in Section 2.1, when an attracting invariant torus exists, the long-term dynamics of the ING oscillator cannot include multiple phase-locked trajectories with different locking ratios, and cannot period-double as parameters change.

As with any limit-cycle oscillator, the invariant torus which exists for $\epsilon = 0$ (no forcing) persists for sufficiently small $\epsilon > 0$. However, due to its distinctive structure, the ING oscillator has a much broader regime throughout which its invariant torus provably persists. First we show that

As discussed in Section 2.1, the existence of the attracting invariant torus is equivalent to the existence of an attracting invariant circle for the map from the system state at one spike to the next. We let $\mathbf{R}$ denote the map from the (s, Φ) state of the system at the right-hand limit of a spike time at $t = 0$ to its (s, Φ) state at the right-hand limit of the next spike time t_s:

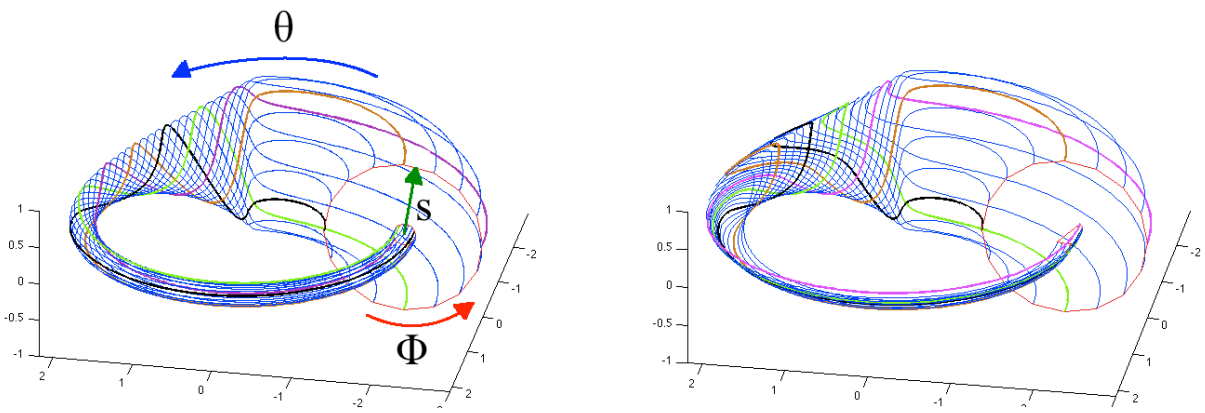

Figure 4: **Left:** Trajectories of ING go to an invariant torus with a jump discontinuity at $\theta = \pi$. θ is represented by the angle around a ring in the x/y plane; s is represented by the length of a vector extending perpendicularly out from this central ring; and Φ is represented by the angle of this vector. around the circular cross-section of the torus. The large red circle is the set $\theta = \pi$, $s = 1$. Sixteen trajectories are initialized from this set, each at a different forcing phase. Four are colored for visibility. **Right:** Under periodic forcing, some trajectories increase and then decrease in the θ direction before spiking; ultimately, they cluster together towards a single trajectory on the cyclinder, giving rise to stable phase-locking.

$$\begin{aligned} \mathbf{R} : [0,1] \times \mathbb{T}^1 &\to [0,1] \times \mathbb{T}^1 \\ (s_0, \Phi_0) &\to (s_{t_s}, \Phi_{t_s}) \end{aligned}$$

In the following, we assume $\epsilon = 1$ because an assumption of weak forcing is not required. We show that an attracting invariant circle exists for $\mathbf{R}$ (and hence an attracting broken invariant torus exists for the dynamical system) when $c = 0$, when c is sufficiently small, and when g is sufficiently large.

3.1.1. *Invariant torus when $c = 0$.* If $c = 0$ (synapses saturate fully at each spike), we can immediately see that since $\rho(s) = 1$ for all s, trajectories reaching $\theta = \pi$ jump onto the circle $s = 1$ in (s, Φ) space. This circle is clearly invariant and attracting under $\mathbf{R}$, and the flow from this circle forms an invariant surface in the full phase space. All we need to show is that this surface is a torus when trajectories are identified across the jump; for this, it is sufficient to show that when the circle $s = 1$ at $\theta = -\pi$ is followed along the flow to the next spike and reset by ρ (i.e., subjected to the return map $\mathbf{R}$), the result is an orientation=preserving homeomorphism on the circle.

We let $\mathbf{P}_{\mathbb{T}^1} : \mathbb{T}^1 \to \mathbb{T}^1$ denote the restriction of $\mathbf{R}$ to the circle $s = 1$, which takes as an argument an initial forcing phase Φ_0 and returns the value of Φ at which a trajectory

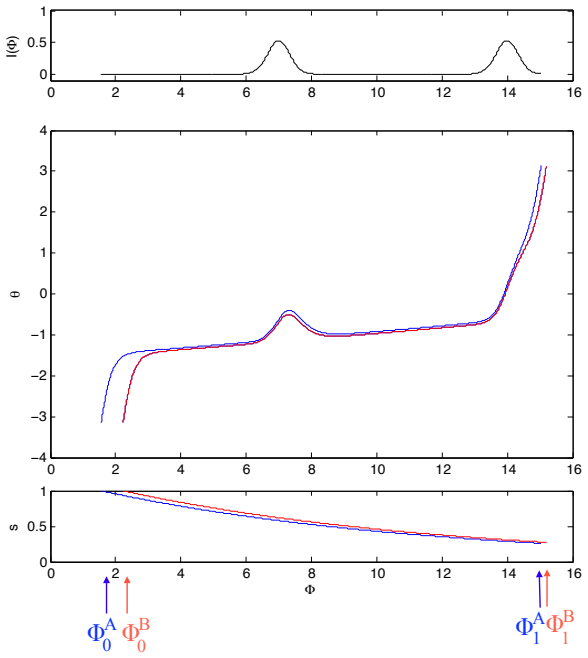

Figure 5: Two trajectories are initialized with $s = 0$, at phases $\bar{\Phi}_0^B > \bar{\Phi}_0^A$. The population phase θ of trajectory B (red) is below that of trajectory A (blue), and cannot cross it because it is under more inhibition. Therefore, trajectory A reaches a spike at an earlier forcing phase: $\bar{\Phi}_1^B > \bar{\Phi}_1^A$.

initialized at $(-\pi, 1, \Phi_0)$ reaches its next spike. If we can show that $\mathbf{P}_{\mathbb{T}^1}$ is an orientation-preserving homeomorphism on the circle, then after points are identified across the jump, the forward flow from $(-\pi, 1, \Phi)$ back to itself traces out a torus.

Theorem 3.1.1. $\mathbf{P}$ *is an orientation-preserving homeomorphism on the circle* $(-\pi, 1, \Phi)$.

The proof below is illustrated in Figure 5.

Proof. Let $\bar{\theta}$ and $\bar{\Phi}$ denote the lifts of θ and Φ to $\mathbb{R}$. Let $\mathbf{P} : \mathbb{R} \to \mathbb{R}$ denote the map $\mathbf{P}_{\mathbb{T}^1}$ for forcing phase lifted to $\mathbb{R}$. Since $\mathbf{P}$ is a lift of the map $\mathbf{P}_{\mathbb{T}^1}$ to $\mathbb{R}$, $\mathbf{P}_{\mathbb{T}^1}$ is an orientation-preserving homeomorphism on $\mathbb{T}^1$ if and only if $\mathbf{P}$ is an orientation-preserving homeomorphism on $\mathbb{R}$.

Consider two trajectories, A and B, which spike at initial time $t = 0$ at forcing phases $\bar{\Phi}_0^A$ and $\bar{\Phi}_0^B$, with $\bar{\Phi}_0^B > \bar{\Phi}_0^A$. We let the state at the right-hand limit of the A spike, $\begin{pmatrix} -\pi \\ 1 \\ \bar{\Phi}_0^A \end{pmatrix}$, flow forward to forcing phase $\bar{\Phi}_0^B$, where we will have $\bar{\theta}^A > -\pi$ and $s^A < 1$. From this point

forward, when the trajectories are at the same forcing phase, the inhibition on trajectory A will be lower. From (3.4), we see that for fixed θ, $\dot{\theta}$ strictly increases as inhibition decreases, so a trajectory under more inhibition can not cross from below to above a trajectory with higher inhibition. From this point forward, $\bar{\theta}^B$ cannot cross $\bar{\theta}^A$ from below, and will stay beneath it until trajectory A reaches another spike at some forcing phase $\bar{\Phi}_1^A$. Hence trajectory b must reach a spike at some $\bar{\Phi}_1^B > \bar{\Phi}_1^A$.

By the preceding argument, $\mathbf{P}$ (the map from $\bar{\Phi}_0^A$ to $\bar{\Phi}_1^A$ described above) preserves ordering. It is continuous because it is a Poincare map on a continuous flow; it is therefore a homeomorphism on $\mathbb{R}$.

The map $\mathbf{P}$ is the lift of the map $\mathbf{P}_{\mathbb{T}^1}$ acting on $\mathbb{T}^1$. Since $\mathbf{P}$ is a periodic order-preserving homeomorphism on $\mathbb{R}$, $\mathbf{P}_{\mathbb{T}^1}$ from Φ_0^A to Φ_1^A must be an orientation-preserving homeomorphism on the circle.

□

As discussed above, this condition is sufficient to prove the existence of a broken invariant torus that can be repaired by identifying points across the jump, and this set absorbs all initial conditions in finite time. $\mathbf{P}_{\mathbb{T}^1}$ is the spike map discussed in Section 2.1, which takes the forcing phase at the right-hand limit of one spike to the forcing phase at the right-hand limit of the next. Once the system has reached a spike, it becomes constrained to the invariant torus, and this spike map fully determines its dynamics.

This proof works because when all other things are equal, a system state with lower s reaches a spike before a system state with higher s. Trajectory B, which spiked more recently than trajectory A, must have a higher value of s at any given time, and therefore its next spike must be later than the next spike of trajectory A. By contrast, a trajectory on the right branch of the FN oscillator will reach a spike sooner if w is higher, whereas a trajectory on the left branch will spike sooner if w is lower, so this proof does not apply.

3.1.2. *Invariant torus for small $c > 0$.* An attracting torus also exists in the case $c > 0$ as long as trajectories contract together sufficiently strongly with time. One possible cause of this contraction is the convergence of trajectories due to the resetting map ρ. When $c = 0$, ρ (and hence the return map $\mathbf{R}$) forces all spiking trajectories onto the circle $s = 1$; when c is small, ρ (and hence $\mathbf{R}$) pushes trajectories close to the circle $s = 1$, and as a result the phase space contracts significantly at each application of the resetting map. Since the net excitation G exceeds zero in bounded time, the time between spikes is bounded, and this contraction occurs regularly; therefore, we expect it to lead to a steady contraction of the whole phase space. In the tradition of contraction-mapping theorems, we expect a strong contraction to lead to the existence of an invariant set, which in this case will be an invariant circle under $\mathbf{R}$ (like the circle $s = 1$ in the $c = 0$ case) and a corresponding broken invariant torus in the full phase space.

Intuitively, it would make sense to apply Niel Fenichel's result on the persistence of invariant manifolds to show that the torus persists when c is perturbed away from zero; however, Fenichel gives his result only for diffeomorphisms and continuous flows, whereas our flow experiences discontinuities and our return map $\mathbf{R}$ is not a diffeomorphism for $c = 0$ (due to the degeneracy of the map ρ in this case). In Appendix 6.2, we use a contraction-mapping result taken from [**Kolesov2003**] and [**shilnikov98**] called the Annulus Principle to show that for any set of system parameters, $c > 0$ may be chosen sufficiently small that there still exists an attracting invariant circle for $\mathbf{R}$ and hence a broken attracting invariant torus for the full system.

3.1.3. *Invariant torus for large g.* A second source of contraction in phase space of the ING system is the convergence of trajectories under sustained inhibition. This second factor in the creation of an invariant torus has been referred to in [**diener85**] and [**dorea2009**] as "rivering" because many voltage trajectories converge tightly under sustained inhibition to form a "river" of trajectories.

In the ING system, s and Φ trajectories evolve independently of θ: $(s_t, \Phi_t) = (s_0 e^{-\frac{t}{\tau_s}}, \Phi_0 + t)$. When the parameters of the ING system force θ to remain sufficiently negative for a sufficiently long time, rivering causes the θ coordinates of sets of trajectories on the same (s, Φ) trajectory to converge into tight rivers. As a result, the time for any system state (θ, s, Φ) to reach a spike comes to depend exclusively on s and Φ and becomes largely independent of θ; equivalently, the next spike time comes to depend only on what (s, Φ) trajectory the system joins at a spike, and becomes largely independent of the specific point along that trajectory that the spike occurs. When $c = 0$, fully-resetting synapses create an attracting invariant torus by causing the set of trajectories reaching a spike at the same forcing phase Φ to converge onto the same trajectory; when strong rivering of θ trajectories occurs, it creates an attracting invariant torus by causing the set of trajectories proceeding from a spike along the same (s, Φ) trajectory to converge on the same trajectory.

For any one-dimensional ODE, we can define a quantitative measure of rivering. Consider the (possibly nonautonomous) ODE $\dot{v} = F(v, t)$. For two nearby initial conditions v_0^* and $v_0^* + \Delta v_0$, we define Δv_t as the difference between the trajectories initialized at these two points after time t. Δv_t evolves according the the linearization of the ODE about the "base trajectory" v_t^*: $\Delta \dot{v}_t = F_v(v_t^*, t)\Delta v_t$. This linear ODE can be solved by ordinary methods:

$$\Delta v_t = \Delta v_0 e^{\int_0^t F_v(v_r^*, r)dr}.$$

We set $\kappa = e^{\int_0^{t_s} F_v(v_t^*, t)dt}$, where t_s is the next spike time after $t = 0$. κ is a measure of the strength of rivering between $t = 0$ and $t = t_s$. If it is close to zero, nearby trajectories converge almost completely; if it is near 1, nearby trajectories stay approximately the same distance apart; if it is large, nearby trajectories diverge. κ is implicitly a function of the initial condition v_0^*.

For the ING system described by (3.1), we can try to define κ for the membrane potential variable V:

$$\Delta V_{t_s} = \kappa \Delta V_0, \text{ where } \kappa = e^{\int_0^{t_s} 2V_t^* dt}.$$

Unfortunately, by this definition the integral in κ explodes at both ends of the interval, where $V = \pm\infty$. Fortunately, we can circumvent this problem by using the change of variables from V to θ as described by (3.4) to define κ for the theta neuron phase θ:

$$\Delta\theta_{t_s} = \kappa \Delta\theta_0, \text{ where } \kappa = e^{\int_0^{t_s} \sin(\theta_t^*)(1-G_t^*)dt}$$

where G_t^* is the net current at time t along the base trajectory $(\theta_t^*, s_t^*, \Phi_t^*)$:

$$G_t^* = b - g s_t^* + I(\Phi_t^*).$$

We can use a change of variables to fully exploit the contraction resulting from the rivering of θ trajectories. We replace the coordinate Φ with $\phi = \Phi + \tau_s \ln(s)$, and then define a map $\tilde{\mathbf{R}}$ analogous to $\mathbf{R}$ that takes the system state (s_0, ϕ_0) at the right-hand limit of a spike at time 0 and returns the system state (s_{t_s}, ϕ_{t_s}) at the right-hand limit of the next spike:

$$\begin{aligned} \tilde{\mathbf{R}} : [0,1] \times \mathbb{T}^1 &\to [0,1] \times \mathbb{T}^1 \\ (s_0, \phi_0) &\to (s_{t_s}, \phi_{t_s}) \end{aligned} \tag{3.5}$$

This new coordinate system is useful because all spikes occurring at the same value of ϕ_0 experience the same timecourse of s and Φ until the next spike, and therefore tend to river together. Thus, though $\mathbf{R}(s_0, \Phi_0)$ may depend strongly on both s_0 and Φ_0, $\tilde{\mathbf{R}}(s_0, \phi_0)$ depends mainly on ϕ_0 and therefore contracts trajectories together strongly in the s direction.

In Appendix 6.2, we show that by choosing the inhibitory conductance parameter g sufficiently large and bounding the allowable magnitude of the forcing current $I(\cdot)$, we can guarantee that κ is small (while other important quantities remain bounded from below). Using the contraction-mapping result described above, we show that if κ is sufficiently small (relative to these other bounded quantities), then $\tilde{\mathbf{R}}$ possesses an attracting invariant torus, and hence a broken attracting invariant torus exists in the full space.

Remark 3.1.1. *In the proof in Appendix 6.2, a second type of convergence of trajectories also occurs for large g: since large g prevents spiking for a long time, all trajectories reach spikes with s close to zero. A measure of convergence of s trajectories due to decay of inhibition is $e^{-\frac{t_s}{\tau_s}}$. In our proof, we show that like κ, this quantity also becomes arbitrarily small with large g, and also contributes to the contraction of phase space that causes the system*

to meet the conditions of the Annulus Principle and converge on an attracting invariant manifold.

3.2. **Monostability.** *Here we use the inter-spike interval function Ψ to study the stability of ING phase-locking, and prove that phase-locking to square pulses is monostable.*

The bistability of the FN oscillator discussed in 2.2.2 is related to its constraint to a plane: excitatory forcing pushes the oscillation phase forward when v is rising but retards the phase when v is falling. In our ING system, excitatory forcing can only cause trajectories to reach spikes earlier. This is possible because the voltage variable lives on a circle, and therefore can continue to move in the same direction throughout the ING period. The uniformity of the ING oscillator's response to excitatory pulses suggests that ING might not lend itself to bistability in the same way as the FN oscillator.

We first consider the case of the forced ING system modeled by the equations (3.1) with $c = 0$, as discussed in section 3.1.1. We may study the number of stably phase-locked states using the spike map $\mathbf{P}$ (from forcing phase at one spike to forcing phase at the next, as defined in section 3.1.1) and its action on $\bar{\Phi}_0 \in \mathbb{R}$: where $\mathbf{P}$ intersects the diagonal line $\mathbf{P}(\bar{\Phi}_0) = \bar{\Phi}_0 + T_I$, phase-locking occurs. Equivalently, we may study the inter-spike interval (ISI) function, defined as

$$\Psi(\Phi_0) = \mathbf{P}(\bar{\Phi}_0) - \bar{\Phi}_0. \tag{3.6}$$

Phases Φ_0 where Ψ crosses the line $\Psi(\Phi_0) = T_I$ are locking phases. By the basic theory of iterated maps (explored and explained more thoroughly in Appendix 6.6), only phases where the crossing is from top to bottom may be stable. In order to show that the ING oscillator may only have one stably phase-locked orbit in response to a particular forcing input, it is sufficient to show that Ψ can only cross T_I in the downward direction once, or equivalently that it can only cross T_I twice.

If we assume that τ is sufficiently small that spikes occur immediately as soon as $G > 0$, we can analytically describe $\Psi(\Phi_0)$ (and illustrate it; see Figure 6). During a pulse, G can only exceed zero if the previous spike took place sufficiently long ago. If the previous spike was too recent, the pulse arrives under slightly too much inhibition to produce a positive net current. When this occurs, the next spike time jumps ahead to the next time the net current is positive, which may be at the next pulse or to the time a spike would naturally occur unforced (after the natural period of oscillation).

Thus, for small τ, $\Psi(\Phi_0)$ a characteristic shape, represented in Figure 6, top. When Φ_0 is in the range marked by purple arrows, the next spike is evoked by the next pulse. In this range, the next spike time does not change with Φ_0, so the interspike interval shrinks steadily as Φ_0 increases and $\frac{d}{d\Phi_0}\Psi = -1$. At some initial forcing phase, the next pulse occurs slightly too early to evoke a spike, and here Ψ jumps up sharply. In the range marked by blue arrows, the next spike occurs after the natural oscillator period T_0, before the following pulse. In this range, the ISI is independent of the initial forcing phase Φ_0,

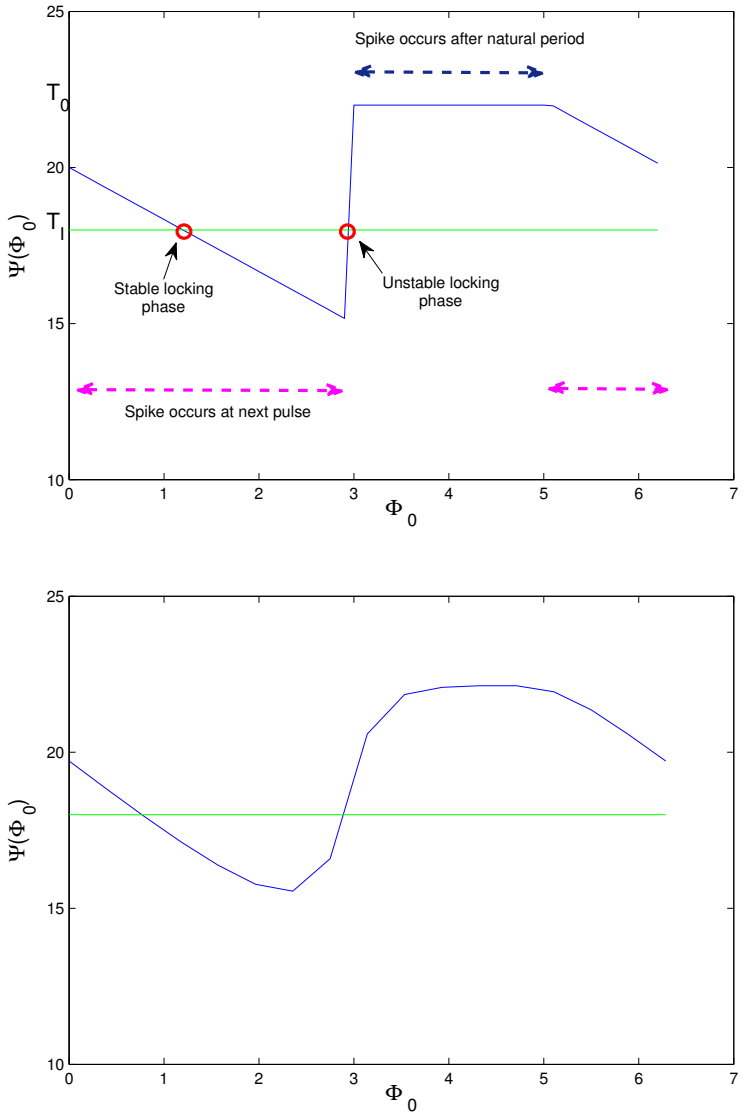

Figure 6: **Top:** The interspike interval function Ψ as a function of initial forcing phase Φ_0 at a spike., for the singular limit case $\tau \to 0$. At the phases where $\Psi(\Phi_0)$ crosses T_I (the green line), phase locking is possible. **Bottom:** Ψ vs. Φ_0 for $0 < \tau \ll 1$. Note the similarity to the singular limit case. We prove that under square-pulse forcing, the direction of Ψ' may only change twice (as it does above), and that therefore Ψ may cross T_I only two times. Only one of the two crossings may be from top to bottom, and this is the requirement for stability, so only one stable phase-locking phase may exist.

so $\frac{d}{d\Phi_0}\Psi = 0$. Beyond this range, the following pulse occurs before T_0 has passed since the last spike, so this pulse evokes the next spike and $\frac{d}{d\Phi_0}\Psi = -1$ again.

When Ψ takes this shape, it can cross the horizontal line $\Psi(\Phi_0) = T_I$ in the downwards direction no more than once in each forcing period. Only at this crossing point can stable phase-locking occur, so phase-locking (if it occurs at all) must be monostable.

Remark 3.2.1. *We make a much more thorough study of the limiting case of small τ in [[[COMPANION PAPER]]].*

When τ is not vanishingly small, the shape of $\Psi(\Phi_0)$ is a smoother approximation of this shape that still has only one peak and one trough (see Figure 6, bottom), so we still expect it to cross $\Psi(\Phi_0) = T_I$ in the downward direction only once.

However, we seek a more rigorous proof of monostability. It is difficult or impossible to write an explicit expression for Ψ, but solving a linear ODE allows us to write an expression for $\Psi'(\Phi)$. We do so in Appendix 6.6, and use it to study the number of stably locked states. We prove that in the case of square pulses, the ISI function on the circle can cross T_I from above only once, proving the monostability of $1:1$ phase-locking in response to square-wave forcing. We also extend this result from the $c = 0$ case to the case of sufficiently small $c > 0$.

Empirical observation of simulations suggests that phase locking to non-square periodic pulses is also generally monostable. A proof for non-square pulses would be more difficult, but might follow along similar lines.

4. PING: A Perturbation of ING

Pyramidal-Interneuronal Network Gamma ("PING") is the name given to gamma rhythms produced by a process requiring both excitatory and inhibitory neuronal populations. In the unforced PING model, a gamma rhythm is again paced by the synchronous firing of interneurons and the subsequent decay of inhibition; however, the first cells to emerge from inhibition are excitatory pyramidal cells. It is the firing of these cells that triggers the next inhibitory volley, rather than the gradual emergence of the I-cells from inhibition. Each cell may fire once each time the inhibition is sufficiently low ("strong PING"), or may fire only on some cycles, while other cells trigger inhibitory volleys on the other cycles ("weak PING").

PING rhythms may be forced by signals to the I-cell or E-cell populations, or by some combination. We focus on the case in which the E-cell population is forced periodically. (We discuss whether these methods may be applied to the general case of forcing to both populations below.) We point out a direct correspondence between models of PING and ING when the rise time of the inhibitory population is small. We then use this correspondence to prove that a periodically-forced PING model with a small inhibitory membrane

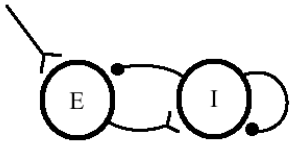

Figure 7: Schema of the PING circuit.

time constant possesses a broken attracting invariant torus. As discussed previously, this shows that forced PING with fast I-cells does not period-double or support shared stability between different types of phase-locking.

To create a simple model of forced PING, we add an additional cell population and an additional synaptic variable to the ING model in (3.1), and again switch from QIF neurons to theta neurons using equation (3.3) to change variables:

$$\begin{cases} \tau_i \dot{\theta^i} & = 1 - \cos(\theta^i) + (1 + \cos(\theta^i)) C G^i \\ \tau_e \dot{\theta^e} & = 1 - \cos(\theta^e) + (1 + \cos(\theta^e)) G^e \\ \dot{s^i} & = -s^i / \tau_{s^i} \\ \dot{s^e} & = -s^e / \tau_{s^e} \\ \dot{\Phi} & = 1 \end{cases} \tag{4.1}$$

with $G^e = b_e - g_{ie} s^i + \epsilon I(\Phi)$ and $G^i = b_i - g_{ii} s^i + g_{ei} s^e$. (We put i and e in superscript for variables that evolve with time and will therefore carry a t subscript.) The inhibitory synaptic activity variable $s^i \in [0, 1]$ resets to $\rho_i(s^i) = 1 + c_i(s^i - 1)$ for some $c_i \in [0, 1)$ in the right-hand limit when $\theta^i = \pi$; the excitatory synaptic activity variable $s^e \in [0, 1]$ resets to $\rho_e(s^e) = 1 + c_e(s^e - 1)$ for some $c_e \in [0, 1)$ in the right-hand limit when $\theta^e = \pi$. The cell phase variables $\theta^e, \theta^i \in [0, 2\pi)$ and the forcing phase $\Phi \in [0, T_I)$ are on circles. $I(\cdot)$ is a T_I-periodic input current to the E-cell; g_{ei}, g_{ie}, and g_{ii} are synaptic gating variables; τ_i and τ_e are the membrane time constants of the two populations; b_e and b_i are the baseline levels of tonic excitation to the two populations; and τ_{s^i} and τ_{s^e} are the decay time constants of inhibition and excitation, respectively.

We have also introduced a parameter C with no analogue in the ING model. This parameter allows us to scale up and down the I-population's synaptic currents together. When C is large, both the excitatory and inhibitory influences on the I-population are very strong, but their magnitudes relative to each other are not affected by C.

We study parameter regimes in which the model gives rise to rhythms by the following process:

- An E-cell volley occurs.

- Immediately afterwards, an I-cell volley follows.
- The I-cell population quickly rivers to an attracting trajectory.
- As inhibition decays, the forcing and lowered inhibition eventually trigger an E-cell volley, etc.

In order to restrict our scope to such models, we make the assumptions:

(1) There exists $K_{IE} < 0$ such that $G^i < K_{IE}$ between an I-spike and an E-spike; thus, once the I-cell has spiked, it cannot spike again until the next E-spike. This assumption can be fulfilled by choosing parameters such that $b_i < 0$ and such that inhibition always outweighs excitation after both have reset.

(2) After an E-spike, an I-spike occurs before the next E-spike. This assumption can be fulfilled by choosing g_{ei} large enough that after an E-spike, θ^i rises faster than θ^e.

(3) There exists a $K_{EI} > 0$ such that $G^i > K_{EI}$ for time $\frac{\pi\tau_i}{K_{EI}}$ after any E-spike; thus, an I-spike necessarily occurs within a certain bounded delay after an E-spike. The natural period of the I-population under constant drive CK_{EI} is $\frac{\pi\tau_i}{\sqrt{CK_{EI}}}$ **[izhikevichDNS]**; this is the time for θ^i to rise from $-\pi$ to π, and a more advanced initial phase or additional current can only shorten this rise time, so this quantity serves as an upper bound on E-spike-to-I-spike lag. This assumption may be met by a combination of sufficiently large g_{ei}, sufficiently small c_e (such that after a spike, $g_{ei}s^e$ is sufficiently large to overwhelm the other terms in G^i) and sufficiently large τ_e (such that $g_{ei}s^e$ stays sufficiently large until an I-spike occurs).

4.1. **Reduction to ING for Small θ^i Rise Time.** If we add one additional assumption to this list, we can create a direct correspondence between the PING and ING models:

(4) C is sufficiently large that the rise time T_{EI} the I-population phase between and E-spike and an I-spike is vanishingly small compared to τ_e, τ_{s^i}, τ_{s^e}, and T_I.

This assumption is justified by several observations. Levy et. al **[Levy2012]** observed in slice that the EPSPs evoked via E-I connections (between pyramidal cells and presumed fast-spiking interneurons, before adaptation) were twice as strong as the IPSPs evoked via I-E connections and three times as strong as the EPSPs evoked via E-E connection. Atallah and Scanziani observed in vivo that the delay time between E-volleys and I-volleys during PING is around 2ms, compared to a gamma period ranging from 12 to 45ms **[Atallah2009]**; in their models, this short lag time is created partially by strong E-to-I connections.

When the I-cell rise time T_{EI} separating the E-spikes and the subsequent I-spikes is vanishingly small on the time scale of the rest of the model, the PING process become indistinguishable from ING: it is as if the E-population is immediately inhibiting itself immediately with every spike. In this case, we know from section 3.1.3 that when c_i is sufficiently small

or g_{ie} is sufficiently large, the subsystem consisting of θ^e, s^i, and Φ asymptotically approaches an invariant torus with a jump discontinuity, and the flow on that manifold can be converted into a flow on an unbroken torus by identifying points across the jump.

Intuition suggests that this invariant torus should correspond with an invariant torus in all five dimensions, and furthermore that the torus and the resulting limitation to periodic and quasiperiodic behavior should persist when the scaling factor C of the I-population synapses is large but finite (and thus the I-cell rise time separating the E-volley and the I-volley is small but nonzero on the other time scales). In Appendix 6.7, we show that in appropriate parameter regimes and for sufficiently large C (i.e. sufficiently strong E-I and I-I synapses to the I cell), the map from the system state at one I-spike to the system state at the next depends only weakly and continuously on the two new variables, and therefore may be considered a small, continuous perturbation of the map $\mathbf{R}$ from the ING case. We extend the Annulus Principle used to prove the existence of an invariant torus for the ING system, first to show that a torus persists when the variable s^e is introduced as long as the decay and reset of s^e induces sufficient contraction, and then again to prove that a torus persists when θ^i is introduced as long as C is sufficiently large.

It is important to note that when such an invariant torus exists, the map from one I-spike time to the next asymptotically approaches a circle, so on the surface of the torus that map is one-dimensional. Thus, even for this high-dimensional system, *there is still a one-dimensional map from one state to the next* that is valid after a transient. It is not guaranteed that this map is well-defined as a map from the forcing phase at an I-spike to the forcing phase at the next; but if the invariant circle at $\theta^i = \pi$ is a graph over Φ (and hence any point on it can be uniquely identified by a single Φ coordinate), as seems to be the case in simulation, this map can indeed be expressed as a map from Φ at one I-spike to Φ at the next.

Remark 4.1.1. *We do not actually need and arbitrarily short θ^i rise time to draw these conclusions. If we make the assumptions that the rise time of θ^i after an E-spike is constant (an assumption made for analytical purposes by [***Malerba2013***] and others) and that $c_i = 0$ (saturating inhibitory synapses), then the dynamics depend only on θ^e, s^i, and Φ, and a similar proof to the one outlined in 3.1.1 may be used to demonstrate that the spike map is a homeomorphism and prove the existence of an attracting invariant torus.*

5. Discussion

5.1. **Major Results.** The ING network's relative simplicity and its fundamental differences from other studied oscillators make it interesting from a purely theoretical perspective: it exemplifies an oscillatory mechanism that is fundamentally different from other archetypical oscillators. This work investigates the dynamics of the simple gamma-rhythmic ING circuit under periodic forcing and contrasts them against those of relaxation oscillators. It identifies two key properties of the ING circuit:

- If synapses saturate sufficiently at each spike volley and/or parameters allow for sufficient rivering of voltage trajectories as inhibition decays, then no matter the forcing strength, the periodically forced ING circuit possesses an attracting invariant torus. As a result, it may achieve only periodic and quasiperiodic dynamics, to the exclusion of period-doubling, coexistence of 1:1 and 2:1 orbits, and any other behaviors impossible on the two-torus. We find that this property is shared by the PING oscillator if the rise time of the inhibitory population is small.
- In the restricted case of saturating synapses and square forcing pulses, the ING circuit can possess only one stable, phase-locked orbit at a time. Phase-locking is also monostable for any pulse shape when the membrane time constant is sufficiently small to make the ISI function take on a shape similar to its shape in the limit as the membrane time constant goes to zero (see Figure 6).

Both of these properties are not shared by the forced relaxation oscillator, which has regimes of period doubling and bistability. The differences can be traced back to the ING oscillator's rapidly-resetting, slowly-decaying feedback inhibition, and the unidirectional influence of decreasing inhibition and excitatory forcing made possible by the ING oscillator's circular (rather than linear) fast variable.

In our models, we have modeled fast-spiking interneurons with theta neurons. This simplification is not completely justified: fast-spiking neurons have been observed to show type-2 rather than type-1 excitability, i.e. they do not initiate spiking by a saddle-node bifurcation like the theta neuron but instead by a Hopf bifurcation. Consistent with this result is the observation that fast-spiking neurons resonate about their resting voltages at slow-gamma-like frequencies. Resonance may compromise the validity of our ING results. In particular, it may not always be the case that the spike map is monotonic: earlier *or* later spike timing may determine whether input pulses align or fail to align with periods of increased excitability, significantly advancing or delaying the next spike. However, preliminary results show that resonance at or near the spiking frequency does not lead to nonmonotonicity of the spike map. Furthermore, in our PING model, our results depend on the E-population being type-1 excitable but do not depend strongly on the excitability type of the I-population as long as they can respond quickly to strong excitatory input.

One major assumption in our models was that each population of cells fires synchronously or not at all. It has repeatedly been observed that during some episodes of PING (dubbed "sparse" or "weak" PING), only a fraction of the E-cells fire on each cycle [**Buhl1998**] [**Burchell1998**] [**Fisahn1998**]. However, our work does not rest heavily on the assumption of synchronous E-cells as long as the I-volley is triggered all at once, creating a sudden onset followed by a slow decay of inhibition. We believe that with a reasonable set of assumptions, sparse PING could be shown to obey the same dynamic restrictions as strong PING.

It has also been observed that some I-cells may fire on only a fraction of cycles, and that different amounts of inhibition may be recruited on each gamma cycle [**Atallah2009**]. The effects of variable inhibitory recruitment on phase-locking has been studied in [**Serenevy**].

Though the authors find that this effect makes phase-locking more robust, their results also show that a volley occurring at a later phase of the periodic drive may be followed by an earlier second volley due to less inhibitory recruitment, creating a non-monotonic spike map and qualitatively different behavior than the dynamics described here. We hypothesize that in some parameter regimes, this effect leads to chaos.

Our brief discussion of PING makes two additional major assumptions: the rise time of the inhibitory population following an E-spike must be small, and the forcing must be delivered only to pyramidal cells. The first assumption has strong basis in experimental findings: Atallah and Scanziani observe that this lag time is about 2ms in vivo. This may be due partially to low membrane time constants. Indeed, fast-spiking interneurons do have lower membrane time constants than most other cortical cells [**Pike2000**]. It also may be due to the strong E-to-I connectivity in these networks.

The second assumption is a caricature: there is reason to believe that fast-spiking interneurons involved in PING do receive input from other cortical areas, as well as evidence that forcing these interneurons can entrain a gamma rhythm [**Cardin2009**]. If we continue to assume that the E- and I-populations are each firing synchronously, we do not expect this complication to significantly impact our conclusions. If excitatory forcing is delivered to the I-population in addition to the E-population, inhibitory spike volleys may be initiated with or without excitatory participation; but in either case, these volleys are created by forcing that pushes them above decaying inhibition, and cause the inhibition to reset quickly, wiping out most history dependence. These dynamics are not significantly different than the dynamics when periodic forcing is delivered exclusively to pyramids.

5.2. **Relationship to Other Work.** To our knowledge, our work is the first to directly compare the network gamma mechanism to the relaxation oscillator, and the first to identify dynamic constraint inherent to the network gamma mechanism under forcing.

In an effort to answer questions about schizophrenia, Vierling-Claassen and Kopell [**dorea2009**] study periodically forced PING circuits using a model very similar to ours. They create a one-dimensional map similar to our spike map using the assumption that the various possible trajectories of both cells river together completely under inhibition and that synapses saturate at every spike. In this manuscript we show that in the case of ING, either one of those assumptions or the combination of partial rivering and partial saturation is sufficient to create an invariant 2-torus, allowing us to define a one-dimensional map describing the asymptotic dynamics. We also show that the same is true of PING if the inhibitory membrane time constant τ_i is small. Their work is aimed at explaining a specific observation in schizophrenic patients, and assume a specific profile of periodic forcing; ours is aimed at deepening our understanding of any instance of forced network gamma with analytical results valid for any periodic input.

The work of Serenevy and Kopell [**Serenevy**] is closely related to ours. It studies forced ING using maps from one spike volley to the next, and demonstrates that variable I-cell participation adds robustness to phase locking. Their work assumes complete rivering of

trajectories in order to define a one-dimensional map description of the interesting phase-locking dynamics that may result from variable participation. Our work applies the language of invariant manifolds and assumes a fixed population of participating cells, allowing us to generalize and relax the assumption of complete rivering as discussed above.

Various authors, including Ermentrout et al. [**Ermentrout2001**] and Kilpatrick and Ermentrout [**Kilpatrick2011**] have studied QIF neurons with adaptation in coupled and forced settings. The QIF-with-adaptation models they use are very similar to our model of ING: instead of decaying and resetting inhibition, they have a decaying and resetting adaptive current. Our work differs from theirs in at least two important ways. First, other work generally uses PRC's that assume weak coupling/forcing or pulsatile forcing; here, we prove the existence of invariant tori given no assumptions about the forcing signal except Lipschitz continuity, and prove monostability assuming forcing by square pulses of finite length. Second, we generalize our result to PING, an interaction of two cell populations. To our knowledge, we are the first to draw a connection between the QIF-with-adaptation model (our ING model) and the PING circuit.

Engelbrecht and Mirollo [**Engelbrecht2012**] also study the existence of attracting invariant manifolds for neuronal systems. In their study of the interaction between periodic forcing and noise in individual neurons, they find that even high-dimensional neuron models asymptote to two-dimensional surfaces (like our ING and PING models), allowing them to describe a forced Hodgkin-Huxley neuron with a one-dimensional spike map. They explain this effect as the persistence of an invariant torus from the unforced oscillatory state, but they do not further examine the factors that allow this torus to persist.

Burden et al. [**Burden2011**] study the existence of attracting invariant manifolds for hybrid dynamical systems like the ones we study here. They prove that if a resetting map in a hybrid system with a periodic orbit is of rank r, then the periodic orbit lies in a $r+1$-dimensional manifold that attracts all initial conditions in finite time. When $c = 0$ in our ING model, the resetting map is rank 1, and we prove that this implies the existence of a two-dimensional invariant manifold. In later unpublished work, they also discuss exponentially attracting manifolds in hyperbolic systems. However, all of the work done by Burden et al. assumes the existence of a periodic orbit, whereas our work proves the existence of invariant tori even if no periodic orbit exists.

Rajan et al. [**Rajan2010**] provide analytical results indicating that strong ongoing input to a chaotic neural network suppresses chaotic behavior. Though their results are for firing rate models of random networks and do not relate to rhythmic behavior, their results tell a story very similar to ours: a driven network displays a limited, non-chaotic repertoire of dynamics, and can therefore respond reliably and reproducibly to an input. Any network receiving ongoing temporally-varying input must strike a balance between its intrinsic dynamics and its response to the input. Rhythms may prove to play an important role in adjusting and maintaining this balance.

5.3. **Implications for Communication Through Coherence.** The properties of gamma rhythms under forcing are particularly interesting in the context of the Communication-Through-Coherence (CTC) hypothesis [**Womelsdorf2007b**]. Briefly, this hypothesis states that oscillations (and in particular gamma rhythms) in neuronal populations create periodic windows during which they are susceptible to input, alternating with windows of insensitivity to input. For two oscillating populations to effectively communicate, the output from one oscillation must be phase-aligned with the susceptible windows of the other.

For CTC to operate, it is necessary (though not sufficient) that a mechanism exist for reliably establishing a consistent phase relationship between the rhythms of the "sending" and "receiving" populations. Several studies have demonstrated that gamma rhythms in the brain cannot be relied upon to sustain a metronome-like periodicity [**Burns2011**] [**Xing2012**], so any phase alignment between gamma rhythms must actively maintained [**Nikolic2013**]. One straightforward method of creating and maintaining such a phase relationship is to allow the rhythmicity of the sending population's output to entrain the receiving population directly. But entrainment is not sufficient: the phase relationship between the two populations must be stable and predictable. As is demonstrated by the case of the FN system, an oscillator given excitatory forcing of moderate strength at a period close to its natural period may align differently with alternate forcing cycles due to period-doubling; or its alignment with the forcing may depend strongly on initial conditions due to bi-stability of phase-locked orbits. The properties of ING identified above guarantee that neither of these behaviors may interfere with the phase alignment of the entrained receiving population, facilitating CTC.

We have proven that phase-locking occurs with a specific, reliable phase relationship to the forcing; but we have not specified *what* phase relationship. This topic is explored in depth in [[[COMPANION PAPER]]], where it is shown that volleys in the gamma circuit generally follow input pulses with short delay. This result places gamma rhythms in a very specific position among the set of all possible oscillators, which may entrain to any phase relationship with periodic forcing. The specific phase relationship created by network gamma rhythms under forcing is optimal for CTC with these networks: when forcing pulses (which presumably also encode information) reach the receiving population, it has been nearly a full gamma period since the last spike volley, so inhibition is low and cells can readily fire in response. In [[[COMPANION PAPER]]], it is also shown that when two gamma circuits are mutually coupled and phase-locking occurs, a phase relationship is created that is optimal for unidirectional transmission of information from the more driven population to the less driven one.

The techniques used here all assume that $\Phi \in \mathbb{T}^1$, i.e., forcing is periodic. However, with almost exactly the same methods, we could study forcing by N periodic signals of different periods by considering $\vec{\Phi} \in \mathbb{T}^N = [0, T_{I,1}) \times ... \times [0, T_{I,N})$ (and setting $\dot{\vec{\Phi}}$ to a vector of ones). A return map could be defined for this system that took the state $(s, \vec{\Phi})$ at one spike to the state at the next; an attracting invariant torus for this map that could be written as a graph of s over $\vec{\Phi}$ would allow us to study the asymptotically stable dynamics of the system as the

dynamics of a highly constrained map on $\mathbb{T}^N$. This method could answer questions about when the system could phase-lock to one periodic signal without interference by others, as discussed and studied through simulation in [**Christoph2008**], and potentially reveal the importance of the network gamma mechanism in selective communication through phase locking.

5.4. **Broader Implications.** The ING/PING mechanism is interesting outside the context of gamma rhythms due to its resemblance to other rhythmic processes across the nervous system. Some bursting mechanisms may be described by a process of overcoming a threshold that decays slowly and resets quickly. For instance, the high-threshold bursting of thalamic relay neurons implicated in alpha rhythms is characterized by the slow activation of h-type cation channel while the cell rests at low voltage, followed by its rapid inactivation during a burst of spikes. As the h-current activates, it requires less excitation to evoke a burst. The ING circuit as defined here might serve as a first approximation of this process, with s replaced by the activation of the h-current and spiking events replaced by bursting events. To the extent that such a model accurately describes the generation of a rhythm, this rhythm may be expected to share the distinctive properties of ING under forcing.

Though the systems treated here are low-dimensional for analytical tractability, the ideas and techniques presented apply equally to higher dimensional systems, e.g. a gamma rhythm generated by Hodgkin-Huxley neurons or by populations that are not completely synchronous. In particular, if all of the variables in a system approach a fixed point that varies slowly with the decay of a single slow variable and persists for sufficient time, the rivering effect will create a strong contraction in phase space. As discussed briefly in Section 3.1.3, this effect may occur when fast variables describing the cell state converge during the slow decay of inhibition, or when synapses rise rapidly towards saturation during a spike. We show here that variational equations may be used to find conditions under which rivering induces sufficient contraction in state space to force the existence of an invariant manifold. If this rivering occurs under inhibition that strictly decays, spikes occurring later relative to the forcing signal remain under greater inhibition until the next spike, and are therefore followed by a later spike (as discussed in Section **??**). We expect that such a monotonic relationship combined with strong rivering will force higher dimensional systems onto an invariant torus as well.

In many neural processes, individual spikes or spike volleys form natural landmarks in the dynamics, so maps from one spiking event to the next are a convenient framework in which to study neural dynamics. The framework of invariant manifolds significantly extends the applicability of spike maps. A map from the time or forcing phase of one spiking event to the time or forcing phase at the next is only well-defined if the system's state at a spike can be completely specified by a single variable, so such a map can only be defined for a system that is effectively two-dimensional. However, even a high-dimensional system may become effectively two-dimensional due to contraction onto an invariant 2-torus. Similarly, the map from the state at one spike to the state at the next may be reduced to a second- or third-order spike map (a map from two or three variables at one spike to the same

variables at the next) if the system converges onto a three- or four-dimensional manifold, respectively.

Conversely, maps from one spike to the next may be used to prove the existence of attracting manifolds of the full system, as we have done here. The search for low-dimensional activity patterns and their causes in the brain is ultimately a search for low-dimensional attracting invariant manifolds in large state-spaces; the techniques we have presented here may prove valuable to that search.

6. Appendix

6.1. **Derivation of linearly-resetting synapses.** Here we derive our instantaneous synaptic resetting rule $\rho(s) = 1+c(s-1)$ from a dynamic model of synaptic rise. Using a standard model of synaptic rise we write:

$$\begin{cases} \tau\dot{\theta} = & 1-\cos(\theta)+(1+\cos(\theta))G \\ \dot{s} = & -\frac{1}{\tau_s}s + \frac{1}{\tau_r}\frac{h}{\gamma}\chi_{[\pi-\gamma,\pi]}(\theta)(1-s) \\ \dot{\Phi} = & 1 \end{cases} \tag{6.1}$$

with

$$G = b - gs + \epsilon I(\Phi).$$

.

where $\chi_{[\pi-\gamma,\pi]}$ is the characteristic function that is one on $[\pi-\gamma,\pi]$ and zero elsewhere. As θ passes through an interval of width γ just before $\theta=\pi$, inhibitory transmitters are present in the synapse at concentration $\frac{h}{\gamma}$, causing s to increase towards 1. The rest of the model is the same as (3.1). We set $\epsilon = 1$ because this result does not depend on weak forcing.

We approximate the effect of a spike on s by assuming that $\gamma \ll 2\pi$, $\frac{\gamma\tau_r}{h} \ll \tau_s$, and $\gamma\tau \ll 1$. During the interval of synaptic rise, our approximations give us $\theta \approx \pi$ and

$$\begin{cases} \dot{\theta} \approx \frac{1}{\tau}\left(1-\cos(\pi)+(1+\cos(\pi))G\right) & = \frac{2}{\tau} \\ \dot{s} = -\frac{1}{\tau_s}s + \frac{1}{\tau_r}\frac{h}{\gamma}(1-s) & \approx \frac{h}{\gamma\tau_r}(1-s) \\ \dot{\Phi} & = 1 \end{cases} \tag{6.2}$$

We let t^i denote the time that $\theta_{t^i} = -\pi-\gamma$, and we let t_f denote the time that $\theta_{t_f} = -\pi$. Between t^i and t_f, the term $\frac{1}{\tau_r}\frac{h}{\gamma}\chi_{[\pi-\gamma,\pi]}(\theta)(1-s)$ in (6.1) is large. We write

$$t_f - t^i = \int_{t^i}^{t_f} dt$$

and changing variables from t to θ, we can write

$$t_f - t^i = \int_{\pi-\gamma}^{\pi} \frac{1}{\frac{d\theta}{dt}} d\theta.$$

Using the approximation for $\dot{\theta}$ from (6.2), we have

$$\begin{aligned} t_f - t^i \approx & \int_{\pi-\gamma}^{\pi} \frac{1}{\frac{2}{\tau}} d\theta \\ \approx & \frac{\gamma\tau}{2} \ll 1 \end{aligned} \tag{6.3}$$

Between t_f and t^i, we have the linear differential equation:

$$\dot{s} \approx \frac{h}{\gamma\tau_r}(1-s)$$

which is solved by

$$s_t \approx 1 + (s_{t^i} - 1)e^{-\frac{h}{\gamma\tau_r}(t-t^i)}$$

So we can solve for for s_{t_f} in terms of s_{t^i}:

$$s_{t_f} \approx 1 + (s_{t^i} - 1)e^{-\frac{h}{\gamma\tau_r}(t_f-t^i)} \tag{6.4}$$

Substituting from (6.3),

$$\begin{aligned} \approx & 1 + (s_{t^i} - 1)e^{-\frac{h}{\gamma\tau_r}\frac{\gamma\tau}{2}} \\ = & 1 + (s_{t^i} - 1)e^{-\frac{h\tau}{2\tau_r}} \\ = & 1 + c(s_{t^i} - 1) \end{aligned}$$

where $c = e^{-\frac{h\tau}{2\tau_r}}$ is in the interval $[0, 1]$. Thus, when a spike occurs at time t, these fast dynamics induce the "reset" map ρ from s just before the spike to s just afterwards:

$$s_{t_f} = \rho(s_{t-}) = 1 + c(s_{t^i} - 1) \tag{6.5}$$

at each spike ($\theta = \pi$), where $c = e^{-\frac{h\tau}{2\tau_r}}$. Since the duration of this reset is very short (see (6.3)), we replace s_{t^i} with s_{t-} and s_{t_f} with s_t, where $t-$ and t denote the left- and right-hand limits of a spike time t. We have now reproduced the reset rule described in (3.2).

6.2. **Invariant Torus in the ING Model, General Case.** *Here we find a sufficient condition for the existence of an attracting invariant 2-dimensional torus in the phase space of the ING model* (3.1) *in terms of integrals over the set of possible inter-spike trajectories.*

Instantaneously resetting synapses helpfully lower the dimensionality of the system; however, because of them we cannot directly apply results from the study of continuous ODEs. Instead, we study a transverse section of the system at $\theta = \pi$ and the associated Poincare

mapping $\mathbf{R}$ from the section to itself. Since we are unable to solve the ODEs, we cannot write an explicit expression for this map. We can, however, solve the associated variational equations. These are defined as the linearization of the ODE about a trajectory, and describe the flow of small variations in state. We use these solutions to estimate the rates of contraction of trajectories. If this contraction is sufficient, a contraction-mapping result guarantees the existence of an attracting manifold.

6.2.1. *Proof Outline.*

(1) We solve the variational equations of the ODE in order to describe the transformation in variations of state from one spike time to the next.

(2) Combining our solution with a mapping describing the transformation of a variation as it reaches the instantaneous reset, we write an explicit expression for the Jacobian $D\mathbf{R}$ of $\mathbf{R}$.

(3) We change to an appropriate set of coordinates and restrict our domain to an appropriate annulus.

(4) We apply the "Annulus Principle," taken from **[Kolesov2003]** and **[shilnikov98]**, to establish conditions under which the return map induces a sufficiently strong contraction in an appropriate direction on the annulus that it must have an attracting invariant torus.

(5) We show by numerical methods that these conditions are met robustly for a range of parameter values.

(6) We show that for a fixed parameter set not including c, the conditions established above are met for sufficiently small $c > 0$.

(7) We show that for a fixed parameter set not including g, the conditions established above are met for sufficiently large g.

6.2.2. *Theorem Used.* First we present the major theorem we will utilize in our proof.

Theorem 6.2.1 (Annulus Principle)**.** *Let us consider a diffeomorphism T:*

$$r_2 = f(r_1, x_1) \tag{6.6}$$

$$x_2 = x_1 + F_0(r_1, x_1) = F(r_1, x_1) \tag{6.7}$$

where $r_1, r_2 \in \mathbb{R}^n, x_1, x_2 \in \mathbb{T}^m, n \geq 1, m \geq 1$, and the smooth functions f and F are 2π-periodic with respect to x_1.

Let $\mathbb{K}$ be an annulus defined by $\mathbb{K} = \{(r, x)$ s.t. $r \in [\delta_1, \delta_2], x \in \mathbb{T}^m\}$.

Let $\|f\|^o$ denote $\sup_{(r,x)\in\mathbb{K}} \|f(r, x)\|$, where $\|\cdot\|$ is the standard Euclidean norm.

If the following conditions are met:

(1) *T maps $\mathbb{K}$ into itself.*

(2) *$\|\frac{\partial f}{\partial r}\|_o < 1$ for any fixed x_1.*

(3) *F is a diffeomorphism for any fixed r_1.*

(4) $\|\left(\frac{\partial F}{\partial x}\right)^{-1}\|^o \cdot \|\frac{\partial f}{\partial r}\|_o + 2\sqrt{\|\left(\frac{\partial F}{\partial x}\right)^{-1}\|^o \cdot \|\frac{\partial F}{\partial r}\|^o \cdot \|\frac{\partial f}{\partial x}\left(\frac{\partial F}{\partial x}\right)^{-1}\|^o} < 1.$

Then T posseses an m-dimensional invariant torus in $\mathbb{K}$ which contains all ω-limit points of all positive semi-trajectories in $\mathbb{K}$. The torus is defined by the graph $s = h^*(x)$ where h^* is a C^1-smooth 2π-periodic function.

6.2.3. *Definitions and Notation.* Given the model (3.1) with phase coordinate defined in (3.4), we set $\epsilon = 1$ as in the previous appendix:

$$\begin{cases} \tau\dot{\theta} = & 1 - \cos(\theta) + (1 + \cos(\theta))G \\ \dot{s} = & -\frac{s}{\tau_s} \\ \dot{\Phi} = & 1 \end{cases} \tag{6.8}$$

where

$$G = b - gs + I(\Phi).$$

We study the trajectory from one spike to the next. We henceforth call the initial spike time 0 and the next spike time t_s. By default, states are specified at the right-hand limits (r.h.l.) of these times; we use the additional subscript $(-)$ to denote values at the left-hand limits so that we can distinguish values of s before and after the instantaneous reset. As we have previously, we use s_t to refer to the value of s at time t.

We define

$$\begin{gathered} \mathbf{R} : \mathbb{T}^1 \times [0,1] \times \mathbb{T}^1 \to \mathbb{T}^1 \times [0,1] \times \mathbb{T}^1 \\ \begin{pmatrix} s_0 \\ \Phi_0 \end{pmatrix} \to \begin{pmatrix} s_{t_s} \\ \Phi_{t_s} \end{pmatrix} \end{gathered} \tag{6.9}$$

to be the mapping from the system state at the right-hand limit of a spike at time 0 to the same values at the right-hand limit of the next spike, at time t_s. $\mathbf{R}$ exists provided that spiking continues indefinitely, which is the case as long as $b > 0$. This mapping is well-defined because forward trajectories are unique in this system. The set $\theta = \pi$ is transverse to the flow: at $\theta = \pi$, $\dot{\theta} = \frac{2}{\tau} > 0$.

6.2.4. *Step 1: Tracking variations.* Here we solve the variational equations associated with the ODE.

We let $\zeta_t = \begin{pmatrix} \Delta\theta_t \\ \Delta s_t \\ \Delta\Phi_t \end{pmatrix}$ denote a variation from a base trajectory $\begin{pmatrix} \theta_t^* \\ s_t^* \\ \Phi_t^* \end{pmatrix}$ at time t. It is helpful to consider ζ_t the difference between this trajectory and a "varied" trajectory $\begin{pmatrix} \theta_t^* + \Delta\theta_t \\ s_t^* + \Delta s_t \\ \Phi_t^* + \Delta\Phi_t \end{pmatrix}$. ζ_t evolves according to the ODEs in (3.1) linearized about the trajectory $\begin{pmatrix} \theta_t^* \\ s_t^* \\ \Phi_t^* \end{pmatrix}$:

$$\begin{cases} \tau \frac{d}{dt}\Delta\theta_t = & (1 - G_t^*)\sin(\theta_t^*)\Delta\theta_t - g(1+\cos(\theta_t^*))\Delta s_t + (1+\cos(\theta_t^*))I'(\Phi_t^*)\Delta\Phi_t \\ \frac{d}{dt}\Delta s_t = & -\frac{1}{\tau_s}\Delta s_t \\ \frac{d}{dt}\Delta\Phi_t = & 0 \end{cases} \tag{6.10}$$

where

$$G_t^* = b - g s_t^* + \epsilon I(\Phi_t^*).$$

As previously mentioned, we set $\epsilon = 1$ because our results will not depend on weak forcing.

Two of the equations in system (6.10) are easily solved in terms of initial conditions at time 0:

$$\Delta\Phi_t = \Delta\Phi_0 \tag{6.11}$$

$$\Delta s_t = e^{-\frac{t}{\tau_s}}\Delta s_0 \tag{6.12}$$

Substituting into the first equation in (6.10),

$$\tau\frac{d}{dt}\Delta\theta_t = (1 - G_t^*)\sin(\theta_t^*)\Delta\theta_t - g(1+\cos(\theta_t^*))e^{-\frac{t}{\tau_s}}\Delta s_0 + (1+\cos(\theta_t^*))I'(\Phi_t^*)\Delta\Phi_0 \tag{6.13}$$

We can solve this equation using an integrating factor. We set

$$\begin{cases} Q_t = & \frac{1}{\tau}(1 - G_t^*)\sin(\theta_t^*) \\ R_t = & \frac{1}{\tau}(1+\cos(\theta_t^*))e^{-\frac{t}{\tau_s}} \\ S_t = & \frac{1}{\tau}(1+\cos(\theta_t^*))I'(\Phi_t^*) \end{cases} \tag{6.14}$$

and substitute into (6.13) to write

$$\begin{aligned}
\frac{d}{dt}\Delta\theta_t =& Q_t\Delta\theta_t - gR_t\Delta s_0 + S_t\Delta\Phi_0 \\
\frac{d}{dt}\Delta\theta_t - Q_t\Delta\theta_t =& -gR_t\Delta s_0 + S_t\Delta\Phi_0 \\
\left(\frac{d}{dt}\Delta\theta_t\right)e^{-\int_0^t Q_r dr} - Q_t\Delta\theta_t e^{-\int_0^t Q_r dr} =& \left(-gR_t\Delta s_0 + S_t\Delta\Phi_0\right)e^{-\int_0^t Q_r dr} \\
\frac{d}{dt}\left(\Delta\theta_t e^{-\int_0^t Q_r dr}\right) =& \left(-gR_t\Delta s_0 + S_t\Delta\Phi_0\right)e^{-\int_0^t Q_r dr}
\end{aligned}$$

Integrating both sides from 0 to t_s,

$$\begin{aligned}
\Delta\theta_{t_s}e^{-\int_0^{t_s} Q_r dr} - \Delta\theta_0 =& \int_0^{t_s}\left(-gR_t\Delta s_0 + S_t\Delta\Phi_0\right)e^{-\int_0^t Q_r dr}dt \\
\Delta\theta_{t_s}e^{-\int_0^{t_s} Q_r dr} =& \Delta\theta_0 + \int_0^{t_s}\left(-gR_t\Delta s_0 + S_t\Delta\Phi_0\right)e^{-\int_0^t Q_r dr}dt \\
\Delta\theta_{t_s} =& \Delta\theta_0 e^{\int_0^{t_s} Q_r dr} + \int_0^{t_s}\left(-gR_t\Delta s_0 + S_t\Delta\Phi_0\right)e^{\int_t^{t_s} Q_r dr}dt \qquad (6.15)
\end{aligned}$$

We write (6.11), (6.12), and (6.15) as a single matrix solution:

$$\zeta_{t_{s-}} = \begin{pmatrix}\Delta\theta_{t_{s-}}\\ \Delta s_{t_{s-}}\\ \Delta\Phi_{t_{s-}}\end{pmatrix} = \mathbf{B}\begin{pmatrix}\Delta\theta_0\\ \Delta s_0\\ \Delta\Phi_0\end{pmatrix} = \mathbf{B}\zeta_0 \qquad (6.16)$$

where

$$\mathbf{B} = \begin{pmatrix} e^{\int_0^{t_s} Q_t dt} & -g\int_0^{t_s} R_t e^{\int_t^{t_s} Q_r dr}dt & \int_0^{t_s} S_t e^{\int_t^{t_s} Q_r dr}dt \\ 0 & e^{-\frac{t_s}{\tau_s}} & 0 \\ 0 & 0 & 1 \end{pmatrix}$$

To condense notation, we define

$$\begin{cases} \kappa := & e^{\int_0^{t_s} Q_t dt} \\ \Sigma := & \frac{g\tau}{2}\int_0^{t_s} R_t e^{\int_t^{t_s} Q_r dr}dt \\ \Omega := & \int_0^{t_s} S_t e^{\int_t^{t_s} Q_r dr}dt \end{cases} \qquad (6.17)$$

such that we can write the matrix solution in the simple form

$$\mathbf{B} = \begin{pmatrix} \kappa & -\frac{2}{\tau}\Sigma & \Omega \\ 0 & e^{-\frac{t_s}{\tau_s}} & 0 \\ 0 & 0 & 1 \end{pmatrix}. \qquad (6.18)$$

6.3. **Step 2: Tracking variations across discontinuities.** Here we use saltation matrices and our solution to the variational equations to derive an expression for $D\mathbf{R}$.

Variations can be followed across discontinuities using saltation matrices [**Aizerman**] [**Dieci2011**]. At a spike, we use a modification of standard saltation matrices to follow the variation ζ_t across the discontinuous resetting map. Our formula for saltation matrices is different from the standard formula: standard saltation matrices let us see what a variation looks like after both the base trajectory and the varied trajectory have crossed a vector field discontinuity; but we want to know what the variation looks like if we let both the base trajectory and the varied trajectory flow only up to the "resetting plane," $\theta = \pi$. We stop here because we need to apply the resetting map to both trajectories when they reach the resetting plane.

Remark 6.3.1 (Derivation of Modified Saltation Matrices)**.** *Consider a system in which* $\dot{\mathbf{x}} = \mathbf{f}(\mathbf{x})$ *(where states are written as column vectors). Let* $\mathbf{x}$ *be a base trajectory and* ζ_t *a variation just before* $\mathbf{x}_t$ *reaches a target plane* ν*, transverse to the flow. Let* η *be a row vector normal to* ν *in the direction of the flow. At the time that* $\mathbf{x}_t$ *reaches* ν*, the varied trajectory* $\mathbf{x}_t + \zeta_t$ *is close to* ν*, but displaced from it by* $\eta\zeta_t$*. If we allow the varied trajectory to flow forward or backward to* ν*, it approaches* ν *at rate* $\eta\mathbf{f}(\mathbf{x}_t)$*, so it reaches* ν *in time* $\Delta t = -\frac{\eta\zeta_t}{\eta\mathbf{f}(\mathbf{x}_t)}$*. So it meets* ν *at the point*

$$\begin{aligned}\mathbf{x}_t + \zeta_t^\nu =& \mathbf{x}_t + \zeta_t - \mathbf{f}(\mathbf{x}_t)\Delta t \\ =& \mathbf{x}_t + \zeta_t - \mathbf{f}(\mathbf{x}_t)\frac{\eta\zeta_t}{\eta\mathbf{f}(\mathbf{x}_t)}.\end{aligned}$$

Thus, we find that

$$\begin{aligned}\zeta_t^\nu =& \zeta_t - \mathbf{f}(\mathbf{x}_t)\frac{\eta\zeta_t}{\eta\mathbf{f}(\mathbf{x}_t)} \\ =& \left(\mathbf{I} - \frac{\mathbf{f}(\mathbf{x}_t)\eta}{\eta\mathbf{f}(\mathbf{x}_t)}\right)\zeta_t = \mathbf{M}_t\zeta_t\end{aligned}$$

where

$$\mathbf{M}_t := \mathbf{I} - \frac{\mathbf{f}(\mathbf{x}_t)\eta}{\eta\mathbf{f}(\mathbf{x}_t)} \tag{6.19}$$

This derivation is illustrated and discussed further in Figure 8.

We shall adopt the convention of using $\hat{\zeta}$ to refer to 2-dimensional vectors representing variations in s and Φ at the plane $\theta = \pi$, and using $\check{\zeta}$ to refer to 3-dimensional vectors representing variations in θ and s at any plane $\Phi = \Phi^*$. (Though $\check{\zeta}$ lives in a plane, we write it in three dimensions with last element zero for ease of notation.)

At the right hand limit of spike time 0, we write $\hat{\zeta}_0 = \begin{pmatrix}\Delta\hat{s}_0 \\ \Delta\hat{\Phi}_0\end{pmatrix}$. We allow the varied trajectory to flow forward to the target plane $\Phi = \Phi_0^*$. We first embed $\hat{\zeta}_0$ in 3-space with

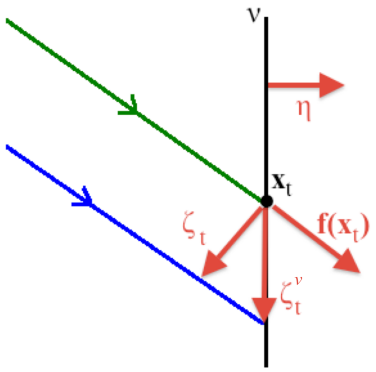

Figure 8: The difference between a base trajectory and a varied trajectory can be measured either when they reach the same time point or when they reach a plane ν that they both cross transversely. To transform one measurement to the other, we use a modification of the saltation matrix. Base trajectory is green; varied trajectory is blue. ζ_t is the distance between trajectories when the base trajectory reaches the plane (at time t, at the point $\mathbf{x}_t$); at this time, the varied trajectory has not yet reached ν. ζ_t^ν is the distance between trajectories at the points where the two trajectories reach ν. An ordinary saltation matrix would go on to determine the difference between the two trajectories at the same time once both have crossed the plane, but since our trajectories reset discontinuously immediately after reaching the plane, it is more useful to stop here. η is a unit vector normal to ν, and $\mathbf{f}(\mathbf{x}_t)$ is the derivative of the base trajectory at ν.

the matrix $\begin{pmatrix} 1 & 0 \\ 0 & 1 \\ 0 & 0 \end{pmatrix}$. Then, applying (6.19), we calculate the 3-D saltation matrix from the plane $\theta = -\pi$ to the plane $\Phi = \Phi_0^*$:

$$\begin{aligned}\mathbf{M}_0 =& \mathbf{I} - \frac{\begin{pmatrix} \dot\theta_0 \\ \dot s_0 \\ \dot\Phi_0 \end{pmatrix} \begin{pmatrix} 0 & 0 & 1 \end{pmatrix}}{\begin{pmatrix} 0 & 0 & 1 \end{pmatrix} \begin{pmatrix} \dot\theta_0 \\ \dot s_0 \\ \dot\Phi_0 \end{pmatrix}} = \mathbf{I} - \frac{\begin{pmatrix} \frac{2}{\tau} \\ -\frac{s_0}{\tau_s} \\ 1 \end{pmatrix} \begin{pmatrix} 0 & 0 & 1 \end{pmatrix}}{\begin{pmatrix} 0 & 0 & 1 \end{pmatrix} \begin{pmatrix} \frac{2}{\tau} \\ -\frac{s_0}{\tau_s} \\ 1 \end{pmatrix}} \\ =& \mathbf{I} - \begin{pmatrix} 0 & 0 & \frac{2}{\tau} \\ 0 & 0 & -\frac{s_0}{\tau_s} \\ 0 & 0 & 1 \end{pmatrix} = \begin{pmatrix} 1 & 0 & -\frac{2}{\tau} \\ 0 & 1 & \frac{s_0}{\tau_s} \\ 0 & 0 & 0 \end{pmatrix}\end{aligned} \tag{6.20}$$

Thus, we have

$$\check{\zeta}_0 = \begin{pmatrix} \Delta\check{\theta}_0 \\ \Delta\check{s}_0 \\ 0 \end{pmatrix} = \mathbf{M}_0 \begin{pmatrix} 1 & 0 \\ 0 & 1 \\ 0 & 0 \end{pmatrix} \hat{\zeta}_0 = \tilde{\mathbf{M}}_0 \hat{\zeta}_0$$

where

$$\tilde{\mathbf{M}}_0 = \begin{pmatrix} 0 & -\frac{2}{\tau} \\ 1 & \frac{s_0}{\tau_s} \\ 0 & 0 \end{pmatrix}. \tag{6.21}$$

Then the variation flows forward to t_{s-} (the left-hand limit of spike time t_s) and is transformed by $\mathbf{B}$, the solution to the linear variational equation:

$$\check{\zeta}_{t_{s-}} = \begin{pmatrix} \Delta\check{\theta}_{t_{s-}} \\ \Delta\check{s}_{t_{s-}} \\ 0 \end{pmatrix} = \mathbf{B}\check{\zeta}_0.$$

Next, the varied trajectory is allowed to join the base trajectory on the resetting plane $\theta = \theta^*_{t_s} = \pi$, and then embedded in 2-dimensional (s, Φ) space by the matrix $\begin{pmatrix} 0 & 1 & 0 \\ 0 & 0 & 1 \end{pmatrix}$. Using $\theta = \pi$ as the target plane, we calculate the saltation matrix:

$$\begin{aligned} \mathbf{M}_{t_{s-}} =& \mathbf{I} - \frac{\begin{pmatrix} \dot{\theta}_{t_s} \\ \dot{s}_{t_{s-}} \\ \dot{\Phi}_{t_s} \end{pmatrix} \begin{pmatrix} 1 & 0 & 0 \end{pmatrix}}{\begin{pmatrix} 1 & 0 & 0 \end{pmatrix} \begin{pmatrix} \dot{\theta}_{t_s} \\ -\frac{s_{t_{s-}}}{\tau_s} \\ \dot{\Phi}_{t_s} \end{pmatrix}} = \mathbf{I} - \frac{\begin{pmatrix} \frac{2}{\tau} \\ -\frac{s_{t_{s-}}}{\tau_s} \\ 1 \end{pmatrix} \begin{pmatrix} 1 & 0 & 0 \end{pmatrix}}{\begin{pmatrix} 1 & 0 & 0 \end{pmatrix} \begin{pmatrix} \frac{2}{\tau} \\ -\frac{s_{t_{s-}}}{\tau_s} \\ 1 \end{pmatrix}} \\ =& \mathbf{I} - \begin{pmatrix} 1 & 0 & 0 \\ -\frac{s_{t_{s-}}\tau}{2\tau_s} & 0 & 0 \\ \frac{\tau}{2} & 0 & 0 \end{pmatrix} = \begin{pmatrix} 0 & 0 & 0 \\ \frac{s_{t_{s-}}\tau}{2\tau_s} & 1 & 0 \\ -\frac{\tau}{2} & 0 & 1 \end{pmatrix} \end{aligned} \tag{6.22}$$

$$\hat{\zeta}_{t_{s-}} = \begin{pmatrix} 0 \\ \Delta\hat{s}_{t_{s-}} \\ \Delta\hat{\Phi}_{t_{s-}} \end{pmatrix} = \begin{pmatrix} 0 & 1 & 0 \\ 0 & 0 & 1 \end{pmatrix} \mathbf{M}_{t_{s-}} \check{\zeta}_{t_{s-}} = \tilde{\mathbf{M}}_{t_{s-}}$$

where

$$\tilde{\mathbf{M}}_{t_{s-}} = \begin{pmatrix} \frac{s_{t_{s-}}\tau}{2\tau_s} & 1 & 0 \\ -\frac{\tau}{2} & 0 & 1 \end{pmatrix} \tag{6.23}$$

Finally, the inhibition on both trajectories jumps up according to the map ρ as defined in (6.5), and $\hat{\zeta}_{t_{s-}}$ in (s, Φ) space is transformed by

$$D\rho = \begin{pmatrix} c & 0 \\ 0 & 1 \end{pmatrix} \tag{6.24}$$

to become $\hat{\zeta}_{t_s}$. All together, we have

$$\begin{aligned} \hat{\zeta}_{t_s} = D\rho\hat{\zeta}_{t_{s-}} =& D\rho\tilde{\mathbf{M}}_{t_{s-}}\check{\zeta}_{t_{s-}} = D\rho\tilde{\mathbf{M}}_{t_{s-}}\mathbf{B}\check{\zeta}_0 \\ =& D\rho\tilde{\mathbf{M}}_{t_{s-}}\mathbf{B}\tilde{\mathbf{M}}_0\hat{\zeta}_0 \\ =& D\mathbf{R}\hat{\zeta}_0 \end{aligned} \tag{6.25}$$

See Figure 6.4 for illustration.

Remark 6.3.2. *The operator* $\mathbf{B}$ *can be applied to any variation in 3-space. Why, then, use saltation matrices before and after applying* $\mathbf{B}$*? We do so because the hybrid structure of the system demands that return maps be computed from one spike to the next (i.e. within the plane* $\theta = \pi$*), be we want to connect the properties of this map to the rivering of* θ*-trajectories, which most accessible to measurement by comparing trajectories with the same* Φ*-coordinate. The relative behavior of trajectories at different* Φ *coordinates is complicated by the fact that they are receiving different inputs* $I(\Phi)$*; but the saltation matrix* $\tilde{\mathbf{M}}_0$ *neatly eliminates the term* Ω*, which is the only term in* $\mathbf{B}$ *that depends explicitly on* $I(\cdot)$*.*

Substituting into (6.25),

$$\begin{aligned} D\tilde{\mathbf{R}} =& D\rho\mathbf{M}_{t_{s-}}\mathbf{B}\tilde{\mathbf{M}}_0 \\ =& \begin{pmatrix} c & 0 \\ 0 & 1 \end{pmatrix} \begin{pmatrix} \frac{s_{t_{s-}}\tau}{2\tau_s} & 1 & 0 \\ -\frac{\tau}{2} & 0 & 1 \end{pmatrix} \begin{pmatrix} \kappa & -\frac{2}{\tau}\Sigma & \Omega \\ 0 & e^{-\frac{t_s}{\tau_s}} & 0 \\ 0 & 0 & 1 \end{pmatrix} \begin{pmatrix} 0 & -\frac{2}{\tau} \\ 1 & \frac{s_0}{\tau_s} \\ 0 & 0 \end{pmatrix} \\ =& \begin{pmatrix} c\tau\frac{s_{t_{s-}}}{2\tau_s} & c & 0 \\ -\frac{\tau}{2} & 0 & 1 \end{pmatrix} \begin{pmatrix} -\frac{2}{\tau}\Sigma & -\frac{2}{\tau}\kappa - \frac{2}{\tau}\Sigma\frac{s_0}{\tau_s} \\ e^{-\frac{t_s}{\tau_s}} & \frac{s_0}{\tau_s}e^{-\frac{t_s}{\tau_s}} \\ 0 & 0 \end{pmatrix} \qquad (6.26) \\ =& \begin{pmatrix} -\Sigma c\frac{s_{t_{s-}}}{\tau_s} + ce^{-\frac{t_s}{\tau_s}} & c\frac{s_{t_{s-}}}{\tau_s}(-\kappa - \Sigma\frac{s_0}{\tau_s}) + c\frac{s_0}{\tau_s}e^{-\frac{t_s}{\tau_s}} \\ \Sigma & \kappa + \Sigma\frac{s_0}{\tau_s} \end{pmatrix} \qquad (6.27) \end{aligned}$$

Substituting $s_{t_{s-}} = s_0 e^{-\frac{t_s}{\tau_s}}$,

$$= \begin{pmatrix} ce^{-\frac{t_s}{\tau_s}}(1 - \Sigma\frac{s_0}{\tau_s}) & ce^{-\frac{t_s}{\tau_s}}\frac{s_0}{\tau_s}(1 - \kappa - \Sigma\frac{s_0}{\tau_s}) \\ \Sigma & \kappa + \Sigma\frac{s_0}{\tau_s} \end{pmatrix} \tag{6.28}$$

We recall the assumption that $I(\cdot)$ was differentiable. We find now that since the term Ω no longer features directly in the expression for $D\tilde{\mathbf{R}}$ (see Remark 6.3.2), the terms in $D\tilde{\mathbf{R}}$ no longer depend on $I'(\cdot)$, so all terms in $D\tilde{\mathbf{R}}$ are continuous with respect to initial conditions regardless of whether $I(\cdot)$ is continuously differentiable.

6.4. **Step 3: Change of variables.** Here we change to coordinates in which the expression for our return map reveals the contraction induced by rivering under inhibition.

Using the terms in $D\mathbf{R}$ from (6.28), we could apply the Annulus Principle (Theorem 6.2.1) to the map $\mathbf{R}$ to determine when an attracting invariant torus must exist *as a graph of s over Φ*. The conditions for the existence of an attracting invariant torus would depend on the smallness of the first row of $D\mathbf{R}$, and would therefore follow from small c and/or small maximum $e^{-\frac{t_s}{\tau_s}}$. However, they would not make clear the role of κ, the measure of rivering of population phase under inhibition, in the formation of an invariant torus. This is because these conditions are conditions that ensure sufficient contraction between states with the same value of Φ; but rivering under inhibition causes contraction in a different direction, and therefore gives rise to a torus that is a graph of s over a different independent variable. Due to contraction by rivering, we expect that any points following the same (s_t, Φ_t) trajectory will reach approximately the same θ state when they spike next, so we let ϕ denote a quantity that is invariant over an (s_t, Φ_t) trajectory and use it as a new coordinate instead of Φ.

After initial time 0, we have $s_t = s_0 e^{-\frac{t}{\tau_s}}$ and $\Phi_t = \Phi_0 + t$. We consider the quantity $\phi = \Phi_t + \tau_s \ln(s_t) \in \mathbb{T}^1$. Along an (s, Φ) trajectory we have

$$\begin{aligned}\dot{\phi} = \frac{d}{dt}\left(\Phi_t + \tau_s \ln(s_t)\right) =& \frac{d}{dt}\left(\Phi_0 + t + \tau_s \ln\left(e^{-\frac{t}{\tau_s}}\right)\right) \\ =& \frac{d}{dt}\left(\Phi_0 + t - t\right) = \frac{d}{dt}\Phi_0 = 0\end{aligned}$$

so ϕ is constant over time for points on the same (s_t, Φ_t) trajectory. (See Figure 6.4.) We change coordinates, replacing Φ with ϕ. We define $\tilde{\mathbf{R}}$ as $\mathbf{R}$ in this new coordinate system, and we use $\tilde{\zeta}$ to represent a variation in the new coordinates. To change coordinates, we write

$$\mathbf{F}\begin{pmatrix} s \\ \Phi \end{pmatrix} = \begin{pmatrix} s \\ \Phi + \tau_s \ln(s) \end{pmatrix} \text{ and } \mathbf{F}^{-1}\begin{pmatrix} s \\ \phi \end{pmatrix} = \begin{pmatrix} s \\ \phi - \tau_s \ln(s) \end{pmatrix}$$

$$D\mathbf{F} = \begin{pmatrix} 1 & 0 \\ \frac{\tau_s}{s} & 1 \end{pmatrix} \text{ and } D\mathbf{F}^{-1} = \begin{pmatrix} 1 & 0 \\ -\frac{\tau_s}{s} & 1 \end{pmatrix}$$

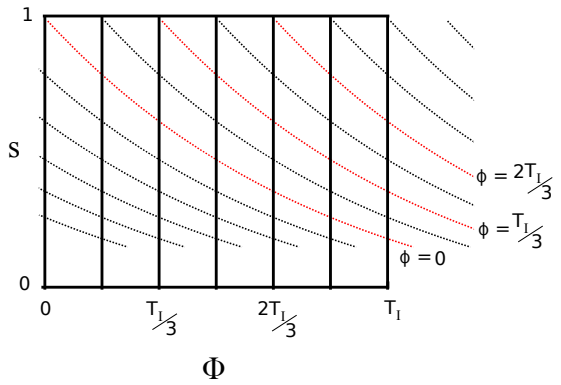

Figure 9: Using s and Φ, we define a new variable ϕ such that ϕ is constant along an (s, Φ) trajectory from one spike to the next.

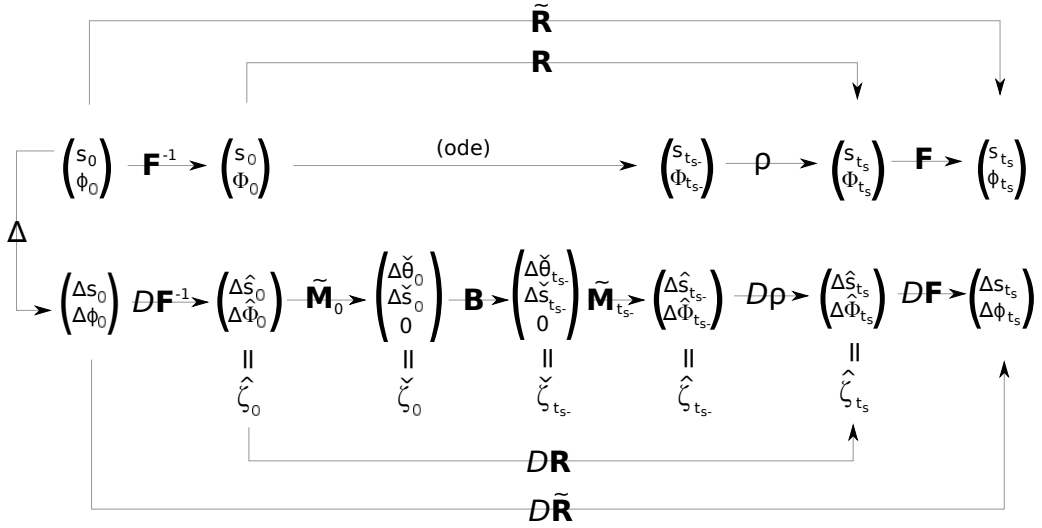

Figure 10: Schematic of the components of the return map $\hat{\mathbf{R}}$ and its derivative $D\hat{\mathbf{R}}$. The state at time 0 in (s, ϕ)-coordinates is transformed to (s, Φ) coordinates by $\mathbf{F}^{-1}$; flows forward from $(-\pi, s_0, \Phi_0)$ to $(\pi, s_{t_s}, \Phi_{t_s})$ according to the ODE (1); is reset by the synaptic rise map ρ; and then is transformed back to (s, ϕ) coordinates by $\mathbf{F}$. An initial variation at a spike in (s, ϕ) coordinates is transformed to (s, Φ) coordinates by $D\mathbf{F}^{-1}$; flows to the $\Phi = \Phi_0^*$ plane via $\tilde{\mathbf{M}}_0$; flows forward to time t_s according to the variational equation (6.10) and its solution $\mathbf{B}$; flows to the $\theta = \pi$ plane via $\tilde{\mathbf{M}}_{t_s}$; is reset by synaptic rise via $D\rho$; and finally, is transformed back to (s, ϕ) coordinates by $D\mathbf{F}$. The variation needs to be transformed by saltation matrices before and a

$$\tilde{\mathbf{R}}\begin{pmatrix} s_0 \\ \phi_0 \end{pmatrix} = \mathbf{F}\left(\mathbf{R}\left(\mathbf{F}^{-1}\begin{pmatrix} s_0 \\ \phi_0 \end{pmatrix}\right)\right)$$
$$D\tilde{\mathbf{R}} = D\mathbf{F}_{t_s} D\mathbf{R} D\mathbf{F}_0^{-1}$$

See Figure 6.4 for illustration.

Substituting from (6.28),

$$\begin{aligned}
D\tilde{\mathbf{R}} &= \begin{pmatrix} 1 & 0 \\ \frac{\tau_s}{s_{t_s}} & 1 \end{pmatrix} \begin{pmatrix} ce^{-\frac{t_s}{\tau_s}}(1-\Sigma\frac{s_0}{\tau_s}) & ce^{-\frac{t_s}{\tau_s}}\frac{s_0}{\tau_s}(1-\kappa-\Sigma\frac{s_0}{\tau_s}) \\ \Sigma & \kappa+\Sigma\frac{s_0}{\tau_s} \end{pmatrix} \begin{pmatrix} 1 & 0 \\ -\frac{\tau_s}{s_0} & 1 \end{pmatrix} \\
&= \begin{pmatrix} 1 & 0 \\ \frac{\tau_s}{s_{t_s}} & 1 \end{pmatrix} \begin{pmatrix} ce^{-\frac{t_s}{\tau_s}}\kappa & ce^{-\frac{t_s}{\tau_s}}\frac{s_0}{\tau_s}(1-\kappa-\Sigma\frac{s_0}{\tau_s}) \\ -\frac{\tau_s}{s_0}\kappa & \kappa+\Sigma\frac{s_0}{\tau_s} \end{pmatrix} \\
&= \begin{pmatrix} ce^{-\frac{t_s}{\tau_s}}\kappa & ce^{-\frac{t_s}{\tau_s}}\frac{s_0}{\tau_s}(1-\kappa-\Sigma\frac{s_0}{\tau_s}) \\ (\frac{ce^{-\frac{t_s}{\tau_s}}}{s_{t_s}}-\frac{1}{s_0})\tau_s\kappa & ce^{-\frac{t_s}{\tau_s}}\frac{s_0}{s_{t_s}}(1-\kappa-\Sigma\frac{s_0}{\tau_s})+\kappa+\Sigma\frac{s_0}{\tau_s} \end{pmatrix} \\
&= \begin{pmatrix} ce^{-\frac{t_s}{\tau_s}}\kappa & ce^{-\frac{t_s}{\tau_s}}\frac{s_0}{\tau_s}(1-\kappa-\Sigma\frac{s_0}{\tau_s}) \\ (\frac{ce^{-\frac{t_s}{\tau_s}}}{s_{t_s}}-\frac{1}{s_0})\tau_s\kappa & (ce^{-\frac{t_s}{\tau_s}}\frac{s_0}{s_{t_s}}-1)(1-\kappa-\Sigma\frac{s_0}{\tau_s})+1 \end{pmatrix} \\
&= \begin{pmatrix} ce^{-\frac{t_s}{\tau_s}}\kappa & ce^{-\frac{t_s}{\tau_s}}\frac{s_0}{\tau_s}(1-\kappa-\Sigma\frac{s_0}{\tau_s}) \\ (\frac{ce^{-\frac{t_s}{\tau_s}}s_0}{s_{t_s}s_0}-\frac{s_{t_s}}{s_{t_s}s_0})\tau_s\kappa & \frac{s_0ce^{-\frac{t_s}{\tau_s}}-s_{t_s}}{s_{t_s}}(1-\kappa-\Sigma\frac{s_0}{\tau_s})+1 \end{pmatrix}
\end{aligned}$$

Substituting $s_{t_s-} = s_0 e^{-\frac{t_s}{\tau_s}}$, we have

$$= \begin{pmatrix} ce^{-\frac{t_s}{\tau_s}}\kappa & ce^{-\frac{t_s}{\tau_s}}\frac{s_0}{\tau_s}(1-\kappa-\Sigma\frac{s_0}{\tau_s}) \\ \frac{cs_{t_s-}-s_{t_s}}{s_{t_s}s_0}\tau_s\kappa & \frac{cs_{t_s-}-s_{t_s}}{s_{t_s}}(1-\kappa-\Sigma\frac{s_0}{\tau_s})+1 \end{pmatrix}$$

Substituting $cs_{t_s-} - s_{t_s} = cs_{t_s-} - \rho(s_{t_s-}) = cs_{t_s-}(1+c(s_{t_s-}-1)) = -(1-c)$, we have

$$= \begin{pmatrix} ce^{-\frac{t_s}{\tau_s}}\kappa & ce^{-\frac{t_s}{\tau_s}}\frac{s_0}{\tau_s}(1-\kappa-\Sigma\frac{s_0}{\tau_s}) \\ -\frac{1-c}{s_{t_s}s_0}\tau_s\kappa & 1-\frac{1-c}{s_{t_s}}(1-\kappa-\Sigma\frac{s_0}{\tau_s}) \end{pmatrix} \tag{6.29}$$

(6.30)

6.5. **Step 4: Applying the Annulus Principle.** Here we use the Annulus Principle to find conditions under which $\tilde{\mathbf{R}}$ possesses an attracting invariant circle.

Using the terms in $D\tilde{\mathbf{R}}$ from (6.29), we will apply the Annulus Principle (Theorem 6.2.1) to the map $\tilde{\mathbf{R}}$. Since $1-c \le s \le 1$ immediately after ever spike, we choose the annulus $\mathbb{K} = \{(s,\phi) | s \in [1-c, 1]\}$. We set $n = 1$ and $m = 1$; we substitute s for r and ϕ for x, and we use T_I as the period of ϕ instead of 2π. We let $\tilde{\mathbf{R}}(s,\phi) = \begin{pmatrix} \tilde{f}(s,\phi) \\ \tilde{F}(s,\phi) \end{pmatrix}$, and let $\|\cdot\|^o$

denote a supremum norm over initial conditions in $\mathbb{K}$ as in the Annulus Principle. Using the bounds $s_0, s_{t_s} \in [1-c, 1]$ which hold on $\mathbb{K}$, we have

$$\begin{cases} \frac{\partial \tilde{F}}{\partial \phi} & = 1 - \frac{1-c}{s_{t_s}}(1 - \kappa - \Sigma\frac{s_0}{\tau_s}) \\ \|\left(\frac{\partial \tilde{F}}{\partial \phi}\right)^{-1}\|^o = \|\frac{1}{1-\frac{1-c}{s_{t_s}}(1-\kappa-\Sigma\frac{s_0}{\tau_s})}\|^o \leq \|\frac{1}{1-(1-\kappa-\Sigma\frac{s_0}{\tau_s})}\|^o & \leq \|\frac{1}{\kappa+\Sigma\frac{s_0}{\tau_s}}\|^o \\ \|\frac{\partial \tilde{F}}{\partial s}\|^o = \|\frac{(1-c)\tau_s}{s_{t_s} s_0}\kappa\|^o & \leq \frac{\tau_s}{1-c}\|\kappa\|^o \\ \|\frac{\partial \tilde{f}}{\partial \phi}\left(\frac{\partial \tilde{F}}{\partial \phi}\right)^{-1}\|^o = \|\frac{ce^{-\frac{t_s}{\tau_s}}\frac{s_0}{\tau_s}(1-\kappa-\Sigma\frac{s_0}{\tau_s})}{1-\frac{1-c}{s_{t_s}}(1-\kappa-\Sigma\frac{s_0}{\tau_s})}\|^o \leq \|ce^{-\frac{t_s}{\tau_s}}\frac{s_0}{\tau_s}\frac{1-\kappa-\Sigma\frac{s_0}{\tau_s}}{1-(1-\kappa-\Sigma\frac{s_0}{\tau_s})}\|^o & \leq c\|e^{-\frac{t_s}{\tau_s}}\|^o\frac{1}{\tau_s}\|\frac{1}{\kappa+\Sigma\frac{s_0}{\tau_s}} - 1\|^o \\ \|\frac{\partial \tilde{f}}{\partial s}\|^o = c\|e^{-\frac{t_s}{\tau_s}}\kappa\|^o & \leq c\|e^{-\frac{t_s}{\tau_s}}\|^o\|\kappa\|^o \end{cases} \tag{6.31}$$

We place simple bounds on these terms by defining

$$M := max(1, \|\frac{1}{\kappa + \Sigma\frac{s_0}{\tau_s}}\|^o) \tag{6.32}$$

and writing

$$\begin{cases} \|\left(\frac{\partial \tilde{F}}{\partial \phi}\right)^{-1}\|^o & \leq M \\ \|\frac{\partial \tilde{F}}{\partial s}\|^o & \leq \frac{\tau_s}{1-c}\|\kappa\|^o \\ \|\frac{\partial \tilde{f}}{\partial \phi}\left(\frac{\partial \tilde{F}}{\partial x}\right)^{-1}\|^o & \leq c\|e^{-\frac{t_s}{\tau_s}}\|^o\frac{1}{\tau_s}M \\ \|\frac{\partial \tilde{f}}{\partial s}\|^o & \leq c\|e^{-\frac{t_s}{\tau_s}}\|^o\|\kappa\|^o \end{cases} \tag{6.33}$$

Two conditions of the Annulus Principle are trivially met:

(1) $\tilde{\mathbf{R}}$ maps $\mathbb{K}$ into itself.

(3) Since κ and Σ are positive and $s_{t_s} \geq 1-c$, the expression $\frac{\partial \tilde{F}}{\partial \phi} = 1-\frac{1-c}{s_{t_s}}(1-\kappa-\Sigma\frac{s_0}{\tau_s}) \geq 1-(1-\kappa-\Sigma\frac{s_0}{\tau_s}) \geq 0$ on the whole annulus. Therefore $\tilde{F}$ is increasing on $\mathbb{T}$. $\tilde{F}$ is a composition of a Poincare section return map and a differentiable map, so it is continuously differentiable; there $\tilde{F}$ is a diffeomorphism on $\mathbb{T}$.

Thus, an attracting invariant torus exists if the other two conditions are met:

(2) $\|\frac{\partial \tilde{f}}{\partial s}\|_o < 1$.

(4) $\|\left(\frac{\partial \tilde{F}}{\partial \Phi}\right)^{-1}\|^o \cdot \|\frac{\partial f}{\partial s}\|_o + 2\sqrt{\|\left(\frac{\partial F}{\partial \Phi}\right)^{-1}\|^o \cdot \|\frac{\partial F}{\partial s}\|^o \cdot \|\frac{\partial f}{\partial \Phi}\left(\frac{\partial F}{\partial \Phi}\right)^{-1}\|^o} < 1$.

Substituting from (6.33), we find that an attracting invariant torus exists if for all initial coordinates $(s_0^*, \phi_0^*) \in \mathbb{K}$,

(2) $c\|e^{-\frac{t_s}{\tau_s}}\|^o\|\kappa\|^o < 1$.

(4) $Mc\|e^{-\frac{t_s}{\tau_s}}\|^o\|\kappa\|^o + 2\sqrt{M\frac{\tau_s}{1-c}\|\kappa\|^o c\|e^{-\frac{t_s}{\tau_s}}\|^o\frac{1}{\tau_s}M} < 1$, or
$M\left[c\|e^{-\frac{t_s}{\tau_s}}\|^o\|\kappa\|^o + \frac{2}{\sqrt{1-c}}\sqrt{c\|e^{-\frac{t_s}{\tau_s}}\|^o\|\kappa\|^o}\right] < 1$

6.5.1. *Validating results through simulation.* Here we use simulation to size up the parameter regime in which $\tilde{\mathbf{R}}$ possesses an attracting invariant circle.

We have proven that given an otherwise full set of parameters, sufficiently large g or sufficiently small c guarantees the existence of an invariant circle for the return map and an invariant broken torus for the full system. We do not, however, produce explicit bounds on these parameters that guarantee the existence of said torus. Here we check that the invariant torus exists for a set of "reasonable" parameter values by numerically calculating $c\|e^{-\frac{t_s}{\tau_s}}\|^o\|\kappa\|^o$ and M (defined in (6.32)) over a dense grid of initial conditions and verifying that the conditions of the Annulus Principle (as formulated in (**??**)) are met everywhere. In particular, we find the maximal values of $e^{-\frac{t_s}{\tau_s}}$, κ, and $\frac{1}{\kappa+\Sigma\frac{s_0}{\tau_s}}$ over a grid of 220 initial conditions spanning the set $\theta_0 = -\pi$, $s_0 \in [1-c, 1]$, $\Phi \in \mathbb{T}^1$; if both $c\|e^{-\frac{t_s}{\tau_s}}\|^o\|\kappa\|^o$ and $N := M\left[c\|e^{-\frac{t_s}{\tau_s}}\|^o\|\kappa\|^o + \frac{2}{\sqrt{1-c}}\sqrt{c\|e^{-\frac{t_s}{\tau_s}}\|^o\|\kappa\|^o}\right]$ are both less than 1 (where $M = max(1, \|\frac{1}{\kappa+\Sigma\frac{s_0}{\tau_s}}\|^o)$ as in (6.32)), then conditions 2 and 4 are met and the Annulus Principle holds.

We use the default parameters $c = 0.4$, $\tau = 1.5$, $\tau_s = 9$, $g = 1.5$, and $b = 0.2$, where $I(\cdot)$ is a series of gaussian pulses bounded above by $B = 0.4$.

Parameter set	$\|e^{-\frac{t_s}{\tau_s}}\|^o$	$\|\kappa\|^o$	$\|\frac{1}{\kappa+\Sigma\frac{s_0}{\tau_s}}\|^o$	$c\|e^{-\frac{t_s}{\tau_s}}\|^o\|\kappa\|^o$	N
(default)	0.1127	0.0061	4.4567	0.0003	0.1917
$\tau = 2.25$	0.0611	0.0275	4.2647	0.0007	0.2883
$g = 1$	0.1683	0.0392	4.5422	0.0026	0.6146
$\tau_s = 6$	0.0787	0.0150	4.2446	0.0005	0.2401
$b = 0.3$	0.1698	0.0153	3.9365	0.0010	0.3320
$B = 0.6$	0.1552	0.0164	6.1150	0.0010	0.5095
$c = 0.6$	0.1683	0.0392	4.5422	0.0040	0.9219

None of the values in the table above exceed 1, so the Annulus Principle hold for all parameter sets described here. Making c, τ, b, or B larger or g or τ_s smaller seems to drive the system towards the regime in which an invariant torus cannot be guaranteed by the methods presented here by limiting the time between spikes and/or the amount of rivering under inhibition. However, the torus seems relatively robust in the neighborhood of our default parameters, especially to changes in the parameters b, τ_s, and τ.

6.5.2. *Small c guarantees an invariant torus.* Here we show that $\tilde{\mathbf{R}}$ possesses an attracting invariant circle for sufficiently small c.

Given any full set of parameters not including c, plus an upper bound B on $I(\cdot)$, κ and Σ are bounded from above and away from zero over the annulus $s \in [\frac{1}{2}, 1]$ and over all $I(\cdot) < B$, and they do not depend on c. So we may choose c such that $c\|e^{-\frac{t_s}{\tau_s}}\|^o\|\kappa\|^o$ is arbitrarily small, whereas M remains bounded above; therefore, for sufficiently small $c > 0$, an attracting invariant circle exists for $\tilde{\mathbf{R}}$ for all $I(\cdot) < B$, and a broken attracting invariant torus exists for the system. The existence of this torus may be attributed to convergence of trajectories due to synaptic resetting.

6.5.3. *Large g guarantees an invariant torus.* Here we show that $\tilde{\mathbf{R}}$ possesses an attracting invariant circle for sufficiently large g, due both to contraction of phase space as s decays and contraction of phase space as θ rivers under inhibition.

Given any full set of parameters not including g, a nonnegative forcing signal $I(\cdot)$, and a bound B on $I(\cdot)$ such that $0 \leq I(\cdot) \leq B < 1 - b$, we can show that g may be chosen sufficiently large that $e^{-\frac{t_s}{\tau_s}}$ and κ become arbitrarily small over the annulus $\mathbb{K}$ while Σ remains bounded away from zero, proving the existence of a broken attracting invariant torus for sufficiently large g. The existence of this torus may be attributed partially to small κ, i.e. due to rivering of trajectories under inhibition.

At any time t, let G_t^1 denote the maximum possible input current: $G_t^1 = b - g(1-c)e^{-\frac{t}{\tau_s}} + B$. Let C_1 denote the curve $0 = 1 - \cos(\theta) + (1 + \cos(\theta))G_t^1$ in θ-vs.-t space: θ cannot cross C_1 from below, so θ remains below $-\frac{\pi}{2}$ until G_t^1 crosses -1 and C_1 crosses $-\frac{\pi}{2}$ at time $t^o := \tau_s \ln\left(\frac{g(1-c)}{b+B+1}\right)$, which grows without bound as $g \to \infty$. Let G_t^2 denote the minimum possible input current: $G_t^2 = b - ge^{-\frac{t}{\tau_s}}$. Let C_2 denote the curve $\frac{1}{\tau} = \frac{1}{\tau}\left[1 - \cos(\theta) + (1 + \cos(\theta))G_t^2\right]$ in θ-vs.-t space: θ increases with slope at least $\frac{1}{\tau}$ below the lower branch of C^2. See Figure 11.

First, we show that M is bounded from above. From definition (6.32), we see that it is sufficient to show that Σ is bounded away from zero. We note that $G < b + B < 1$, so $1 - G > 0$. For $\theta \in [0, \pi]$, we have

$$Q_t = (1 - G_t)\sin(\theta_t) \geq 0. \tag{6.34}$$

From (6.17),

$$\Sigma = \frac{g}{2}\int_0^{t_s} R_t e^{\int_t^{t_s} Q_r dr} dt \tag{6.35}$$

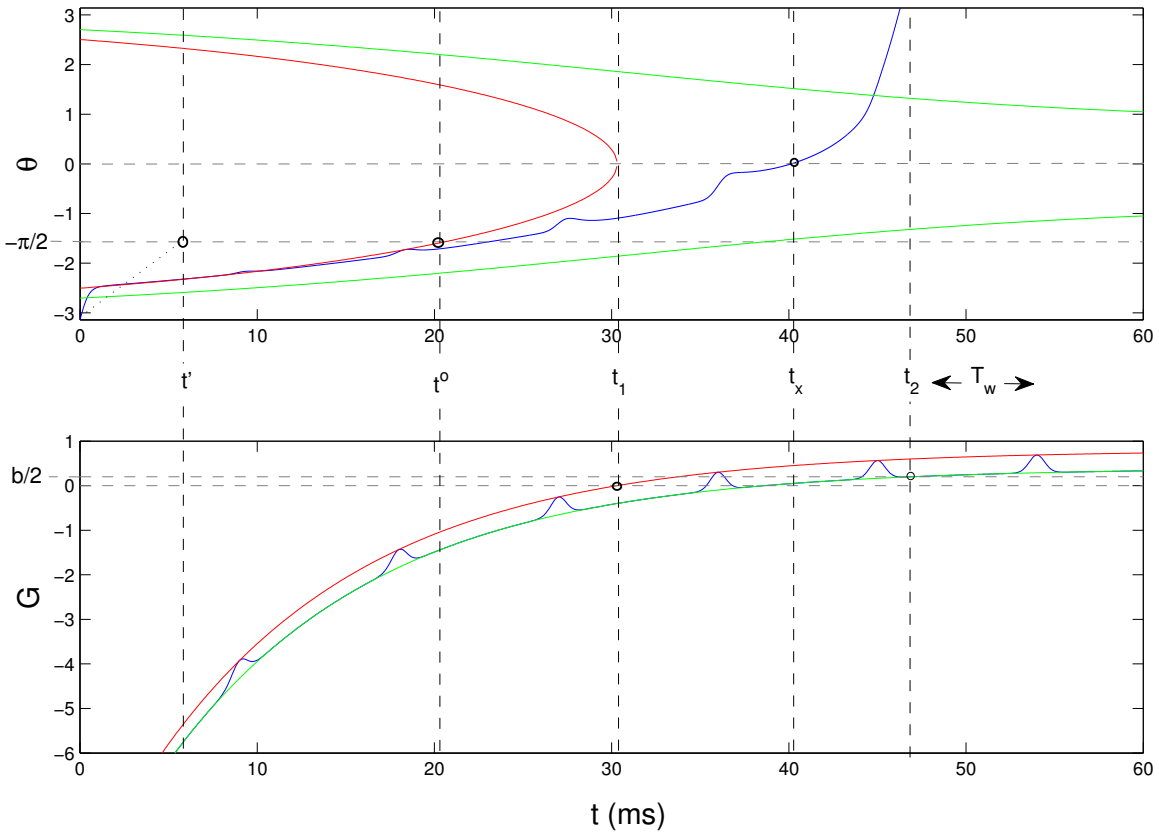

Figure 11: **Above:** θ_t trajectory is blue, C^1 is red, C^2 is green. θ_t cannot cross $\frac{\pi}{2}$ until C^1 crosses it at t^o. θ_t rises faster than $\frac{1}{\tau}$ below C^2, and C^2 is below $\frac{\pi}{2}$ before t^o, so the trajectory must cross C^2 before $t' := \frac{\pi\tau}{2}$. (In fact, it crosses much sooner.) t_x is defined as the last time θ_t crosses zero before a spike (or in this case, the only time). **Below:** G_t is blue, G_t^1 is red, G_2^t is green. A spike cannot occur until G_t^1 reaches 0 at time t_1; a spike must occur within a window of T_w after G_t^2 crosses $\frac{b}{2}$ at time t_2. (In fact, the spike occurs much sooner.)

Let t_x denote the last time θ crosses 0 before a spike. Using $R_t > 0$, we can bound the integral from below by restricting it to just the final rise time $[t_x, t_s]$:

$$> \frac{g}{2} \int_{t_x}^{t_s} R_t e^{\int_t^{t_s} Q_r dr} dt \tag{6.36}$$

For $t \in [t_x, t_s]$, $\theta \in [0, \pi]$, so from (6.34),

$$> \frac{g}{2} \int_{t_x}^{t_s} R_t dt \tag{6.37}$$

From (6.14),

$$> \frac{g}{2}\int_{t_x}^{t_s}\frac{1}{\tau}(1+\cos(\theta_t^*))e^{-\frac{t}{\tau_s}}dt \tag{6.38}$$

$$= \frac{1}{2\tau}\int_{t_x}^{t_s}\frac{1}{\tau}(1+\cos(\theta_t^*))(ge^{-\frac{t}{\tau_s}})dt \tag{6.39}$$

Once the level of inhibition, $gs_0e^{-\frac{t}{\tau_s}}$, has dropped to $\frac{b}{2}$, we have $G_t^2 = b - gs_0e^{-\frac{t}{\tau_s}} = \frac{b}{2}$; after this point, since the input current must be positive and bounded away from zero, a spike must occur within some maximum time window T_w. During this time $gs_0e^{-\frac{t}{\tau_s}}$ can drop no further than $\frac{b}{2}e^{-\frac{T_w}{\tau_s}}$. Thus, $gs_0e^{-\frac{t}{\tau_s}} > \frac{b}{2}e^{-\frac{T_w}{\tau_s}}$, and, using $s_0 < 1$, $ge^{-\frac{t}{\tau_s}} > \frac{b}{2}e^{-\frac{T_w}{\tau_s}}$:

$$\Sigma > \frac{1}{2\tau}\int_{t_x}^{t_s}(1+\cos(\theta_t^*))\frac{b}{2}e^{-\frac{T_w}{\tau_s}}dt \tag{6.40}$$

Finally, we change variables from an integral over time to an integral over θ using $dt = \frac{d\theta}{\dot\theta}$:

$$= \frac{b}{4\tau}e^{-\frac{T_w}{\tau_s}}\int_0^{\pi}(1+\cos(\theta))\frac{d\theta}{\dot\theta} \tag{6.41}$$

Since $G < 1$, $\dot\theta := \frac{1}{\tau}\left[1-\cos(\theta)+(1+\cos(\theta))G\right] < \frac{2}{\tau}$:

$$\Sigma > \frac{b}{4\tau}e^{-\frac{T_w}{\tau_s}}\int_0^{\pi}(1+\cos(\theta))\frac{d\theta}{\frac{2}{\tau}} \tag{6.42}$$

$$= \frac{1}{8}e^{-\frac{T_w}{\tau_s}}\pi \tag{6.43}$$

so Σ is bounded away from zero.

Next, we show that by choosing g large, $c\|e^{-\frac{t_s}{\tau_s}}\|^o\|\kappa\|^o$ can be made arbitrarily small. We note that a spike cannot occur until $b - gs_0e^{-\frac{t}{\tau_s}} + B > 0$, so we must have $e^{-\frac{t_s}{\tau_s}} < \frac{b+B}{gs_0}$. By choosing g large, we can make this bound arbitrarily close to zero, so the term $e^{-\frac{t_s}{\tau_s}}$ in $c\|e^{-\frac{t_s}{\tau_s}}\|^o\|\kappa\|^o$ may be made arbitrarily small by choosing g large.

κ, too, becomes arbitrarily small for g sufficiently large. We prove this in two steps: first, we show that the positive component of the integral in the exponent of κ is bounded for all g, and then we show that the negative component becomes arbitrarily negative for large g.

A spike cannot occur until it is possible for G to be greater than zero, i.e. until $G_t^1 >$, or $gs_0e^{-\frac{t}{\tau_s}} < b+B$. However, as previously discussed, once $G_t^2 = \frac{b}{2}$, a spike must occur within a bounded time window T_w. The first event occurs at $t_1 = \tau_s\ln\left(\frac{gs_0}{b+B}\right)$, and the second occurs at $t_2 = \tau_s\ln\left(\frac{2gs_0}{b}\right)$, so the time between them is $t_2 - t_1 = \tau_s\ln\left(\frac{2(b+B)}{b}\right)$, independent of g.

Therefore there is a window of time of bounded duration $\tau_s \ln\left(\frac{2(b+B)}{b}\right) + T_w$ during which θ (and hence $\sin(\theta)$) may be greater than zero. During this window, $G > b - gs_0 e^{-\frac{t}{\tau_s}} > -B$, so $Q_t = (1 - G_t)\sin(\theta_t)$ is bounded from above; hence, the integral of Q_t over this window is also bounded from above. Since this time window is the only time during which $\sin(\theta)$ can be positive, and $1 - G_t > 0$, this window is the only time during which Q_t may be positive.

The rest of the integral of Q_t between spikes grows more negative without bound as $g \to \infty$. To prove this, we show that although Q_t starts at zero, it exceeds a certain lower bound after a bounded transient, and the time it remains above that lower bound grows unboundedly with g.

The lower branch of C^2 is below the lower branch of C^1, so before t^o, the lower branch of C^2 is below $-\frac{\pi}{2}$. Therefore, θ must cross C^2 less than time $t' := \frac{-\frac{\pi}{2}}{\frac{1}{\tau}} = -\frac{\pi\tau}{2}$ after its initial spike, and then must stay between the lower branches of C^1 and C^2 until t^o.

Along C^2, we have $\theta = -\cos^{-1}\left(\frac{G_t^2}{1-G_t^2}\right)$. Applying basic rules of trigonometry, this gives us $\sin(\theta) = -\frac{\sqrt{1-2G_t^2}}{1-G_t^2}$. Before t^o, $\theta < -\frac{\pi}{2}$ below C^1, so between C^1 and C^2 we have $\sin(\theta) \in [-1, -\frac{\sqrt{1-2G_t^2}}{1-G_t^2}]$, and in particular $\sin(\theta) < -\frac{\sqrt{1-2G_t^2}}{1-G_t^2}$. This gives us

$$Q_t = \sin(\theta_t)(1 - G_t) < -\frac{\sqrt{1-2G_t^2}}{1-G_t^2}(1 - G_t) \tag{6.44}$$

$$< -\frac{\sqrt{1-2G_t^2}(1 - G_t^1)}{1-G_t^2} \tag{6.45}$$

$G_t^2 > -ge^{-\frac{t}{\tau_s}}$, and for $t < t^o$, $G_t^1 < -1$, so

$$< -\frac{\sqrt{3}(1 - b + g(1-c)e^{-\frac{t}{\tau_s}} - B)}{1 + ge^{-\frac{t}{\tau_s}}} \tag{6.46}$$

$b + B < 1$, so

$$< -\sqrt{3}\frac{g(1-c)e^{-\frac{t}{\tau_s}}}{1 + ge^{-\frac{t}{\tau_s}}} \tag{6.47}$$

$$= -\sqrt{3}\frac{1-c}{\frac{1}{ge^{-\frac{t}{\tau_s}}} + 1} \tag{6.48}$$

Since $G_t^1 = b - g(1-c)e^{-\frac{t}{\tau_s}} + B < -1$, we have $ge^{-\frac{t}{\tau_s}} > \frac{1+b+B}{1-c}$, and

$$< -\sqrt{3}\frac{1-c}{\frac{1-c}{1+b+B} + 1} \tag{6.49}$$

This quantity is obviously negative and bounded away from zero, so as the interval $[0, t^o]$ becomes arbitrarily long, the integral of Q_t over this interval becomes arbitrarily negative. As $g \to \infty$, this arbitrarily large negative component of the integral arbitrarily outweighs the bounded positive component, making $\kappa := e^{\int_0^{t_s} Q_t dt}$ arbitrarily close to zero.

6.6. **ING Monostability.** *Here we prove the theorem:*

Theorem 6.6.1. *When the ING oscillator described in* (1) *with* $c = 0$ *or sufficiently small* $c > 0$ *is forced by periodic square pulses, stable* $1:1$ *phase locked spiking can occur at only one forcing phase.*

We do so by studying the T_I-periodic interspike interval function $\Psi(\Phi)$, which maps an initial forcing phase Φ at a spike time to the time interval until the next spike and is well-defined for $c = 0$. When $\Psi(\Phi) = T_I$, the next spike occurs at forcing phase $\Phi + T_I$, after exactly one forcing cycle, i.e. the system is phase locked to the forcing. We show here that when the forcing consists of a T_I-periodic square pulse, $\Psi(\Phi)$ may cross T_I on only two intervals of Φ on the circle, and $\Psi'(\Phi)$ may change signs only once on each. It is easy to check that this allows for only two crossings of T_I. (See Figure 13.) From the basic theory of one-dimensional maps, only a downward crossing may be stable; therefore, stable 1:1 phase locking can only occur at one phase. This result persists for small $c > 0$.

6.6.1. *Proof Outline.*

(1) Working from system with $c = 0$ and using the variational techniques from the previous appendix, we show that $\Psi'(\Phi_0)$ can be written as an integral over the θ trajectory between spikes.

(2) Using the standard change of variables from the theta neuron to the QIF neuron, we write $\Psi'(\Phi_0)$ as an integral over the V trajectory of the corresponding QIF neuron.

(3) We let $I(\cdot)$ be a square pulse of duration σ and positive height I_{step}. A simple argument shows that $\Psi(\Phi_0)$ can only cross T_I on one of two subintervals of $[0, T_I)$: on one, spikes occur between pulses, and on the other, spikes occur during the pulse.

(4) On the first subinterval, we use the integral expression for $\Psi(\Phi_0)$ to show that its sign is opposite the sign of $\int_{u=0}^{\sigma} 2V_{u+t_p}(\Phi_0)du$, where t_p is the time between a spike and the arrival of a pulse; therefore, the sign of $\Psi'(\Phi_0)$ is the same as the sign of $\int_{u=0}^{\sigma} 2V_{u+t_p}(\Phi_0)du$.

(5) We present Lemma 6.6.1, which states that V_t strictly increases for as long after a spike as the input current is flat. Using this lemma, we show that $\int_{u=0}^{\sigma} 2V_{u+t_p}(\Phi_0)du$ increases with t_p, which decreases as Φ_0 increases; therefore $\Psi'(\Phi_0)$ can change signs only once (negative to positive) on the first subinterval of $[0, T_I)$.

(6) An argument paralleling that of the preceding two steps shows that on the second subinterval, $\Psi'(\Phi_0)$ may change signs only once (positive to negative).

(7) A simple argument shows that these conditions on $\Psi'(\Phi_0)$ allow Δ to cross T_I only twice transversely or once tangentially. Only a transverse downward crossing is asymptotically stable, so only one stable 1:1 phase locked trajectory may exist.

(8) The above analysis holds only for $c = 0$. However, for sufficiently small $c > 0$, an attracting invariant torus exists (see previous appendix) that must contain all stable orbits and on which an interspike interval map $\Psi(\cdot)$ is uniquely defined. This map is a differentiable perturbation of the same map for $c = 0$, so for sufficiently small $c > 0$, $\Psi(\cdot)$ may only cross T_I twice and only one stable 1:1 phase locked trajectory may exist.

(9) We prove Lemma 6.6.1.

Remark 6.6.1. *This proof relies heavily on the strictly-decreasing inhibition: without it, the lemma stating that V_t strictly increases while the input current is flat might not hold.*

6.6.2. *Step 1: $\Psi'(\Phi_0)$ expressed as the solution to a variational equation.* Let $t = 0$ denote an initial spike time, and let t_s denote the next spike time. In section 3.1.1, we showed that for $c = 0$, the map $\mathbf{P}(\bar{\Phi}) = \bar{\Phi} + \Psi(\Phi)$ on the real line (from the forcing phase at $t = 0$ to the forcing phase at t_s) is a T_I-periodic orientation-preserving homeomorphism on $\mathbb{R}$. Its derivative is the ratio between a variation in forcing phase at the first spike and the resulting variation in forcing phase at the second:

$$\mathbf{P}'(\bar{\Phi}) = \frac{\Delta\hat{\Phi}_{t_s}}{\Delta\hat{\Phi}_0}. \tag{6.50}$$

We can write a similar expression for $\Psi'(\Phi)$:

$$\begin{aligned} \Psi(\Phi) =& \mathbf{P}(\bar{\Phi}) - \bar{\Phi} \\ \Psi'(\Phi) =& \mathbf{P}'(\bar{\Phi}) - 1 = \frac{\Delta\hat{\Phi}_{t_s}}{\Delta\hat{\Phi}_0} - 1 \end{aligned} \tag{6.51}$$

In the previous appendix, we used a saltation matrix to project a variation $\hat{\zeta}_0$ at initial spike time 0 onto the plane $\Phi = \Phi_0^*$; we followed it to the next spike at time t_s using the linearized ODE; we projected it onto the plane $\theta = \pi$; and we followed it through a synaptic resetting event. In this appendix, we will skip the first step and use the linearized ODE to track a variation that is initialized at the plane $\theta = -\pi$. Following the form of equation (6.25) from the previous appendix but leaving off the initial projection by the saltation matrix $\hat{\mathbf{M}}_0$, we write

$$\hat{\zeta}_{t_s} = D\rho\mathbf{M}_{t_s-}\mathbf{B}\hat{\zeta}_0$$

where $\mathbf{B}$ is defined in (6.18), $\mathbf{M}_{t_{s-}}$ is defined in (6.22), and $D\rho$ is defined in (6.24).

$$= \begin{pmatrix} 1 & 0 & 0 \\ 0 & c & 0 \\ 0 & 0 & 1 \end{pmatrix} \begin{pmatrix} 0 & 0 & 0 \\ \frac{1}{2}\frac{s_{t_{s-}}}{\mu} & 1 & 0 \\ -\frac{1}{2} & 0 & 1 \end{pmatrix} \mathbf{B}\hat{\zeta}_0$$

For $c = 0$:

$$\begin{aligned} &= \begin{pmatrix} 0 & 0 & 0 \\ 0 & 0 & 0 \\ -\frac{1}{2} & 0 & 1 \end{pmatrix} \mathbf{B}\hat{\zeta}_0 \\ &= \begin{pmatrix} 0 & 0 & 0 \\ 0 & 0 & 0 \\ -\frac{1}{2} & 0 & 1 \end{pmatrix} \begin{pmatrix} \kappa & -2g\Sigma & \Omega \\ 0 & e^{-\frac{t_s}{\tau_s}} & 0 \\ 0 & 0 & 1 \end{pmatrix} \hat{\zeta}_0 \\ &= \begin{pmatrix} 0 & 0 & 0 \\ 0 & 0 & 0 \\ -\frac{1}{2}\kappa & 0 & -\frac{1}{2}\Omega + 1 \end{pmatrix} \hat{\zeta}_0 \end{aligned}$$

$\hat{\zeta}_0$ is a variation at the plane $\theta = -\pi$, so $\Delta\hat{\theta}_0 = 0$:

$$\begin{aligned} &= \begin{pmatrix} 0 & 0 & 0 \\ 0 & 0 & 0 \\ -\frac{1}{2}\kappa & 0 & -\frac{1}{2}\Omega + 1 \end{pmatrix} \begin{pmatrix} 0 \\ \Delta\hat{s}_0 \\ \Delta\hat{\Phi}_0 \end{pmatrix} \\ \begin{pmatrix} \Delta\hat{\theta}_{t_s} \\ \Delta\hat{s}_{t_s} \\ \Delta\hat{\Phi}_{t_s} \end{pmatrix} &= \begin{pmatrix} 0 \\ 0 \\ (-\frac{1}{2}\Omega + 1)\Delta\hat{\Phi}_0 \end{pmatrix} \\ \Delta\hat{\theta}_{t_s} &= (-\frac{1}{2}\Omega + 1)\Delta\hat{\Phi}_0 \end{aligned} \tag{6.52}$$

Substituting into (6.51),

$$\Psi'(\Phi_0) = \frac{(-\frac{1}{2}\Omega + 1)\Delta\hat{\Phi}_0}{\Delta\hat{\Phi}_0} - 1 = -\frac{1}{2}\Omega + 1 - 1 = -\frac{1}{2}\Omega \tag{6.53}$$

or, substituting from (6.14) and (6.17) and using $\Phi_t^* = \Phi_0^* + t$,

$$\Psi'(\Phi_0) = -\frac{1}{2\tau}\int_0^{t_s} (1 + \cos(\theta_t^*))I'(\Phi_0 + t)e^{\frac{1}{\tau}\int_t^{t_s}(1-G_r^*)\sin(\theta_r^*)dr}dt. \tag{6.54}$$

$$\begin{aligned}\Psi'(\Phi_0) &= -\frac{1}{2}\int_0^{t_s}(1+\cos(\theta_t^*))I'(\Phi_0+t)e^{\int_t^{t_s}(1-G_r^*)\sin(\theta_r^*)dr}dt \\ &= -\frac{1}{2}\int_0^{t_s}e^{\ln(1+\cos(\theta_t^*))}I'(\Phi_0+t)e^{\int_t^{t_s}(1-G_r^*)\sin(\theta_r^*)dr}dt \\ &= -\frac{1}{2}\int_0^{t_s}e^{\int_{\theta_t^*}^{\pi}\frac{\sin(\theta)}{1+\cos(\theta)}d\theta}I'(\Phi_0+t)e^{\int_t^{t_s}(1-G_r^*)\sin(\theta_r^*)dr}dt\end{aligned}$$

We change coordinates in the integral to integrate along the path θ_t^*, using $d\theta = \dot{\theta}_t^* dt$ and $\theta_{t_s}^* = \pi$:

$$\begin{aligned}&= -\frac{1}{2}\int_0^{t_s}e^{\int_t^{t_s}\frac{\sin(\theta_r^*)}{1+\cos(\theta_r^*)}\dot{\theta}_r^* dr}I'(\Phi_0+t)e^{\int_t^{t_s}(1-G_r^*)\sin(\theta_r^*)dr}dt \\ &= -\frac{1}{2}\int_0^{t_s}I'(\Phi_0+t)e^{\int_t^{t_s}\frac{\sin(\theta_r^*)}{1+\cos(\theta_r^*)}\dot{\theta}_r^*+(1-G_r^*)\sin(\theta_r^*)dr}dt\end{aligned}$$

Substituting for $\dot{\theta}_t^*$ from (1),

$$\begin{aligned}&= -\frac{1}{2}\int_0^{t_s}I'(\Phi_0+t)e^{\int_t^{t_s}\frac{\sin(\theta_r^*)}{1+\cos(\theta_r^*)}\left[1-\cos(\dot{\theta}_r^*)+(1+\cos(\dot{\theta}_r^*))G_r\right]+(1-G_r^*)\sin(\theta_r^*)dr}dt \\ &= -\frac{1}{2}\int_0^{t_s}I'(\Phi_0+t)e^{\int_t^{t_s}\frac{\sin(\theta_r^*)(1-\cos(\dot{\theta}_r^*))}{1+\cos(\theta_r^*)}+\sin(\theta_r^*)dr}dt \\ &= -\frac{1}{2}\int_0^{t_s}I'(\Phi_0+t)e^{\int_t^{t_s}\frac{2\sin(\theta_r^*)}{1+\cos(\theta_r^*)}dr}dt\end{aligned}$$

Applying the trigonometric identity $\tan\left(\frac{\theta}{2}\right) = \frac{\sin(\theta)}{1+\cos(\theta)}$,

$$= -\frac{1}{2}\int_0^{t_s}I'(\Phi_0+t)e^{\int_t^{t_s}2\tan\left(\frac{\theta_r^*}{2}\right)dr}dt$$

And changing to the V variable of the QIF neuron using (3.3),

$$= -\frac{1}{2}\int_0^{t_s}I'(\Phi_0+t)e^{\int_t^{t_s}2V_r^* dr}dt$$

V_r^* depends on the initial forcing phase Φ_0. We reintroduce this dependency into our notation:

$$\Psi'(\Phi_0) = -\frac{1}{2}\int_0^{t_s}I'(\Phi_0+t)e^{\int_t^{t_s}2V_r^*(\Phi_0)dr}dt \tag{6.55}$$

6.6.3. *Step 3: Phase locking to a square pulse.* Let us consider a T_I-periodic input consisting of a periodic square pulse of height I_{step} and duration $\sigma < T_I$. The input as a function of forcing phase Φ can be written as

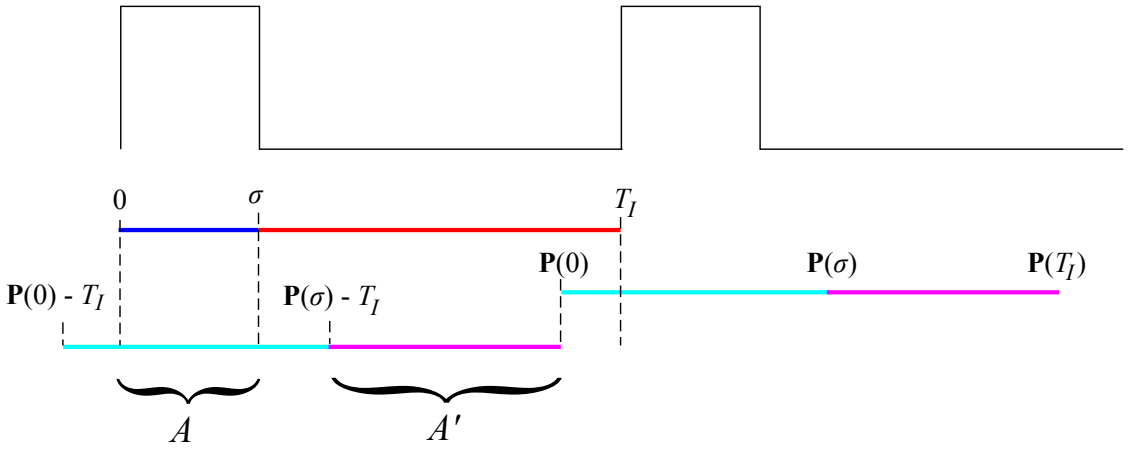

Figure 12: Illustration of the intervals in which 1:1 phase locking can occur. If phase locked spikes occur at phase $\bar{\Phi}$, then $\mathbf{P}(\bar{\Phi}) - T_I = \bar{\Phi}$. Therefore, if $\bar{\Phi} \in [\sigma, T_I)$, i.e., spikes occur between pulses, then $\bar{\Phi} \in A$, where $A = [\sigma, T_I) \cap [\mathbf{P}(\sigma) - T_I, \mathbf{P}(T_I) - T_I]$. Similarly, if $\bar{\Phi} \in [0, \sigma)$, i.e., spikes occur during pulses, then $\bar{\Phi} \in A'$, where $A' = [0, \sigma) \cap [\mathbf{P}(0) - T_I, \mathbf{P}(\sigma) - T_I]$. Phase locking cannot occur for $\bar{\Phi}$ outside these intervals.

$$I(\Phi) = \begin{cases} I_{step} & \text{when } \Phi \in [0, \sigma) \\ 0 & \text{when } \Phi \in [\sigma, T_I) \end{cases} \tag{6.56}$$

and we can write its distributional derivative as

$$I'(\Phi) = I_{step}\delta(\Phi) - I_{step}\delta(\Phi - \sigma) \tag{6.57}$$

where δ is the Dirac delta function on the circle $\mathbb{T}^1 = [0, T_I)$.

We showed in section 3.1.1 that the map $\mathbf{P}(\bar{\Phi})$ on the real line from the forcing phase at $t = 0$ to the forcing phase at t_s is a T_I-periodic orientation-preserving homeomorphism on $\mathbb{R}$. The image of $[0, \sigma)$ under $\mathbf{P}$ is therefore an interval on $\mathbb{R}$. 1:1 phase locking occurs at any phase Φ where $\mathbf{P}(\bar{\Phi}) = \bar{\Phi} + T_I$. By the T_I-periodicity of $\mathbf{P}$, a 1:1 locking phase $\bar{\Phi} \in \mathbb{R}$ exists if and only if there exists a 1:1 locking phase $\bar{\Phi} \in [0, T_I)$. If this point is on $[\sigma, T_I)$, then it must fall in the subinterval $A = [\sigma, T_I) \cap [\mathbf{P}(\sigma) - T_I, \mathbf{P}(T_I) - T_I)$; if it is in $[0, \sigma)$, then it must fall in the subinterval $A' = [0, \sigma) \cap [\mathbf{P}(0) - T_I, \mathbf{P}(\sigma) - T_I)$. In the first case, phase locked spiking occurs between pulses; in the second, phase locked spiking occurs during the pulse. (See Figure 6.6.3.)

In the following two steps, we shall assume the first case ($\Phi_0 \in A$), such that the upward step of current arrives before the downward step. The upward step arrives at time t_p, where

$$t_p = -\Phi_0 \bmod T_I \tag{6.58}$$

and the downward step arrives at time $t_p + \sigma$. The same argument will apply to the second case ($\Phi_0 \in A'$), in which the downward step arrives before the upward step; we simply need to replace I_{step} with $-I_{step}$ and $t_p + \sigma$, the time of the second step, with $t_p + (T_I - \sigma)$.

6.6.4. *Step 4: $sgn(\Psi'(\Phi_0)$ for a square pulse.* We substitute the derivative (6.57) into (6.55):

$$\Psi'(\Phi_0) = -\frac{1}{2\tau}\int_0^{t_s} (1+\cos(\theta_t^*))\left(I_{step}\delta(\Phi_0+t) - I_{step}\delta(\Phi_0+t-\sigma)\right) e^{\frac{1}{\tau}\int_t^{t_s}(1-G_r^*)\sin(\theta_r^*)dr}dt$$

From (6.58), we see that these delta functions will pick out $t = t_p$ and $t = t_p+\sigma$, respectively, so

$$\Psi'(\Phi_0) = -\frac{I_{step}}{2\tau}\left((1+\cos(\theta_{t_p}^*))e^{\frac{1}{\tau}\int_{t_p}^{t_s}(1-G_r^*)\sin(\theta_r^*)dr} - (1+\cos(\theta_{t_p+\sigma}^*))e^{\frac{1}{\tau}\int_{t_p+\sigma}^{t_s}(1-G_r^*)\sin(\theta_r^*)dr}\right) \tag{6.59}$$

Factoring out $(1+\cos(\theta_{t_p+\sigma}^*))e^{\frac{1}{\tau}\int_{t_p+\sigma}^{t_s}(1-G_r^*)\sin(\theta_r^*)dr}$ from both exponentials:

$$= -\frac{I_{step}}{2\tau}e^{\frac{1}{\tau}\int_{t_p+\sigma}^{t_s}(1-G_r^*)\sin(\theta_r^*)dr}\left(\frac{1+\cos(\theta_{t_p}^*)}{1+\cos(\theta_{t_p+\sigma}^*)}e^{\frac{1}{\tau}\int_{t_p}^{t_p+\sigma}(1-G_r^*)\sin(\theta_r^*)dr} - 1\right) \tag{6.60}$$

$$= -\frac{I_{step}}{2\tau}e^{\frac{1}{\tau}\int_{t_p+\sigma}^{t_s}(1-G_r^*)\sin(\theta_r^*)dr}\left(e^{\ln(1+\cos(\theta_{t_p}^*))-\ln(1+\cos(\theta_{t_p+\sigma}^*))}e^{\frac{1}{\tau}\int_{t_p}^{t_p+\sigma}(1-G_r^*)\sin(\theta_r^*)dr} - 1\right) \tag{6.61}$$

$$= -\frac{I_{step}}{2\tau}e^{\frac{1}{\tau}\int_{t_p+\sigma}^{t_s}(1-G_r^*)\sin(\theta_r^*)dr}\left(e^{\int_{\theta_{t_p}^*}^{\theta_{t_p}^*+\sigma}\frac{\sin(\theta)}{1+\cos(\theta)}d\theta}e^{\frac{1}{\tau}\int_{t_p}^{t_p+\sigma}(1-G_r^*)\sin(\theta_r^*)dr} - 1\right) \tag{6.62}$$

We take our integral from $\theta^*_{t_p}$ to $\theta^*_{t_p+\sigma}$ along the path θ^*_r, and change variables from θ to the time variable r using $d\theta = \dot{\theta}^*_r dr$.

$$= -\frac{I_{step}}{2\tau} e^{\frac{1}{\tau}\int_{t_p+\sigma}^{t_s}(1-G^*_r)\sin(\theta^*_r)dr}\left(e^{\int_{t_p}^{t_p+\sigma}\frac{\sin(\theta^*_r)}{1+\cos(\theta^*_r)}\dot{\theta}^*_r dr} e^{\frac{1}{\tau}\int_{t_p}^{t_p+\sigma}(1-G^*_r)\sin(\theta^*_r)dr} - 1\right) \tag{6.63}$$

$$= -\frac{I_{step}}{2\tau} e^{\frac{1}{\tau}\int_{t_p+\sigma}^{t_s}(1-G^*_r)\sin(\theta^*_r)dr}\left(e^{\int_{t_p}^{t_p+\sigma}\frac{\sin(\theta^*_r)}{1+\cos(\theta^*_r)}(1-\cos(\theta^*_r)+(1+\cos(\theta^*_r))G^*_r dr} e^{\frac{1}{\tau}\int_{t_p}^{t_p+\sigma}(1-G^*_r)\sin(\theta^*_r)dr} - 1\right) \tag{6.64}$$

$$= -\frac{I_{step}}{2\tau} e^{\frac{1}{\tau}\int_{t_p+\sigma}^{t_s}(1-G^*_r)\sin(\theta^*_r)dr}\left(e^{\int_{t_p}^{t_p+\sigma}\sin(\theta^*_r)G^*_r+\frac{\sin(\theta^*_r)(1-\cos(\theta^*_r))}{1+\cos(\theta^*_r)}dr} e^{\frac{1}{\tau}\int_{t_p}^{t_p+\sigma}\sin(\theta^*_r)-\sin(\theta^*_r)G^*_r dr} - 1\right) \tag{6.65}$$

Combining the integrals,

$$= -\frac{I_{step}}{2\tau} e^{\frac{1}{\tau}\int_{t_p+\sigma}^{t_s}(1-G^*_r)\sin(\theta^*_r)dr}\left(e^{\int_{t_p}^{t_p+\sigma}\frac{\sin(\theta^*_r)(1-\cos(\theta^*_r))}{1+\cos(\theta^*_r)}+\sin(\theta^*_r)dr} - 1\right) \tag{6.66}$$

$$= -\frac{I_{step}}{2\tau} e^{\frac{1}{\tau}\int_{t_p+\sigma}^{t_s}(1-G^*_r)\sin(\theta^*_r)dr}\left(e^{\int_{t_p}^{t_p+\sigma}\frac{2\sin(\theta^*_r)}{1+\cos(\theta^*_r)}dr} - 1\right) \tag{6.67}$$

Applying the trigonometric identity $\tan\left(\frac{\theta}{2}\right) = \frac{\sin(\theta)}{1+\cos(\theta)}$,

$$= -\frac{I_{step}}{2\tau} e^{\frac{1}{\tau}\int_{t_p+\sigma}^{t_s}(1-G^*_r)\sin(\theta^*_r)dr}\left(e^{\int_{t_p}^{t_p+\sigma}2\tan\left(\frac{\theta^*_r}{2}\right)dr} - 1\right) \tag{6.68}$$

And changing to the V variable of the QIF neuron using (3.3),

$$= -\frac{I_{step}}{2\tau} e^{\frac{1}{\tau}\int_{t_p+\sigma}^{t_s}(1-G^*_r)\sin(\theta^*_r)dr}\left(e^{\int_{t_p}^{t_p+\sigma}2V^*_r dr} - 1\right) \tag{6.69}$$

V^*_r depends on the initial forcing phase Φ_0. We reintroduce this dependency into our notation:

$$\Psi'(\Phi_0) = -\frac{I_{step}}{2\tau} e^{\frac{1}{\tau}\int_{t_p+\sigma}^{t_s}(1-G^*_r)\sin(\theta^*_r)dr}\left(e^{\int_{t_p}^{t_p+\sigma}2V^*_r(\Phi_0)dr} - 1\right) \tag{6.70}$$

In order to show that $\Psi'(\Phi_0)$ changes sign only once on interval A, it is sufficient to note the $\pm$ sign of $\Psi'(\Phi_0)$:

$$sgn\left(\Psi'(\Phi_0)\right) = sgn\left(-\frac{I_{step}}{2\tau}\right) sgn\left(e^{\frac{1}{\tau}\int_{t_p+\sigma}^{t_s}(1-G^*_r)\sin(\theta^*_r)dr}\right) sgn\left(e^{\int_{t_p}^{t_p+\sigma}2V^*_r(\Phi_0)dr} - 1\right) \tag{6.71}$$

$$= -\,sgn\left(I_{step}\right) sgn\left(e^{\int_{t_p}^{t_p+\sigma}2V^*_r(\Phi_0)dr} - 1\right) \tag{6.72}$$

$$= -\,sgn\left(I_{step}\right) sgn\left(\int_{t_p}^{t_p+\sigma}2V^*_r(\Phi_0)dr\right) \tag{6.73}$$

To eliminate the dependence of the bounds of integration on t_p, we change variables in the integral to $q = r - t_p$:

$$= - \, sgn\,(I_{step})\, sgn\left(\int_0^{\sigma} 2V^*_{q+t_p}(\Phi_0)dq\right) \tag{6.74}$$

$$\tag{6.75}$$

6.6.5. *Step 5: $\Psi'(\Phi_0)$ may change signs only once.* Before the arrival of the pulse, $V_t^*(\Phi_0)$ is independent of Φ_0 because the cell receives the same flat current before the first step no matter the initial forcing phase, so we write V_t^*. We prove in Lemma 6.6.1 below that during this time, $\frac{d}{dt}V_t^* > 0$. Therefore the value of V when the pulse arrives increases with t_p, the time between the initial spike and the arrival of the pulse.

For $q \in [0, \sigma)$, $V^*_{q+t_p}$ is an autonomous 1-D dynamical system with respect to q:

$$\frac{\partial}{\partial q}V^*_{q+t_p} = {V^*_{q+t_p}}^2 - ge^{-\frac{q+t_p}{\tau_s}} + I_{step} \tag{6.76}$$

with initial condition $V^*_{t_p}$ at $q = 0$. Trajectories cannot cross, so as the initial condition increases with t_p, so does $V^*_{q+t_p}$ for any $q \in [0, \sigma)$, at which point the pulse ends.

Since $\frac{\partial}{\partial t_p}V^*_{q+t_p} > 0$, we also have

$$\frac{\partial}{\partial t_p}\int_0^{\sigma} 2V^*_{q+t_p}dr = \int_0^{\sigma} 2\frac{\partial}{\partial t_p}V^*_{q+t_p}dq > 0. \tag{6.77}$$

From (6.58), we see that t_p decreases with Φ_0, so $\int_{q=0}^{\sigma} 2V^*_{q+t_p}dq$ decreases with Φ_0. This integral can change signs (from positive to negative) only once as Φ_0 increases, and must cross zero transversely. So by (6.74), $\Psi'(\Phi_0)$ may change signs once (from negative to positive) with the increase of Φ_0, and must also cross zero transversely.

6.6.6. *Step 6: Steps 3 and 4 for $\Phi_0 \in [0, \sigma)$.* The preceding two steps assumed that Φ_0 was on the arc $A = [\sigma, T_I) \cap [\mathbf{P}(\sigma)T_I, \mathbf{P}(T_I)T_I)$. As previously explained, Δ may also cross T_I on the arc $A' = [0, \sigma) \cap [\mathbf{P}(0) - T_I, \mathbf{P}(\sigma) - T_I)$. In this case, we can repeat the same derivation substituting $-I_{step}$ for I_{step} and $T_I - \sigma$ for σ in (6.73), and conclude that

$$sgn(\Psi'(\Phi_0)) = -sgn(-I_{step})sgn\left(\int_0^{T_I-\sigma} 2V^*_{q+t_p}(\Phi_0)dq\right) = sgn\left(\int_0^{T_I-\sigma} 2V^*_{q+t_p}(\Phi_0)dq\right) \tag{6.78}$$

where $\int_0^{T_I-\sigma} 2V_{q+t_p}(\Phi_0)dq$ decreases with Φ_0. Therefore, on A', $\Psi'(\Phi_0)$ can change signs only once (from positive to negative) as Φ_0 increases, and must cross zero transversely.

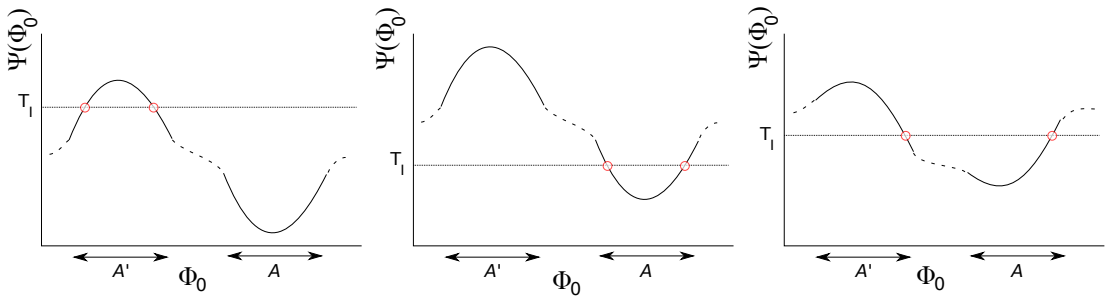

Figure 13: If $\Psi(\Phi_0)$ crosses T_I, it may do so only on A (on which it must be concave) and A' (on which it must be convex), and only in three ways. **Left:** If two crossings occur on A', none can occur on A. **Center:** If two crossings occur on A, none can occur on A'. **Right:** If one crossing occurs on A, only one can occur on A'.

6.6.7. *Step 7: Ψ may only cross T_I twice.* On A, Ψ may switch from decreasing to increasing, and may therefore cross T_I once downwards and then once upwards. In this case, $\Psi(\Phi) > T_I$ at both ends of A. Any other crossings must occur on A'; therefore, $\Psi(\Phi) > T_I$ at both ends of A'. For additional crossings to occur on A', Ψ would have to decrease and then increase on this interval; but we have shown that the sign of the derivative can switch signs from positive to negative on this interval, so no additional crossings are possible.

If only one crossing occurs on A, then $\Psi(\Phi) > T_I$ on one side of A' and $\Psi(\Phi) < T_I$ on the other. Therefore an odd number of crossings must occur on A'; but for three crossings to occur on A', the sign of the derivative would have to switch twice, which is not permitted. Therefore, in this case only one crossing may occur on A'.

A parallel argument to the first shows that if there are no crossings on A, a maximum of two may occur on A'.

In all of these cases, when two crossings occur one is from above to below and the other from below to above. An asymptotically stable 1:1 phase lock is only possible when the map $\mathbf{P} - T_I$ has a fixed point Φ at which $-1 \leq \mathbf{P}'(\Phi) \leq 1$. We recall that $\mathbf{P}(\Phi) = \Psi(\Phi) + \Phi$, so at such a fixed point we must have $-1 \leq \Psi'(\Phi) + 1 \leq 1$, or $-2 \leq \Psi'(\Phi) \leq 0$. In other words, only when Ψ crosses T_I downwards can the associated fixed point be asymptotically stable. Therefore, only one asymptotically stable 1:1 phase locked trajectory may exist.

See Figure 13 for illustration.

6.6.8. *Step 8: for $c > 0$.* It is not immediately clear how to define Ψ for $c > 0$: at any initial forcing phase Φ, the system may have a range of initial values of s, so the subsequent interspike interval is not uniquely determined. However, if the return map $\mathbf{R}$ from (s, Φ) just after one spike to (s, Φ) at the next possesses an asymptotically stable invariant circle (see previous appendix) *and* that circle is a graph of s over Φ, then after a sufficient transient,

the initial value of s after a spike at any forcing phase Φ *is* uniquely determined by the graph, and $\Psi(\Phi)$, the interspike interval following this initial condition, is uniquely defined. For $c = 0$, the graph $s = 1$ serves this purpose: immediately after any spike, $s = 1$, so this circle of initial conditions forms an attracting invariant circle for the return map.

The only part of the evolution of the system that depends on c is the resetting map, which depends smoothly on c; therefore, by Fenichel's theorem for maps [**Fenichel**], for a sufficiently small c the invariant circle persists and depends smoothly on c. Therefore, for sufficiently small c, the invariant circle is still a graph over Φ, and the interspike intervals following the initial condition parametrized by Φ depend smoothly on c. Thus, $\Psi(\Phi)$ depends smoothly on c. For $c = 0$, Δ only crosses T_I transversely, so for a sufficiently small smooth perturbation no additional crossings can be created. Therefore, for sufficiently small $c > 0$, Δ can cross T_I only twice, and only one crossing can correspond to an asymptotically stable 1:1 phase lock; in other words, 1:1 phase locking is monostable.

6.6.9. *Step 9: Proof of Lemma 6.6.1.*

Lemma 6.6.1. *If an ING oscillator receives a flat current I_0 after a spike, its voltage strictly increases.*

Proof. In the V vs. t plane, the V-nullcline is the set $V = \sqrt{ge^{-\frac{t}{\tau_s}} - b - I_0}$. This nullcline vanishes at a saddle-node bifurcation when $b - ge^{-\frac{t}{\tau_s}} + I_0 < 0$, which occurs when $t > \tau_s \ln\left(\frac{b+I_0}{g}\right)$. After a spike at $t = 0$, the voltage begins below the V-nullcline. The branch of the nullcline accessible from below slants up and right, and on the nullcline all vectors point horizontally to the right, so the nullcline cannot be crossed from below. Therefore V remains below this nullcline, and $\dot{V} > 0$ until $t > \tau_s \ln\left(\frac{b+I_0}{g}\right)$. And for all $t > \tau_s \ln\left(\frac{b+I_0}{g}\right)$, we also have $\dot{V} = V^2 + b - ge^{-\frac{t}{\tau_s}} + I_0 > V^2 + 0 > 0$. See Figure 14 for illustration. □

6.7. **Existence of an Attracting Invariant Torus for PING.** *Here we show that for sufficiently strong synapses to the I-population and an appropriate choice of parameters for excitatory synapses, an attracting invariant torus exists in the PING phase space.*

Theorem 6.7.1.

6.7.1. *Proof Outline.*

(1) First, we extend the ING system described in (1) to four dimensions by adding the variable s^e, and rename the map from spike to spike $\mathring{\mathbf{R}}$. We show that if an attracting invariant torus exists for the return map for (1), then a corresponding attracting invariant manifold exists for the map $\mathring{\mathbf{R}}$.

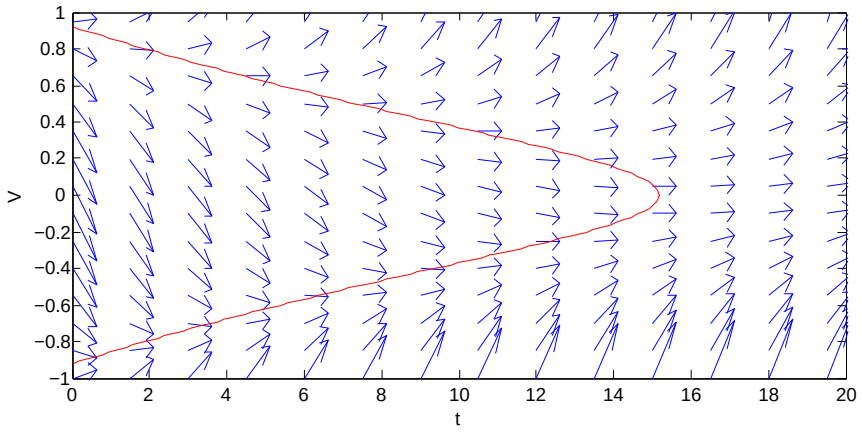

Figure 14: System is receiving flat current I_0 after a spike at $t = 0$. In the V vs. t plane, the V nullcline (red) cannot be crossed from underneath. All arrows to the right of the nullcline point upwards, so V is always increasing.

(2) We show that if the rise time T_{EI} of the I-population and its derivative with respect to initial conditions go to zero as $C \to \infty$, then the map from the state at one I-spike to the state at the next becomes C^1 close to the map $\mathring{\mathbf{R}}$ described above. By Fenichel's persistence result [**Fenichel**], this guarantees the existence of the attracting invariant torus for sufficiently large C.

(3) We prove the lemma that $T_{EI} \to 0$ as $C \to \infty$.

(4) We use variational equations to prove the lemma that $\|\nabla T_{EI}\| \to 0$ as $C \to \infty$, using several supporting lemmas.

(5) We prove all supporting lemmas.

6.7.2. *Step 1: From three to four dimensions.* Here we prove that if we add the variable s_e to the ING model, we may still ensure that an attracting invariant manifold exists by picking g sufficiently large or picking c_i and c_e sufficiently small.

We extend (1) to a four-dimensional model by changing the names of θ and s to θ^e and s^i, respectively, and adding an ODE for s^e:

$$\begin{cases} \tau_e \dot{\theta}^e = & 1 - \cos(\theta) + (1 + \cos(\theta))CG \\ \dot{s}^i = & -\frac{s^i}{\tau_{si}} \\ \dot{s}^e = & -\frac{s^e}{\tau_{se}} \\ \dot{\Phi} = & 1 \end{cases} \tag{6.79}$$

where

$$G = b - gs^i + I(\Phi).$$

We let s^i reset to $\rho_i(s^i) = 1 + c_i(s^i - 1)$ for some $0 < c_i < 1$ in the right-hand limit when $\theta^e = \pi$; we let $s^e \in [0, 1]$ reset to $\rho_e(s^e) = 1 + c_e(1 - s^e)$ for some $0 < c_e < 1$ in the right-hand limit when $\theta^e = \pi$. Φ is again on the circle $\mathbb{T}^1 = [0, T_I)$. We assume that $I(\cdot)$ is T_I-periodic. This is slightly different than the PING model described by (4.1) in that θ^i is left out and s^i resets at E-spikes instead of I-spikes.

We let $\mathring{\mathbf{R}}$ denote the four-dimensional map from $(\theta_0^e, s_0^i, s_0^e, \Phi_0)$ at the r.h.l. of a spike time $t = 0$ to the state at the r.h.l. of the next spike time, t_s, acting on the annulus $\mathbb{K} = \{(\theta_0^e, s_0^i, s_0^e, \Phi) | \theta_0^e \in U, s_0^i \in [1 - c_i, 1],\ s_0^e \in [1 - c_e, 1]\}$ where U is some small neighborhood of $\pm\pi$ on $\mathbb{T}^1$.

Remark 6.7.1. *We note that the evolution of s^e under the map $\mathring{\mathbf{R}}$ depends on the state of the rest of the system, but the rest of the system is independent of s^e. This type of system, with "independent" and "dependent" state variables, is called a"skew product" map. Jaroslav Stark [**Stark1997**] and others have proven that if a skew product map produces a uniform contraction in the direction of the dependent variables and the map is invertible on the independent system, then it approaches an attracting invariant manifold that is a graph of*

the dependent variables over the independent variables. In our case, the map $\mathring{\mathbf{R}}$ *restricted to the independent system is just* $\mathbf{R}$*, which is indeed invertible as long as* $c_i > 0$*. However, the invariant manifold produced by contracting skew product systems is not necessarily robust to the perturbation of introducing a weak dependence of the independent variables upon the dependent variables, which is what we now must do. Therefore, we cannot directly make use of the skew product structure of our system, and instead restrict our parameter space such that we may again apply the Annulus Principle to prove the existence of an invariant torus.*

We again use subscripts 0 and t_s to label the states of variables at the r.h.l. of the initial and final spike times, and t_{s-} to label the states of variables at the l.h.l. of t_s. We follow section 6.2, solving the variational equations and calculating the saltation matrices with one extra variable, and then use (6.25) to write the expression

$$
\begin{aligned}
D\mathbf{R} =& D\rho \mathbf{M}_{t_{s-}} \mathbf{B} \tilde{\mathbf{M}}_0 \\
=& \begin{pmatrix} 1 & 0 & 0 & 0 \\ 0 & c_i & 0 & 0 \\ 0 & 0 & c_e & 0 \\ 0 & 0 & 0 & 1 \end{pmatrix} \begin{pmatrix} 0 & 0 & 0 & 0 \\ \frac{s^i_{t_{s-}}\tau}{2\tau_{s^i}} & 1 & 0 & 0 \\ \frac{s^e_{t_{s-}}\tau}{2\tau_{s^e}} & 0 & 1 & 0 \\ -\frac{\tau}{2} & 0 & 0 & 1 \end{pmatrix} \begin{pmatrix} \kappa & -\frac{2}{\tau}\Sigma & 0 & \Omega \\ 0 & e^{-\frac{t_s}{\tau_{s^i}}} & 0 & 0 \\ 0 & 0 & e^{-\frac{t_s}{\tau_{s^i}}} & 0 \\ 0 & 0 & 0 & 1 \end{pmatrix} \begin{pmatrix} 1 & 0 & 0 & -\frac{2}{\tau} \\ 0 & 1 & 0 & \frac{s^i_0}{\tau_{s^i}} \\ 0 & 0 & 1 & \frac{s^e_0}{\tau_{s^e}} \\ 0 & 0 & 0 & 0 \end{pmatrix} \\
=& \begin{pmatrix} 0 & 0 & 0 & 0 \\ c_i \frac{s^i_{t_{s-}}\tau}{2\tau_{s^i}} & c_i & 0 & 0 \\ c_e \frac{s^e_{t_{s-}}\tau}{2\tau_{s^e}} & 0 & c_e & 0 \\ -\frac{\tau}{2} & 0 & 0 & 1 \end{pmatrix} \begin{pmatrix} \kappa & -\frac{2}{\tau}\Sigma & 0 & -\frac{2}{\tau}\kappa - \frac{2}{\tau}\Sigma\frac{s^i_0}{\tau_{s^i}} \\ 0 & e^{-\frac{t_s}{\tau_{s^i}}} & 0 & \frac{s^i_0}{\tau_{s^i}} e^{-\frac{t_s}{\tau_{s^i}}} \\ 0 & 0 & e^{-\frac{t_s}{\tau_{s^e}}} & \frac{s^e_0}{\tau_{s^e}} e^{-\frac{t_s}{\tau_{s^e}}} \\ 0 & 0 & 0 & 0 \end{pmatrix} \\
=& \begin{pmatrix} 0 & 0 & 0 & 0 \\ c_i \frac{s^i_{t_{s-}}\tau}{2\tau_{s^i}}\kappa & -c_i \frac{s^i_{t_{s-}}}{\tau_{s^i}}\Sigma + c_i e^{-\frac{t_s}{\tau_{s^i}}} & 0 & c_i \frac{s^i_{t_{s-}}}{\tau_{s^i}}(-\kappa - \Sigma\frac{s^i_0}{\tau_{s^i}}) + c_i \frac{s^i_0}{\tau_{s^i}} e^{-\frac{t_s}{\tau_{s^i}}} \\ c_e \frac{s^e_{t_{s-}}\tau}{2\tau_{s^e}}\kappa & -c_e \frac{s^e_{t_{s-}}}{\tau_{s^e}}\Sigma & c_e e^{-\frac{t_s}{\tau_{s^e}}} & c_e \frac{s^e_{t_{s-}}}{\tau_{s^e}}(-\kappa - \Sigma\frac{s^i_0}{\tau_{s^i}}) + c_e \frac{s^e_0}{\tau_{s^e}} e^{-\frac{t_s}{\tau_{s^e}}} \\ -\frac{\tau}{2}\kappa & \Sigma & 0 & \kappa + \Sigma\frac{s^i_0}{\tau_{s^i}} \end{pmatrix}
\end{aligned}
$$

Substituting $s_{t_{s-}} = s_0 e^{-\frac{t_s}{\tau_s}}$,

$$
= \begin{pmatrix} 0 & 0 & 0 & 0 \\ c_i e^{-\frac{t_s}{\tau_{s^i}}} \frac{s^i_0\tau}{2\tau_{s^i}}\kappa & c_i e^{-\frac{t_s}{\tau_{s^i}}}(1 - \frac{s^i_0}{\tau_{s^i}}\Sigma) & 0 & c_i \frac{s^i_0}{\tau_{s^i}} e^{-\frac{t_s}{\tau_{s^i}}}(1 - \kappa - \Sigma\frac{s^i_0}{\tau_{s^i}}) \\ c_e e^{-\frac{t_s}{\tau_{s^e}}} \frac{s^e_0\tau}{2\tau_{s^e}}\kappa & c_e e^{-\frac{t_s}{\tau_{s^e}}}(1 - \frac{s^e_0}{\tau_{s^e}}\Sigma) & c_e e^{-\frac{t_s}{\tau_{s^e}}} & c_e \frac{s^e_0}{\tau_{s^e}} e^{-\frac{t_s}{\tau_{s^e}}}(1 - \kappa - \Sigma\frac{s^i_0}{\tau_{s^i}}) \\ -\frac{\tau}{2}\kappa & \Sigma & 0 & \kappa + \Sigma\frac{s^i_0}{\tau_{s^i}} \end{pmatrix} \tag{6.80}
$$

Remark 6.7.2. *For clarity and simplicity, we do not change variables from Φ to ϕ in this section. Thus, in the following we can only study the existence of invariant tori for PING systems in parameter regimes for which the corresponding ING return map $\mathbf{R}$ possesses an invariant circle that is a graph of s over Φ. Restricting ourselves to these regimes, we cannot fully exploit the effects of rivering under inhibition. The analysis in this section could be repeated with a similar result using an appropriate change of variables.*

We let F denote the component of $\mathring{\mathbf{R}}$ mapping (s_0^i, s_0^e, Φ_0) to Φ_{t_s}, and we let f denote the component of $\mathring{\mathbf{R}}$ mapping (s_0^i, s_0^e, Φ_0) to $(s_{t_s}^i, s_{t_s}^e)$.

$$\begin{cases} \frac{\partial \tilde{F}}{\partial \Phi} & = \kappa + \Sigma \frac{s_0^i}{\tau_{s^i}} \\ \|\left(\frac{\partial \tilde{F}}{\partial \Phi}\right)^{-1}\|^o & = \|\frac{1}{\kappa + \Sigma \frac{s_0^i}{\tau_{s^i}}}\|^o \\ \|\frac{\partial \tilde{F}}{\partial s}\|^o & = \|\begin{pmatrix} -\frac{\tau}{2}\kappa & \Sigma & 0 \end{pmatrix}\|^o \\ \|\frac{\partial \tilde{f}}{\partial \Phi}\left(\frac{\partial \tilde{F}}{\partial \Phi}\right)^{-1}\|^o = \|\frac{\begin{pmatrix} 0 \\ c_i \frac{s_0^i}{\tau_{s^i}} e^{-\frac{t_s}{\tau_{s^i}}}(1 - \kappa - \Sigma \frac{s_0^i}{\tau_{s^i}}) \\ c_e \frac{s_0^e}{\tau_{s^e}} e^{-\frac{t_s}{\tau_{s^e}}}(1 - \kappa - \Sigma \frac{s_0^i}{\tau_{s^i}}) \end{pmatrix}}{\kappa + \Sigma \frac{s_0^i}{\tau_{s^i}}}\|^o & = \|\begin{pmatrix} 0 \\ c_i \frac{s_0^i}{\tau_{s^i}} e^{-\frac{t_s}{\tau_{s^i}}} \left(\frac{1}{\kappa + \Sigma \frac{s_0^i}{\tau_{s^i}}} - 1\right) \\ c_e \frac{s_0^e}{\tau_{s^e}} e^{-\frac{t_s}{\tau_{s^e}}} \left(\frac{1}{\kappa + \Sigma \frac{s_0^i}{\tau_{s^i}}} - 1\right) \end{pmatrix}\|^o \\ \|\frac{\partial \tilde{f}}{\partial s}\|^o & = \|\begin{pmatrix} 0 & 0 & 0 \\ c_i e^{-\frac{t_s}{\tau_{s^i}}} \frac{s_0^i \tau}{2\tau_{s^i}} \kappa & c_i e^{-\frac{t_s}{\tau_{s^i}}}(1 - \frac{s_0^i}{\tau_{s^i}}\Sigma) & 0 \\ c_e e^{-\frac{t_s}{\tau_{s^e}}} \frac{s_0^e \tau}{2\tau_{s^e}} \kappa & c_e e^{-\frac{t_s}{\tau_{s^e}}}(1 - \frac{s_0^e}{\tau_{s^e}}\Sigma) & c_e e^{-\frac{t_s}{\tau_{s^e}}} \end{pmatrix}\|^o \end{cases} \tag{6.81}$$

In Appendix 6.2, we determined that c could be chosen independently of all other terms in $D\tilde{\mathbf{R}}$, and g could be chosen large enough to make κ and $e^{-\frac{t_s}{\tau_s}}$ arbitrarily small while Σ remained bounded from below. (This result depended upon the θ trajectory being initialized at $-\pi$, but the same result can be derived for θ_0 sufficiently close to $-\pi$, i.e., for U sufficiently small.) Using these results and a bound on the standard matrix norm $\|A\|_2 < \sqrt{\|A\|_1 \|A\|_\infty}$, where $\|A\|_1$ is the maximum absolute row sum of A and $\|A\|_\infty$ is the maximum absolute column sum, it is easy to check that by choosing g sufficiently large or c_i and c_e sufficiently small, these partial derivatives may be made to satisfy the conditions of the Annulus Principle.

6.7.3. *Step 2: Persistence due to small T_{EI}.* We now turn to the full PING model, (4.1):

$$\begin{cases} \tau_i \dot{\theta^i} & = 1 - \cos(\theta^i) + (1 + \cos(\theta^i))CG^i \\ \tau_e \dot{\theta^e} & = 1 - \cos(\theta^e) + (1 + \cos(\theta^e))G^e \\ \dot{s^i} & = -s^i/\tau_{s^i} \\ \dot{s^e} & = -s^e/\tau_{s^e} \\ \dot{\Phi} & = 1 \end{cases} \tag{6.82}$$

with $G^e = b_e - g_{ie}s^i + I(\Phi)$ and $G^i = b_i - g_{ii}s^i + g_{ei}s^e$. We assume that this model meets all assumptions from section 4 for $C = 1$. As in the PING model (4.1): The inhibitory synaptic activity variable $s^i \in [0, 1]$ reset to $\rho_i(s^i) = 1 + c_i(s^i - 1)$ for some $0 \leq c_i < 1$ in the right-hand limit when $\theta^i = \pi$; the excitatory synaptic activity variable $s^e \in [0, 1]$ resets to $\rho_e(s^e) = 1 + c_e(s^e - 1)$ for some $0 \leq c_e < 1$ in the right-hand limit when $\theta^e = \pi$. The cell phase variables $\theta^e, \theta^i \in [0, 2\pi)$ and the forcing phase $\Phi \in [0, T_I)$ are on circles. $I(\cdot)$ is a periodic input current to the with bound $B > 0$; g_{ei}, g_{ie}, and g_{ii} are gating variables; τ_i and τ_e are the two membrane time constants; b_e and b_i are the baseline levels of tonic excitation to both populations; and τ_{s^i} and τ_{s^e} are the decay time constants of inhibition and excitation, respectively.

We let T_{EI} denote the function that takes a state at initial time t_{E0} and returns the time for θ^i to rise from its initial state at t_{E0} up to π. In the following, we frequently suppress the dependence of T_{EI} on state.

We prove in Lemma 6.7.1 below that as $C \to \infty$, $T_{EI} \to 0$ uniformly over initial conditions at t_{E0}. Here we demonstrate that as T_{EI} and its derivative ∇T_{EI} go to zero, the return map for θ^i approaches the map $\mathring{\mathbf{R}}$ defined above in C^1 space.

In order to define the return map for the PING model (6.82), we first define the map from the state at the r.h.l. of an I-spike at time t_{I0} (not including θ^i, which must be $-\pi$) to the state at the r.h.l. of the next E-spike, at time t_{E0} (not including θ^e, which must be $-\pi$):

$$\begin{aligned} \mathbf{R}_E : \mathbb{T}^1 \times [0,1] \times [0,1] \times \mathbb{T}^1 \to & \mathbb{T}^1 \times [0,1] \times [0,1] \times \mathbb{T}^1 \\ \begin{pmatrix} \theta^e_{t_{I0}} \\ s^i_{t_{I0}} \\ s^e_{t_{I0}} \\ \Phi_{t_{I0}} \end{pmatrix} \to & \begin{pmatrix} \theta^i_{t_{E0}} \\ s^i_{t_{E0}} \\ s^e_{t_{E0}} \\ \Phi_{t_{E0}} \end{pmatrix} \end{aligned} \tag{6.83}$$

The model makes unique forward trajectories, and we have assumed that every trajectory eventually leads to another E-spike, so this map is well-defined.

Similarly, we define

$$\begin{aligned}\mathbf{R}_I : \mathbb{T}^1 \times [0,1] \times [0,1] \times \mathbb{T}^1 \to &\mathbb{T}^1 \times [0,1] \times [0,1] \times \mathbb{T}^1 \\ \begin{pmatrix} \theta^i_{t_{E0}} \\ s^i_{t_{E0}} \\ s^e_{t_{E0}} \\ \Phi_{t_{E0}} \end{pmatrix} \to &\begin{pmatrix} \theta^e_{t_{I2}} \\ s^i_{t_{I2}} \\ s^e_{t_{I2}} \\ \Phi_{t_{I2}} \end{pmatrix}\end{aligned} \tag{6.84}$$

which takes the state at the right hand limit of an E-spike at time t (except θ^e) and returns the state at the right hand limit of the next I-spike at time t_{I2} (except θ^i).

We define the map $\mathbf{R}_{IE}$ as the composition of the two maps: $\mathbf{R}_{IE} = \mathbf{R}_I \circ \mathbf{R}_E$ takes the state at time 0 to the state at the r.h.l. of the I-spike that follows the next E-spike.

As $T_{EI} \to 0$, the distance traveled by θ^e from $\pm\pi$ between t_{E0} and t_{I2} (as a function of state at t_{E0}) is linearly approximated by $\dot\theta^e_{t_{E0}} T_{EI}$:

$$\theta^e_{t_{I2}} - (\pm\pi) \approx \dot\theta^e_{t_{E0}} T_{EI}.$$

Similarly,

$$\begin{aligned} s^i_{t_{I2-}} - s^i_{t_{E0}} &\approx \dot s^i_{t_{E0}} T_{EI} \\ s^e_{t_{I2}} - s^e_{t_{E0}} &\approx \dot s^e_{t_{E0+}} T_{EI} \\ \Phi_{t_{I2}} - \Phi_{t_{E0}} &\approx \dot\Phi_{t_{E0}} T_{EI} \end{aligned}$$

where $+$ and $-$ are added as subscripts to distinguish between values before $(-)$ and after $(+)$ synaptic resetting. At the end of the EI interval, s^i resets in the right-hand limit, contracting distances by $\rho_i'(s^i) = c_i$; therefore

$$\begin{aligned} s^i_{t_{I2+}} - \rho_i(s^i_{t_{E0}}) &\approx \rho_i(s^i_{t_{I2-}}) - \rho_i(s^i_{t_{E0}}) \\ &\approx \rho_i'(s^i_{t_{E0}})(s^i_{t_{I2-}} - s^i_{t_{E0}}) = c_i \dot s^i_{t_{E0}} T_{EI}. \end{aligned}$$

All of these approximations are up to $O(T_{EI}^2)$. Therefore,

$$\mathbf{R}_I \begin{pmatrix} \theta^i_{t_{E0}} \\ s^i_{t_{E0}} \\ s^e_{t_{E0+}} \\ \Phi_{t_{E0}} \end{pmatrix} - \begin{pmatrix} \pm\pi \\ \rho_i(s^i_{t_{E0}}) \\ s^e_{t_{E0+}} \\ \Phi_{t_{E0}} \end{pmatrix} = \begin{pmatrix} \dot\theta^e_{t_{E0}} \\ c_i \dot s^i_{t_{E0}} \\ \dot s^e_{t_{E0+}} \\ \dot\Phi_{t_{E0}} \end{pmatrix} T_{EI} + O(T_{EI}^2) \tag{6.85}$$

$\mathbf{R}_E$ is exactly the same as the map $\mathring{\mathbf{R}}$ from the previous step, except that $\mathbf{R}_E$ returns the quantity θ^i at the next E-spike instead of θ^e, and $\mathring{\mathbf{R}}$ includes an s^i reset at the end while $\mathbf{R}_E$ does not:

$$\mathring{\mathbf{R}}\begin{pmatrix}\theta^e_{t_{I0}}\\ s^i_{t_{I0+}}\\ s^e_{t_{I0}}\\ \Phi_{t_{I0}}\end{pmatrix}=\begin{pmatrix}\pm\pi\\ \rho_i\left(s^i_{t_{E0}}\right)\\ s^e_{t_{E0+}}\\ \Phi_{t_{E0}}\end{pmatrix} \tag{6.86}$$

From (6.86),

$$\begin{aligned}\mathbf{R}_{IE}\begin{pmatrix}\theta^e_{t_{I0}}\\ s^i_{t_{I0+}}\\ s^e_{t_{I0}}\\ \Phi_{t_{I0}}\end{pmatrix}-\mathring{\mathbf{R}}\begin{pmatrix}\theta^e_{t_{I0}}\\ s^i_{t_{I0+}}\\ s^e_{t_{I0}}\\ \Phi_{t_{I0}}\end{pmatrix}=&\mathbf{R}_I\left(\mathbf{R}_E\begin{pmatrix}\theta^e_{t_{I0}}\\ s^i_{t_{I0+}}\\ s^e_{t_{I0}}\\ \Phi_{t_{I0}}\end{pmatrix}\right)-\begin{pmatrix}\pm\pi\\ \rho_i\left(s^i_{t_{E0}}\right)\\ s^e_{t_{E0+}}\\ \Phi_{t_{E0}}\end{pmatrix}\\ =&\mathbf{R}_I\begin{pmatrix}\theta^i_{t_{E0}}\\ s^i_{t_{E0}}\\ s^e_{t_{E0+}}\\ \Phi_{t_{E0}}\end{pmatrix}-\begin{pmatrix}\pm\pi\\ \rho_i\left(s^i_{t_{E0}}\right)\\ s^e_{t_{E0+}}\\ \Phi_{t_{E0}}\end{pmatrix}\end{aligned}$$

From (6.85),

$$=\begin{pmatrix}\dot\theta^e_{t_{E0}}\\ \dot s^i_{t_{E0+}}\\ \dot s^e_{t_{E0+}}\\ \dot\Phi_{t_{E0}}\end{pmatrix}T_{EI}+O(T_{EI}^2)$$

Making explicit the dependence of T_{EI} on the state at time t_{E0}:

$$=\begin{pmatrix}\dot\theta^e_{t_{E0}}\\ \dot s^i_{t_{E0+}}\\ \dot s^e_{t_{E0+}}\\ \dot\Phi_{t_{E0}}\end{pmatrix}T_{EI}\circ\mathbf{R}_E\begin{pmatrix}\theta^e_{t_{I0}}\\ s^i_{t_{I0+}}\\ s^e_{t_{I0}}\\ \Phi_{t_{I0}}\end{pmatrix}+O(T_{EI}^2) \tag{6.87}$$

C does not directly affect the magnitudes of $\dot\theta^e$, $\dot s^i$, $\dot s^e$, or $\dot\Phi$, so they remain bounded as $C\to\infty$. We prove below in Lemma 6.7.1 that $\lim_{C\to\infty}T_{EI}=0$ (uniformly over initial state at t_{E0}); we conclude that $\mathbf{R}_{IE}$ and $\mathring{\mathbf{R}}$ approach each other in function space C^0 on the annulus $\mathbb{K}$, and in particular, for sufficiently large C, $\mathbf{R}_{IE}$ maps $\mathbb{K}$ into itself, fulfilling the first condition of the Annulus Principle.

Differentiating both sides of (6.87) with respect to initial state,

$$D\mathbf{R}_{IE}-D\mathring{\mathbf{R}}=\begin{pmatrix}\dot\theta^e_{t_{E0}}\\ c_i\dot s^i_{t_{E0}}\\ \dot s_{t_{E0+}}\\ \dot\Phi_{t_{E0}}\end{pmatrix}\nabla T_{EI}D\mathbf{R}E+O(T_{EI})\le\begin{pmatrix}\dot\theta^e_{t_{E0}}\\ c_i\dot s^i_{t_{E0}}\\ \dot s_{t_{E0+}}\\ \dot\Phi_{t_{E0}}\end{pmatrix}\|\nabla T_{EI}\|\|D\mathbf{R}E\|+O(T_{EI})$$

We prove below in Lemma 6.7.2 that $\|\mathbf{R}_E\|$ is bounded as $C \to \infty$; we prove below in lemma 6.7.3 that $\lim_{C\to\infty}\|\nabla T_{EI}\| = 0$ (this result does *not* immediately follow from $\lim_{C\to\infty} T_{EI} = 0$); we conclude that $D\mathbf{R}_{IE}$ and $D\mathring{\mathbf{R}}$ also approach each other on $\mathbb{K}$. Thus, $\mathbf{R}_{IE}$ and $\mathring{\mathbf{R}}$ approach each other in function space C^1 on $\mathbb{K}$ as $C \to \infty$. In particular, the partial derivatives of $\mathbf{R}_{IE}$ still fulfill conditions 2, 3, and 4 of the annulus principle for sufficiently large C.

We conclude that if we choose C sufficiently large, and either c_e and c_i sufficiently small or g_{ie} sufficiently large, the return map $\mathbf{R}_{IE}$ for the PING system possesses an attracting invariant circle, and the full PING system therefore possesses a broken attracting invariant torus and is limited to periodic and quasiperiodic dynamics.

6.7.4. *Step 3: T_{EI} gets small as C grows.* In support of our previous conclusion we prove the lemma:

Lemma 6.7.1. *As $C \to \infty$, $T_{EI} \to 0$ uniformly over $\mathbb{K}$.*

Proof. Let $T_{EI}(C)$ denote the time between an E-population spike and the subsequent I-population spike as a function of C. (T_{EI} also depends on initial conditions, though we suppress this dependence with this notation.) The period of a theta neuron with membrane time constant τ_i and constant current I is $\frac{\tau\pi}{\sqrt{I}}$. By assumption 3 in Section 4, for $C = 1$, the current to the I-cell is bounded away from zero until an I-spike: $G^i > K_{EI} > 0$ for time $T_{EI}(1)$. This bound holds over all initial conditions. For $C > 1$, G^i during this time is at least CK_{EI}, so $T_{EI}(C) < \frac{\tau_i\pi}{\sqrt{CK_{EI}}}$. As $C \to \infty$, this bound goes to zero, so $T_{EI}(C) \to 0$ uniformly over all initial conditions. □

6.7.5. *Step 4: T_{EI} does not vary sharply with initial state for large C.* In support of our previous conclusion we prove two lemmas. The first says that $\|D\mathbf{R}_E\|$ is bounded as $C \to \infty$; the second says that as $C \to \infty$, $\|\nabla T_{EI}\| \to 0$ as (where the gradient is taken with respect to system state at t_{E0}). In combination, these show that the variation in T_{EI} in response to variation in the initial state at t_{I0} goes to zero as $C \to \infty$.

Lemma 6.7.2. *$\|D\mathbf{R}_E\|$ is bounded as $C \to \infty$,*

Proof. The only terms in $D\mathbf{R}_E$ that depend on C are the derivatives of $\theta^i_{t_{E0}}$ with respect to state at t_{I0}. Variations in Φ and θ^e at t_{I0} may affect $\theta^i_{t_{E0}}$ only by making time t_{E0} earlier or later; the amount by which such a variation affects t_{E0} is not affected by C, and the resulting variation in θ^i is simply $\dot\theta^i$ times the variation in t_{E0}, so we need only show that $\dot\theta^i$ is bounded as $C \to \infty$. Variations in s_i and s_e affect the evolution of θ^i directly; we must show that their effect is bounded throughout the interval $[t_{I0}, t_{E0}]$ as $C \to \infty$.

When $C = 1$, by assumption 1 from Section 4 $G^i < K_{IE} < 0$ between an I-spike and an E-spike. Therefore for $C > 1$, $G^i < CK_{IE} < 0$ between I-spike and E-spike. During

this interval, if $\theta^i > -\cos^{-1}\left(\frac{1+CK_{IE}}{1-CK_{IE}}\right)$, then $\dot{\theta}^i < 0$; therefore, θ^i cannot cross above $-\cos^{-1}\left(\frac{1+CK_{IE}}{1-CK_{IE}}\right)$ until the next E-spike, and until then

$$\cos(\theta^i) < \frac{1+CK_{IE}}{1-CK_{IE}}. \tag{6.88}$$

We also have $|G^i| = |C(b_i + g_{ei}s_e - g_{ii}s_i)| \leq C(-b_i + g_{ei} + g_{ii})$. These results allow us to bound $|\dot{\theta}^i|$ during this interval:

$$\begin{aligned}
\tau_i|\dot{\theta}^i| =& |1 - \cos(\theta^i) + (1+\cos(\theta^i))G^i| \\
\leq& 2 + |1+\cos(\theta^i)||G^i| \\
\leq& 2 + |1 + \frac{1+CK_{IE}}{1-CK_{IE}}|C(-b_i + g_{ei} + g_{ii}) \\
=& 2 + |\frac{2}{1-CK_{IE}}|C(-b_i + g_{ei} + g_{ii}) \\
\leq& 2 + \frac{2(-b_i + g_{ei} + g_{ii})|}{|\frac{1}{C} - K_{IE}|}
\end{aligned}$$

which is bounded as $C \to \infty$; therefore, the variations in $\theta^i_{t_{E0}}$ produced by variations in $\theta^e_{t_{I0}}$ and $\Phi_{t_{I0}}$ are bounded as $C \to \infty$.

Differentiating the first equation in (6.82) with respect to the system state, we have

$$\frac{d}{dt}\Delta\theta^i_t = \frac{1}{\tau_i}(1 - G^i_t)\sin(\theta^i_t)\Delta\theta^i_t + \frac{C}{\tau_i}(1+\cos(\theta^i))(g_{ei}\Delta s^e_t - g_{ii}\Delta s^i_t)$$

with initial condition $\Delta\theta^i_t = 0$. This ODE is solved at t_{E0} by

$$\Delta\theta^i_{t_{E0}} = \frac{C}{\tau_i}\int_{t_{I0}}^{t_{E0}} (1+\cos(\theta^i_t))e^{\frac{1}{\tau_i}\int_t^{t_{E0}}(1-CG^i_r)\sin(\theta^i_r)dr}(-g_{ii}\Delta s^i_t + g_{ei}\Delta s^e_t)dt$$

By the triangle inequality,

$$|\Delta\theta^i_{t_{E0}}| \leq \frac{C}{\tau_i}\int_{t_{I0}}^{t_{E0}} (1+\cos(\theta^i_t))e^{\frac{1}{\tau_i}\int_t^{t_{E0}}(1-CG^i_r)\sin(\theta^i_r)dr}|-g_{ii}\Delta s^i_t + g_{ei}\Delta s^e_t|dt$$

The term $\frac{1}{\tau_i}(1-G^i)\sin(\theta^i)$ is negative during this interval:

$$|\Delta\theta^i_{t_{E0}}| \leq \frac{C}{\tau_i}\int_{t_{I0}}^{t_{E0}} (1+\cos(\theta^i_t))\left(g_{ii}|\Delta s^i_t| + g_{ei}|\Delta s^e_t|\right)dt$$

Δs_t^i and Δs_t^e decrease exponentially, so during this interval they are less or equal to their initial values at t_{I0}:

$$|\Delta\theta^i_{t_{E0}}| \leq \frac{C}{\tau_i}\int_{t_{I0}}^{t_{E0}} (1+\cos(\theta_t^i))\left(g_{ii}|\Delta s^i_{t_{I0+}}| + g_{ei}|\Delta s^e_{t_{I0+}}|\right)$$

From (6.7.5),

$$\begin{aligned}
&\leq \frac{C}{\tau_i}\int_{t_{I0}}^{t_{E0}} \left(1+\frac{1+CK_{IE}}{1-CK_{IE}}\right)\left(g_{ii}|\Delta s^i_{t_{I0+}}| + g_{ei}|\Delta s^e_{t_{I0+}}|\right)\\
&= \frac{C}{\tau_i}\int_{t_{I0}}^{t_{E0}} \left(\frac{2}{\frac{1}{C}-K_{IE}}\right)\left(g_{ii}|\Delta s^i_{t_{I0+}}| + g_{ei}|\Delta s^e_{t_{I0+}}|\right)
\end{aligned}$$

which is bounded as $C \to \infty$. Therefore, the magnitude of the derivatives of $\theta^i_{t_{E0}}$ with respect to $s^i_{t_{I0+}}$ and $s^e_{t_{I0+}}$ are bounded as $C \to \infty$.

□

Lemma 6.7.3. *As $C \to \infty$, $\|\nabla T_{EI}\| \to 0$ (where the gradient is taken with respect to system state at t_{E0}).*

Proof. We want to show that the derivative of T_{EI} with respect to any initial state variable at t_{E0} goes to zero uniformly over all initial conditions as $\tau_i \to 0$ or $C \to \infty$. To do so, we track variations from one spike to the next, as in Appendix 6.2. The amount of change in T_{EI} per unit variation in each initial condition gives us the gradient ∇T_{EI}; we want to show that the magnitude of this gradient goes to zero as $C \to \infty$.

Between the E-spike and the following I-spike, variations in Φ make no difference to the I-population rise time. The variation in θ^i at t_{E0} determines the change in the initial state of θ^i at the beginning of its rise; the variations in s^i and s^e determine the change in the rise speed. We will show that for any $\Delta\theta^i$, Δs^i, and Δs^e at time t_{E0}, the resulting variation in the rise time of the I-population goes to zero as $C \to \infty$.

The first variational equation of (6.82) is solved at time t_{I2} by

$$\Delta\theta^i_{t_{I2}} = \Delta\theta^i_{t_{E0}} e^{\frac{1}{\tau_i}\int_{t_{E0}}^{t_{I2}}(1-CG_t^i)\sin(\theta_t^i)dt} + \frac{C}{\tau_i}\int_{t_{E0}}^{t_{I2}}(1+\cos(\theta_t^i))e^{\frac{1}{\tau_i}\int_t^{t_{I2}}(1-CG_r^i)\sin(\theta_r^i)dr}(-g_{ii}\Delta s_t^i + g_{ei}\Delta s_t^e)dt$$

By the triangle inequality,

$$|\Delta\theta^i_{t_{I2}}| \leq |\Delta\theta^i_{t_{E0}}| e^{\frac{1}{\tau_i}\int_{t_{E0}}^{t_{I2}}(1-CG_t^i)\sin(\theta_t^i)dt} + \frac{C}{\tau_i}\int_{t_{E0}}^{t_{I2}}(1+\cos(\theta_t^i))e^{\frac{1}{\tau_i}\int_t^{t_{I2}}(1-CG_r^i)\sin(\theta_r^i)dr}(g_{ii}|\Delta s_t^i| + g_{ei}|\Delta s_t^e|)dt$$

As noted above, $|\Delta s^e|$ and $|\Delta s^i|$ only decay after t_{E0}, so

$$|\Delta\theta^i_{t_{I2}}| \leq |\Delta\theta^i_{t_{E0}}| e^{\frac{1}{\tau_i}\int_{t_{E0}}^{t_{I2}}(1-CG_t^i)\sin(\theta_t^i)dt} + \frac{C}{\tau_i}\int_{t_{E0}}^{t_{I2}}(1+\cos(\theta_t^i))e^{\frac{1}{\tau_i}\int_t^{t_{I2}}(1-CG_r^i)\sin(\theta_r^i)dr}(g_{ii}|\Delta s^i_{t_{E0}}| + g_{ei}|\Delta s^e_{t_{E0}}|)$$

Setting $k = g_{ii}|\Delta s^i_{t_{E0}}| + g_{ei}|\Delta s^e_{t_{E0}}|$,

$$\begin{aligned}|\Delta\theta^i_{t_{I2}}| \leq & |\Delta\theta^i_{t_{E0}}| e^{\frac{1}{\tau_i}\int_{t_{E0}}^{t_{I2}}(1-CG^i_t)\sin(\theta^i_t)dt} + \frac{kC}{\tau_i}\int_{t_{E0}}^{t_{I2}}(1+\cos(\theta^i_t))e^{\frac{1}{\tau_i}\int_t^{t_{I2}}(1-CG^i_r)\sin(\theta^i_r)dr}dt \\ = & |\Delta\theta^i_{t_{E0}}| e^{\frac{1}{\tau_i}\int_{t_{E0}}^{t_{I2}}(1-CG^i_t)\sin(\theta^i_t)dt} + \frac{k\sqrt{C}}{\tau_i}\int_{t_{E0}}^{t_{I2}}(1+\cos(\theta^i_t))\sqrt{C}e^{\frac{1}{\tau_i}\int_t^{t_{I2}}(1-CG^i_r)\sin(\theta^i_r)dr}dt\end{aligned}$$

where we define

$$\Gamma(t) := (1+\cos(\theta^i_t))\sqrt{C}e^{\frac{1}{\tau_i}\int_t^{t_{I2}}(1-CG^i_r)\sin(\theta^i_r)dr}.$$

We have already determined that $t_{I2} - t_{E0} < \frac{\tau_i\pi}{\sqrt{CK_{EI}}}$, so we have $\frac{\sqrt{C}}{\tau_i} < \frac{\pi}{(t_{I2}-t_{E0})\sqrt{K_{EI}}}$, and we can write

$$|\Delta\theta^i_{t_{I2}}| < |\Delta\theta^i_{t_{E0}}| e^{\frac{1}{\tau_i}\int_{t_{E0}}^{t_{I2}}(1-CG^i_t)\sin(\theta^i_t)dt} + \frac{k\pi}{\sqrt{K_{EI}}}\frac{1}{t_{I2}-t_{E0}}\int_{t_{E0}}^{t_{I2}}\Gamma(t)dt.$$

The term $\frac{1}{t_{I2}-t_{E0}}\int_{t_{E0}}^{t_{I2}}\Gamma(t)dt$ is an average value of the function Γ over the interval $[t_{E0}, t_{I2}]$, and is therefore bounded by the supremum of Γ:

$$|\Delta\theta^i_{t_{I2}}| < |\Delta\theta^i_{t_{E0}}| e^{\frac{1}{\tau_i}\int_{t_{E0}}^{t_{I2}}(1-CG^i_t)\sin(\theta^i_t)dt} + \frac{k\pi}{K_{EI}}\sup_{t\in[t_{E0},t_{I2}]}\Gamma(t).$$

Since $\dot\theta^i > 0$ during this interval, we can invert θ^i_t and write time as a function of I-population phase t_Θ rather than the other way around: t_Θ shall denote the time at which θ^i reaches Θ. We change variables in all of our integrals and integrate over phase rather than time using $dt = \frac{d\Theta}{\dot\theta^i_{t_\Theta}}$:

$$|\Delta\theta^i_{t_{I2}}| < |\Delta\theta^i_{t_{E0}}| e^{\frac{1}{\tau_i}\int_{\theta^i_{t_{E0}}}^{\pi}(1-CG^i_{t_\Theta})\sin(\Theta)\frac{d\Theta}{\dot\theta^i_{t_\Theta}}} + \frac{k\pi}{K_{EI}}\sup_{\Theta\in[\theta^i_{t_{E0}},\pi]}\Gamma_2(\Theta) \tag{6.89}$$

where Γ_2 is Γ as a function of Θ rather than t, a function with the same supremum on $[\theta^i_{t_{E0}}, \pi]$ as Γ has on $[t_{E0}, t_{I2}]$:

$$\Gamma_2(\Theta) := (1+\cos(\Theta))\sqrt{C}e^{\frac{1}{\tau_i}\int_\Theta^\pi(1-CG^i_{t_\theta})\sin(\theta)\frac{d\theta}{\dot\theta^i_{t_\theta}}}.$$

The term $e^{\frac{1}{\tau_i}\int_{\theta^i_{t_{E0}}}^{\pi}(1-CG^i_{t_\Theta})\sin(\Theta)\frac{d\Theta}{\dot\theta^i_{t_\Theta}}}$ in (6.89) can be broken into two parts:

$$e^{\frac{1}{\tau_i}\int_{\theta^i_{t_{E0}}}^{\pi}(1-CG^i_{t_\Theta})\sin(\Theta)\frac{d\Theta}{\dot\theta^i_{t_\Theta}}} = \left[e^{\frac{1}{\tau_i}\int_{\theta^i_{t_{E0}}}^{0}(1-CG^i_{t_\Theta})\sin(\Theta)\frac{d\Theta}{\dot\theta^i_{t_\Theta}}}\right]\left[e^{\frac{1}{\tau_i}\int_0^{\pi}(1-CG^i_{t_\Theta})\sin(\Theta)\frac{d\Theta}{\dot\theta^i_{t_\Theta}}}\right].$$

In Lemma 6.7.5(2), we prove that the first of these terms is bounded as $C \to \infty$; in Lemma 6.7.5(1), we prove that the second goes to zero as $C \to \infty$; in Lemma 6.7.6, we prove that the term $\sup_{\Theta \in [\theta^i_{t_{E0}}, \pi]} \Gamma_2(\Theta)$ in (6.89) goes to zero as $C \to \infty$. Thus, the magnitude of the variation $\Delta\theta^i_{t_{I2}}$ caused by bounded variation in the initial state variables $\theta^i_{t_{E0}}$, $s^i_{t_{E0}}$, and $s^e_{t_{E0}}$ goes to zero as $C \to \infty$.

At time t_{I2}, θ^i crosses π at speed $\frac{2}{\tau_i}$, so a variation in θ^i translates into a variation in spike time:

$$\lim_{C\to\infty} \Delta t = \lim_{C\to\infty} \frac{\Delta\theta^i_{t_{I2}}}{\frac{2}{\tau_i}} = 0.$$

So the impact of any variation in initial conditions at time t_{E0} is reduced to zero as $C \to \infty$; in other words, $\lim_{C\to\infty} \|\nabla T_{EI}\| = 0$.

□

6.7.6. *Step 5: Auxiliary lemmas.* Here we prove the lemmas that support the proof of our previous lemmas. First we provide several definitions that will help us in the proofs of our auxiliary lemmas:

$$\Gamma_2(\Theta) := (1 + \cos(\Theta))\sqrt{C} e^{\frac{1}{\tau_i} \int_\Theta^\pi (1 - CG^i_{t_\theta}) \sin(\theta) \frac{d\theta}{\dot{\theta}^i_{t_\theta}}}. \tag{6.90}$$

Given θ^i_t, the path of the I-population rise between t_{E0} and t_{I2},

$$\begin{cases} G_{min} := \inf_{t\in[t_{E0},t_{I2}]} G^i_t > K_{EI} > 0 \\ G_{max} := \sup_{t\in[t_{E0},t_{I2}]} G^i_{t_\theta} > G_{min} \end{cases}$$

$$W(C) := \frac{1 - CG_{min}}{1 - CG_{max}} < 1$$

Lemma 6.7.4. *G_{min} and G_{max} converge uniformly to $G^i_{t_{E0}}$ as $C \to \infty$.*

Proof. During the I-cell rise, G^i_t is changing at a bounded rate:

$$\begin{aligned} \frac{d}{dt} G^i_t =& - g_{ii} \frac{d}{dt} s^i + g_{ei} \frac{d}{dt} s^e \\ =& g_{ii} \frac{s^i}{\tau_{s^i}} - g_{ei} \frac{s^e}{\tau_{s^e}} \\ \left|\frac{d}{dt} G^i_t\right| \leq& \min\left(\frac{g_{ei}}{\tau_{s^e}}, \frac{g_{ii}}{\tau_{s^i}}\right) \end{aligned}$$

From the proof of Lemma 6.7.1, we know that the rise time of θ^i is bounded by $\frac{\tau_i \pi}{\sqrt{CK_{EI}}}$. For $t \in [t_{E0}, t_{I2}]$, G_t^i must stay close to its initial value, $G_{t_{E0}}^i$:

$$|G_t^i - G_{t_{E0}}^i| \leq \min\left(\frac{g_{ei}}{\tau_{s^e}}, \frac{g_{ii}}{\tau_{s^i}}\right) \frac{\tau_i \pi}{\sqrt{CK_{EI}}}, G_{t_{E0}}^i$$

so both G_{min} and G_{max} must approach $G_{t_{E0}}$ as $C \to \infty$. □

Lemma 6.7.5. *Assume C is sufficiently large that $1 - CG_{min} < 0$. Given some $\theta^i \in [\theta_{t_{E0}}^i, \pi]$,*

(1) *If $\theta_i \in [0, \pi]$,*

$$e^{\frac{1}{\tau_i}\int_{\theta^i}^{\pi}(1-CG_{t_\Theta}^i)\sin(\Theta)\frac{d\Theta}{\dot{\theta}_{t_\Theta}^i}} \leq \left(\frac{2}{1-\cos(\theta^i)+(1+\cos(\theta^i))CG_{max}}\right)^{W(C)}.$$

(2) *If $\theta_i \in [-\pi, 0]$,*

$$e^{\frac{1}{\tau_i}\int_{\theta^i}^{0}(1-CG_{t_\Theta}^i)\sin(\Theta)\frac{d\Theta}{\dot{\theta}_{t_\Theta}^i}} \leq \left(\frac{2CG_{min}}{1-\cos(\theta^i)+(1+\cos(\theta^i))CG_{min}}\right)^{\frac{1}{W(C)}}.$$

(3) $\lim C \to \infty W(C) = 1$.

Proof. (1) If $\theta_i \in [0, \pi]$, then $\sin(\Theta) \geq 0$ for $\Theta \in [\theta^i, \pi]$. We can use this and the definitions of G_{max} and G_{min} above, along with the assumption $1 - CG_{min} < 0$, to place an upper bound on our expression of interest:

$$\begin{aligned}
e^{\frac{1}{\tau_i}\int_{\theta^i}^{\pi}(1-CG_{t_\Theta}^i)\sin(\Theta)\frac{d\Theta}{\dot{\theta}_{t_\Theta}^i}} &= e^{\frac{1}{\tau_i}\int_{\theta^i}^{\pi}(1-CG_{t_\Theta}^i)\sin(\Theta)\frac{d\Theta\tau_i}{1-\cos(\Theta)+(1+\cos(\Theta))CG_{t_\Theta}^i}} \\
&\leq e^{\int_{\theta^i}^{\pi}(1-CG_{min})\sin(\Theta)\frac{d\Theta}{1-\cos(\Theta)+(1+\cos(\Theta))CG_{max}}} \\
&= e^{\frac{1-CG_{min}}{CG_{max}-1}\int_{\theta^i}^{\pi}\frac{d\Theta\sin(\Theta)(CG_{max}-1)}{CG_{max}+1+(CG_{max}-1)\cos(\Theta)}} \\
&= e^{\frac{1-CG_{min}}{CG_{max}-1}(-\ln(CG_{max}+1+(CG_{max}-1)\cos(\Theta)))|_{\Theta=\theta^i}^{\pi}} \\
&= e^{\frac{1-CG_{min}}{1-CG_{max}}\ln\left(\frac{2}{CG_{max}+1+(CG_{max}-1)\cos(\theta^i)}\right)} \\
&= \left(\frac{2}{1-\cos(\theta^i)+(1+\cos(\theta^i))CG_{max}}\right)^{W(C)}
\end{aligned}$$

(2) If $\theta_i \in [-\pi, 0]$, then $\sin(\Theta) \leq 0$ for $\Theta \in [\theta^i, \pi]$. We follow the same steps as above but switch G_{min} and G_{max} to establish an upper bound on our new expression of interest:

$$\begin{aligned}
e^{\frac{1}{\tau_i}\int_{\theta^i}^{0}(1-CG^i_{t_\Theta})\sin(\Theta)\frac{d\Theta}{\dot\theta^i_{t_\Theta}}} &\leq e^{\int_{\theta^i}^{0}(1-CG_{max})\sin(\Theta)\frac{d\Theta}{1-\cos(\Theta)+(1+\cos(\Theta))CG_{min}}} \\
&= e^{\frac{1-CG_{max}}{CG_{min}-1}\int_{\theta^i}^{0}\frac{d\Theta\sin(\Theta)(CG_{max}-1)}{CG_{max}+1+(CG_{max}-1)\cos(\Theta)}} \\
&= e^{\frac{1-CG_{max}}{CG_{min}-1}(-\ln(CG_{min}+1+(CG_{min}-1)\cos(\Theta)))|^{0}_{\Theta=\theta^i}} \\
&= e^{\frac{1-CG_{max}}{1-CG_{min}}\ln\left(\frac{2CG_{min}}{CG_{min}+1+(CG_{min}-1)\cos(\theta^i)}\right)} \\
&= \left(\frac{2CG_{min}}{1-\cos(\theta^i)+(1+\cos(\theta^i))CG_{min}}\right)^{\frac{1}{W(C)}}
\end{aligned}$$

(3) By Lemma 6.7.4, G_{max} and G_{min} both approach $G_{t_{E0}}$ as $C \to \infty$:

$$\begin{aligned}
\lim_{C\to\infty} W(C) &= \lim_{C\to\infty}\frac{1-CG_{min}}{1-CG_{max}} \\
&= \lim_{C\to\infty}\frac{\frac{1}{C}-G_{min}}{\frac{1}{C}-G_{max}} \\
&= \lim_{C\to\infty}\frac{-G_{t_{E0}}}{-G_{t_{E0}}} = 1
\end{aligned}$$

□

Lemma 6.7.6. *Given an initial I-population phase $\theta^i_{t_{E0}} \in [-\pi, 0]$,*

$$\lim_{C\to\infty}\sup_{\Theta\in[\theta^i_{t_{E0}},\pi]}\Gamma_2(\Theta) = 0$$

Proof. First, consider $\theta^i \in [0, \pi]$. We show in Lemma 6.7.5(1) that

$$e^{\frac{1}{\tau_i}\int_{\theta^i}^{\pi}(1-CG^i_{t_\Theta})\sin(\Theta)\frac{d\Theta}{\dot\theta^i_{t_\Theta}}} \leq \left(\frac{2}{CG_{max}+1+(CG_{max}-1)\cos(\theta^i)}\right)^{W(C)}$$

where, by Lemma 6.7.5(**??**), $\lim_{C\to\infty} W(C) = 1$.

We can use this expression to bound $\Gamma_2(\theta^i)$:

$$\begin{aligned}\Gamma_2(\theta^i) =&(1+\cos(\theta^i))\sqrt{C}e^{\frac{1}{\tau_i}\int_{\theta^i}^{\pi}(1-CG^i_{t_\Theta})\sin(\Theta)\frac{d\Theta}{\dot\theta^i_{t_\Theta}}}\\ \leq&(1+\cos(\theta^i))\sqrt{C}\left(\frac{2}{1-\cos(\theta^i)+(1+\cos(\theta^i))CG_{max}}\right)^{W(C)}\\ =&(1+\cos(\theta^i))^{1-W(C)}C^{\frac{1}{2}-W(C)}\left(\frac{2}{G_{max}}\right)^{W(C)}\left(\frac{(1+\cos(\theta^i))CG_{max}}{1-\cos(\theta^i)+(1+\cos(\theta^i))CG_{max}}\right)^{W(C)} \qquad (6.91)\\ =&(1+\cos(\theta^i))^{1-W(C)}C^{\frac{1}{2}-W(C)}\left(\frac{2}{G_{max}}\right)^{W(C)}\left(1-\frac{1-\cos(\theta^i)}{1-\cos(\theta^i)+(1+\cos(\theta^i))CG_{max}}\right)^{W(C)}\end{aligned}$$

$\frac{1-\cos(\theta^i)}{1-\cos(\theta^i)+(1+\cos(\theta^i))CG_{max}} \in [0,1]$, so $\left(1-\frac{1-\cos(\theta^i)}{1-\cos(\theta^i)+(1+\cos(\theta^i))CG_{max}}\right)^{W(C)} < 1$:

$$\Gamma_2(\theta^i) \leq (1+\cos(\theta^i))^{1-W(C)}C^{\frac{1}{2}-W(C)}\left(\frac{2}{G_{max}}\right)^{W(C)} \qquad (6.92)$$

By Lemma 6.7.5(refbothstep3), $W(C)\to 1$, so for sufficiently large C, $\frac{1}{2}-W(C)$ is bounded below zero and $C^{\frac{1}{2}-W(C)}$ goes to zero as C grows.

We also have $W(C)<1$, so for sufficiently large C, $1-W(C)\in(0,1]$ and $(1+\cos(\theta^i))^{1-W(C)}\in[0,2]$.

Finally, by Lemma 6.7.4, $\lim_{C\to 0} G_{max} = G_{t_{E0}}$, so $\left(\frac{2}{G_{max}}\right)^{W(C)} \to \frac{2}{G_{t_{E0}}}$.

The terms in (6.92) are all bounded uniformly over θ^i as $C\to 0$, and one term goes to zero, so $\Gamma_2(\theta^i)$ goes uniformly to zero as $C\to\infty$.

Next, consider $\theta^i\in[-\pi,0]$. We split (6.90) into two pieces:

$$\begin{aligned}\Gamma_2(\theta^i) =&(1+\cos(\theta^i))\sqrt{C}e^{\frac{1}{\tau_i}\int_{\theta^i}^{\pi}(1-CG^i_{t_\Theta})\sin(\Theta)\frac{d\Theta}{\dot\theta^i_{t_\Theta}}}\\ =&\left[\frac{(1+\cos(\theta^i))}{1+\cos(0)}e^{\frac{1}{\tau_i}\int_{\theta^i}^{0}(1-CG^i_{t_\Theta})\sin(\Theta)\frac{d\Theta}{\dot\theta^i_{t_\Theta}}}\right]\left[(1+\cos(0))\sqrt{C}e^{\frac{1}{\tau_i}\int_{0}^{\pi}(1-CG^i_{t_\Theta})\sin(\Theta)\frac{d\Theta}{\dot\theta^i_{t_\Theta}}}\right]\\ =&\left[\frac{(1+\cos(\theta^i))}{2}e^{\frac{1}{\tau_i}\int_{\theta^i}^{0}(1-CG^i_{t_\Theta})\sin(\Theta)\frac{d\Theta}{\dot\theta^i_{t_\Theta}}}\right]\Gamma_2(0).\end{aligned}$$

By Lemma 6.7.5(2), the first term of (**??**) is bounded uniformly over C and θ^i for sufficiently large C. We have shown above that $\Gamma_2(0)\to 0$ uniformly as $C\to 0$. Therefore, for $\theta^i\in[-\pi,0]$, $\Gamma_2(\theta^i)$ goes uniformly to zero as $C\to\infty$. Our proof is complete.

□

7. References